

SIMULATION AND EXPERIMENTAL METHODS FOR CHARACTERIZATION OF NONLINEAR MECHANICAL SYSTEMS

Martin Magnevall

Blekinge Institute of Technology
Doctoral Dissertation Series No. 2011:14
School of Engineering



**Simulation and Experimental Methods
for Characterization of Nonlinear
Mechanical Systems**

Martin Magnevall

Blekinge Institute of Technology doctoral dissertation series
No 2011:14

Simulation and Experimental Methods for Characterization of Nonlinear Mechanical Systems

Martin Magnevall

Doctoral dissertation in
Mechanical Engineering



School of Engineering
Blekinge Institute of Technology
SWEDEN

© 2011 Martin Magnevall
School of Engineering
Publisher: Blekinge Institute of Technology,
SE-371 79 Karlskrona, Sweden
Printed by Printfabriken, Karlskrona, Sweden 2011
ISBN: 978-91-7295-218-8
ISSN 1653-2090
urn:nbn:se:bth-00513

Acknowledgements

This work was carried out at the Department of Mechanical Engineering, School of Engineering, Blekinge Institute of Technology, Karlskrona, Sweden and at AB Sandvik Coromant, Sandviken, Sweden under the supervision of Professor Kjell Ahlin and Professor Göran Broman.

I wish to express my sincere appreciation to Professor Kjell Ahlin for being a great mentor and true source of inspiration. Special gratitude is extended to Professor Göran Broman for his professional support and inspiring guidance throughout the work.

To all my colleagues at the department of mechanical engineering; thank you for the pleasant and productive working environment you help to create. A special thanks to my closest co-worker, Dr. Andreas Josefsson, for all fruitful discussions and a very good collaboration. I would also like to thank my colleagues at AB Sandvik Coromant for creating a truly enjoyable and productive working atmosphere, especially Anders Liljerehn for a fruitful collaboration and Mikael Lundblad for all support and ideas.

Financial support from AB Sandvik Coromant, the Swedish Knowledge Foundation and the Faculty Board of Blekinge Institute of Technology is gratefully acknowledged.

Finally, I would like to extend my deepest gratitude to my family for all their love and support throughout the work.

Karlskrona, November 2011

Martin Magnevall

Abstract

Trial and error and the use of highly time-consuming methods are often necessary for investigation and characterization of nonlinear systems. However, for the rather common case where a nonlinear system has linear relations between many of its degrees of freedom there are opportunities for more efficient approaches. The aim of this thesis is to develop and validate new efficient simulation and experimental methods for characterization of mechanical systems with localized nonlinearities. The purpose is to contribute to the development of analysis tools for such systems that are useful in early phases of the product innovation process for predicting product properties and functionality. Fundamental research is combined with industrial case studies related to metal cutting. Theoretical modeling, computer simulations and experimental testing are utilized in a coordinated approach to iteratively evaluate and improve the methods. The nonlinearities are modeled as external forces acting on the underlying linear system. In this way, much of the linear theories behind forced response simulations can be utilized. The linear parts of the system are described using digital filters and modal superposition, and the response of the system is recursively solved for together with the artificial external forces. The result is an efficient simulation method, which in conjunction with experimental tests, is used to validate the proposed characterization methods.

A major part of the thesis addresses a frequency domain characterization method based on broad-band excitation. This method uses the measured responses to create artificial nonlinear inputs to the parameter estimation model. Conventional multiple-input/multiple-output techniques are then used to separate the linear system from the nonlinear parameters. A specific result is a generalization of this frequency domain method, which allows for characterization of continuous systems with an arbitrary number of localized zero-memory nonlinearities in a structured way. The efficiency and robustness of this method is demonstrated by both simulations and experimental tests. A time domain simulation and characterization method intended for use on systems with hysteresis damping is also developed and its efficiency is demonstrated by the case of a dry-friction damper. Furthermore, a method for improved harmonic excitation of nonlinear systems using numerically optimized input signals is developed. Inverse filtering is utilized to remove unwanted dynamic effects in cutting force measurements, which increases the frequency range of the force dynamometer and significantly improves the experimental results compared to

traditional methods. The new methods form a basis for efficient analysis and increased understanding of mechanical systems with localized nonlinearities, which in turn provides possibilities for more efficient product development as well as for continued research on analysis methods for nonlinear mechanical structures.

Keywords: *nonlinear structural dynamics, simulation, system characterization, experimental techniques.*

Appended Papers

The appended papers have been reformatted from their original layouts to fit the format of this thesis; the content is, however, unchanged.

Paper A

Josefsson, A., Magnevall, M. and Ahlin, K. Control Algorithm for Sine Excitation on Nonlinear Systems, In *Proceedings of IMAC-XXIV, Conference & Exposition on Structural Dynamics*, St. Louis, USA, 2006.

Paper B

Magnévall, M., Josefsson, A. and Ahlin, K. On Nonlinear Parameter Estimation, In *Proceedings of International Conference on Noise and Vibration Engineering (ISMA) 2006*, Leuven, Belgium, 2006.

Paper C

Josefsson, A., Magnevall, M. and Ahlin, K. On Nonlinear Parameter Estimation with Random Noise Signals, In *Proceedings of IMAC-XXV, Conference & Exposition on Structural Dynamics*, Orlando, USA, 2007.

Paper D

Magnévall, M., Josefsson, A., Ahlin, K. and Broman, G. Nonlinear Structural Identification by the “Reverse Path” Spectral Method, *Journal of Sound and Vibration*, vol. 331, no. 4, pp. 938-946, 2012.

Paper E

Magnévall, M., Josefsson, A., Ahlin, K. and Broman, G. A Simulation and Characterization Method for Hysteretically Damped Vibrations, *Submitted for publication*, 2011.

Paper F

Magnevall, M., Lundblad, M., Ahlin, K. and Broman, G. High Frequency Measurements of Cutting Forces in Milling by Inverse Filtering, Accepted for publication in *Machining Science and Technology*, November 2011.

The Author's Contribution to the Papers

The appended papers were written together with co-authors. The present author's contributions to the individual papers are as follows:

Paper A

Took part in planning and writing the paper.
Responsible for the modeling and simulations.

Paper B

Responsible for planning and writing the paper.
Took part in modeling and simulations related to random excitation.
Responsible for modeling and simulations concerning sinusoidal excitation.

Paper C

Took part in planning and writing the paper.
Took part in the modeling, simulations and measurements.

Paper D

Responsible for planning and writing the paper.
Carried out all the modeling, simulations and measurements.

Paper E

Responsible for planning and writing the paper.
Carried out all the modeling, simulations and measurements.

Paper F

Responsible for planning and writing the paper.
Carried out all the modeling, simulations and measurements.

Related publications

Publications authored or co-authored during the period of Ph.D studies which are not included in the written thesis.

Magnévall, M., Josefsson, A., Ahlin, K. Experimental Verification of a Control Algorithm for Nonlinear Systems, In *Proceedings of IMAC-XXIV, Conference & Exposition on Structural Dynamics*, St. Louis, USA, 2006.

Ahlin K., Magnévall M. and Josefsson A. Simulation of Forced Response in Linear and Nonlinear Mechanical Systems using Digital Filters, In *Proceedings of International Conference on Noise and Vibration Engineering (ISMA)*, Leuven, Belgium, 2006.

Magnévall, M., Josefsson, A., Ahlin, K. Parameter Estimation of Hysteresis Elements using Harmonic Input, In *Proceedings of IMAC-XXV, Conference & Exposition on Structural Dynamics*, Orlando, USA, 2007.

Josefsson A., Magnévall M. and Ahlin K. Estimating the Location of Structural Nonlinearities From Random Data, In *Proceedings of IMAC-XXVI, Conference & Exposition on Structural Dynamics*, Orlando, USA, 2008.

Magnévall M., Josefsson A. and Ahlin K. On Parameter Estimation and Simulation of Zero Memory Nonlinear Systems, In *Proceedings of IMAC-XXVI, Conference & Exposition on Structural Dynamics*, Orlando, USA, 2008.

Magnévall M. Methods for Characterization and Simulation of Nonlinear Mechanical Structures, *Licentiate Dissertation*, Karlskrona, Sweden, 2008.

Magnévall M., Liljerehn A., Lundblad M. and Ahlin K. Improved Cutting Force Measurements in High Speed Milling Using Inverse Structural Filtering, In *Proceedings of 2nd CIRP Conference on Process Machine Interaction (PMI)*, Vancouver, Canada, 2010.

Josefsson, A., Magnévall, M., Ahlin, K., Broman, G. Spatial Location Identification of Structural Nonlinearities from Random Data, *Mechanical Systems and Signal Processing*, Elsevier, 2011, (In Print).

Josefsson, A., Magnevall, M., Ahlin, K. Identification of a Beam Structure with a Local Nonlinearity Using Reverse-Path Analysis, *Submitted for publication*, 2011.

Contents

1	Introduction	1
1.1	Background	1
1.2	Aim and Scope	2
1.3	Research Design	3
1.4	Thesis outline	4
2	Linear versus Nonlinear Systems	5
2.1	Zero-Memory Nonlinearities	6
2.2	Hysteretic Nonlinearities	8
3	Time Domain Forced Response Simulation	10
4	Experimental Testing	13
4.1	Random Excitation	13
4.2	Harmonic Excitation	13
5	Characterization of Nonlinear Systems	16
5.1	Frequency Domain	16
5.2	Time/Frequency Domain	17
6	Summary of Papers	20
7	Concluding Discussion	23
References		26
Paper A		33
Paper B		49
Paper C		73
Paper D		95
Paper E		117
Paper F		147

1 Introduction

This section presents a background to the research presented in the thesis and the aim and scope of this research. A description of the research design used is also given together with an overview of the thesis structure.

1.1 Background

Modal parameter estimation, or *modal analysis*, is the most commonly used method to analyze and describe the dynamic behavior of linear mechanical systems. This method provides a small set of parameters in the form of natural frequencies, mode shapes and damping ratios, describing the system's behavior for any input [1, 2, 3].

However, almost all mechanical systems show some form of nonlinear behavior. The nonlinear effects are often due to a combination of several factors, such as nonlinear material properties, geometric effects, structural joints and nonlinear boundary conditions. For simplicity, these effects are often neglected, i.e. the system is linearized within some working range. However, a linear analysis is generally insufficient in relation to the required accuracy. On the other hand, a nonlinear analysis often requires much more computation capacity and time. This is part of the general challenge of product innovation, i.e. there are increasing demands on product performance, requiring more development efforts, at the same time as there are increasing demands on shorter development times. This, in turn, implies increasing demands on simulation models [1, 4] and recent studies [5, 6, 7, 8, 9] indicate that the potential of simulation-driven design is best utilized when virtual and physical prototyping are combined in a systematic way so that the simulation models contribute to the physical prototyping and vice versa. This is especially valid when nonlinear analysis is necessary. Thus, robust and reliable methods for nonlinear system characterization based on experimental data are essential for qualitative assessment of both theoretical and physical models.

In recent years, numerous techniques for structural dynamics detection and identification of nonlinear systems have been developed [1]. These methods are generally very case specific and only applicable to a sparse set of available engineering structures. For example, methods based on single-degree-of-freedom systems or systems with well separated modes [10]. Also, few examples where

nonlinear characterization methods have been tested on experimental data exist in the literature, giving little insight regarding the robustness and performance of many of the existing methods in real applications. Extracting relevant parameters from experimental data to create condensed models of a studied system is a key feature for high quality experimental testing. Since external factors that are hard to simulate and/or foresee can have a significant impact on the results, experimental tests are important to evaluate the performance of new and existing nonlinear characterization methods. At the same time, experimental testing on nonlinear systems is challenging. Many of the existing characterization methods assumes that the system is excited with a single harmonic force signal at constant amplitude, which is often hard to realize in actual physical testing. Additionally, force dropouts around the resonances can make it difficult to drive a structure into its nonlinear regimes hindering nonlinear characterization.

In many practical application it is reasonable to assume that the nonlinearities are local [10, 11, 12, 13, 14]. In that case, there is a potential to combine high accuracy with high computational and experimental efficiency.

1.2 Aim and Scope

The aim of this thesis is to develop and validate new efficient simulation and experimental methods for characterization of mechanical systems with localized nonlinearities. The purpose is to contribute to the development of analysis tools for such systems that are useful in early phases of the product innovation process for predicting product properties and functionality.

In the present work, *simulation* refers to reproducing the dynamic characteristics, given the system parameters and external excitation. *Experimental techniques* refers to methods that can assist in acquiring and evaluating experimental data, while *characterization* refers to the process of extracting relevant parameters based on input-output data. The studied systems are seen as predominantly linear but with local significant nonlinear effects, giving the total system a *weak nonlinear behavior*. *Weak nonlinear behavior* or *weak nonlinearity* lacks a distinct mathematical definition in the literature [15]. However, *weakly nonlinear* systems can be characterized by the fact that the system's response to harmonic excitation is approximately harmonic [1, 16, 17, 18].

1.3 Research Design

This thesis comprises six studies concerning development and validation of efficient methods for simulation, experimental testing and characterization of mechanical systems with localized nonlinearities. The research has been carried out in close collaboration with the following industrial partners: *AB Sandvik Coromant*, *Faurecia Exhaust System AB* and *Axiom Edutech*. Fundamental research has been combined with participatory action research in ongoing product development and research projects at these companies. The research methodology employed in this thesis builds on a *coordinated approach*, Figure 1, which has evolved through several preceding studies [5, 6, 7, 8, 9, 19].

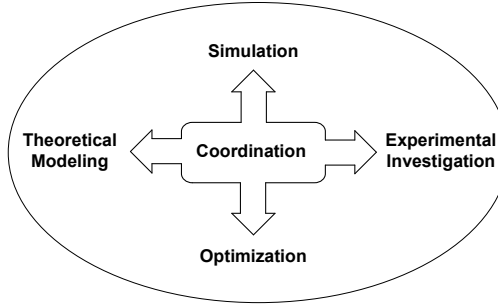


Figure 1: Coordinated approach. The aim is an efficient product development support by a systematic development and use of theoretical models, simulation procedures, experimental tests and optimization procedures.

The main principle of the coordinated approach is to systematically assess and improve product properties by a balanced use of theoretical and physical models to take full advantage of the cross-benefits between simulations and experiments already in the early product innovation phases [5, 8].

In this thesis, the coordinated approach is utilized by combining theoretical modeling with extensive simulations to develop and improve methods for experimental testing and characterization of nonlinear systems. Experimental tests are then conducted in order to further validate the methods and provide insight about the robustness of the methods regarding, e.g., sensitivity to external disturbances not accounted for in the simulations. The results from the experimental tests provide vital feedback which is used to improve the theoret-

ical models, experimental procedures and characterization methods.

1.4 Thesis outline

The basis of this thesis is constituted by six studies, reported in papers A to F. As a general background to the appended papers, this introductory part discuss the basic concepts and theories used throughout the thesis and provides an overview of related research within the field. The simulation, experimental investigation and characterization methods used are then described, followed by a summary of the appended papers and their specific contributions and a concluding discussion.

2 Linear versus Nonlinear Systems

Most engineering systems are nonlinear or become nonlinear if excited with a high enough force. A system is considered nonlinear if the output response data is not a linear function of the input excitation. Thus, for a system, H , to be considered linear it has to be both *additive* and *homogeneous*, thereby fulfilling the equality [20]:

$$H\{\alpha_1 f_1(t) + \alpha_2 f_2(t)\} = \alpha_1 H\{f_1(t)\} + \alpha_2 H\{f_2(t)\} \quad (1)$$

where α_1 and α_2 are constants and $H\{f(t)\}$ refers to the systems response due to $f(t)$. In practice this means that: (i) if the input force to the system is doubled, the response of the system also doubles and (ii) if two or more forces are applied to the structure simultaneously, the system's response will be equal to the sum of the responses obtained if the same forces were applied individually (i.e. the principle of superposition holds). A frequency domain representation of a linear, time invariant, mechanical system with P inputs and Q outputs, is illustrated in Figure 2 and described by Equation (2).

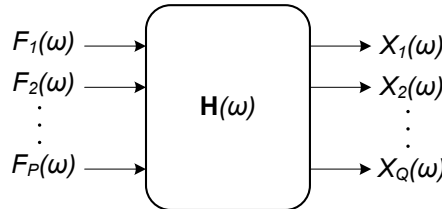


Figure 2: A general linear, time invariant, system with P inputs and Q outputs.

$$\begin{bmatrix} H_{11}(\omega) & \cdots & H_{1P}(\omega) \\ \vdots & \ddots & \vdots \\ H_{Q1}(\omega) & \cdots & H_{QP}(\omega) \end{bmatrix} \begin{Bmatrix} F_1(\omega) \\ \vdots \\ F_P(\omega) \end{Bmatrix} = \begin{Bmatrix} X_1(\omega) \\ \vdots \\ X_Q(\omega) \end{Bmatrix} \quad (2)$$

Here ω is the frequency variable. The frequency response function (FRF), $H(\omega)$, describes the linear relation between the applied force $F(\omega)$ and the system's response $X(\omega)$. For linear systems, $H(\omega)$ is independent of both the

amplitude and characteristics of the excitation signal.

For nonlinear systems, however, no strict definition of FRFs exist [1]. Due to the system's dependence on, e.g., acceleration, velocity or displacement the estimated FRF will appear as if it is dependent on the amplitude and characteristics of the input signal. Thus, different types of excitation signals, e.g., sinusoidal (narrow-band), transient and random noise (broad-band), will generally result in different estimations of the FRF due to the energy distribution of the force over frequency.

FRFs obtained by excitation at different force levels are useful for detecting the presence of a nonlinearity and can also provide information about the nonlinear functional form [1, 15]. However, the nonlinear effects on the FRF are non-unique, i.e. one class of nonlinearity can exhibit the same behavior as another for a certain input-output amplitude range. Thus, the shape or changes in the FRF is not conclusive evidence of a specific type of nonlinearity and/or functional form [10].

Two different classes of nonlinearities are studied in this thesis, zero-memory and hysteretic. A short description of these nonlinearities and how they differ from each other is given in the following two sections.

2.1 Zero-Memory Nonlinearities

Zero-memory nonlinearities refers to functions $g(\ddot{x}(t), \dot{x}(t), x(t))$ having output at any given time t that are nonlinear functions of $\ddot{x}(t), \dot{x}(t), x(t)$ at the same instant of time [21]. Systems which can be described by zero-memory nonlinearities are, e.g., bilinear systems (standard automotive shock absorbers/dampers), systems with clearance, clipped systems, hardening spring systems (systems subjected to large displacements exhibiting geometrical nonlinear effects) and softening spring systems [1, 15, 21]. As an example, the Duffing oscillator, Figure 3, is used in forced response simulations with both harmonic and random excitation at different force amplitudes. The FRFs obtained from these simulations are shown in Figure 4.

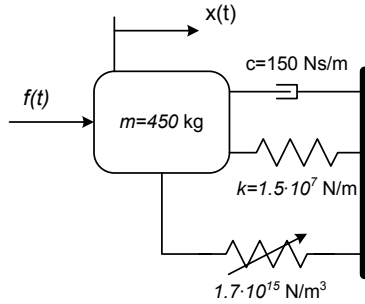


Figure 3: The Duffing oscillator, a SDOF system with a cubic (hardening) zero-memory nonlinearity. $m\ddot{x}(t) + cx(t) + kx(t) + 1.7 \cdot 10^{15} (x(t))^3 = f(t)$.

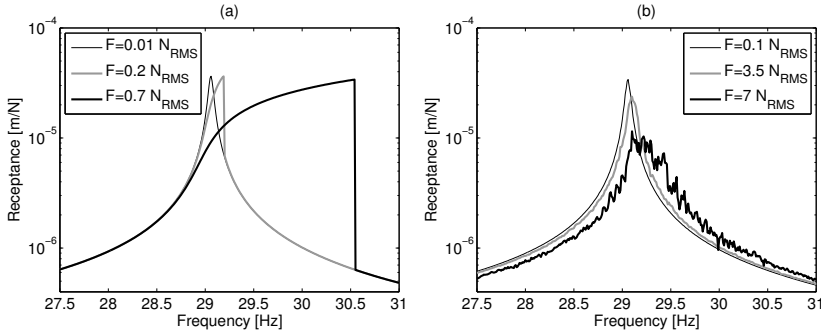


Figure 4: FRFs obtained at different excitation amplitudes: (a) Upward sinusoidal sweep. (b) Random excitation (The force is low-pass filtered using a Butterworth filter of order 3 and cutoff frequency 100 Hz).

As the excitation amplitude increases, the resonance frequency shift upwards since the effective stiffness in the system increases. The FRFs obtained from harmonic excitation and random excitation differs substantially, the distortion in the FRFs due to the nonlinearity is evident when the system is excited with a sinusoidal signal, while the FRFs obtained by random excitation appears linearized at each specific force level.

2.2 Hysteretic Nonlinearities

Hysteretic nonlinearities are very common in engineering structures and are encountered in, e.g., different types of vibration isolators [22, 23], in sandwich composite structures [24] and in mechanical joints [14, 25]. What differs the hysteretic nonlinearity from a zero-memory nonlinearity is its dependence on past values. The current restoring force from a hysteretic nonlinearity is not only dependent on the present displacement but also on past history displacements. An example of a system with nonlinear hysteresis is shown in Figure 5a, a single-degree-of-freedom (SDOF) system with a friction damper described by the stick-slip/Coulomb macro-slip model [26, 27].

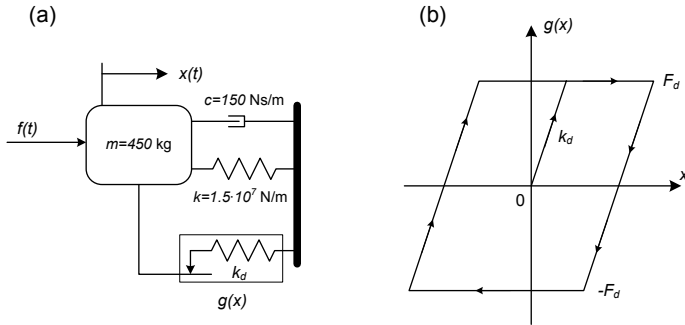


Figure 5: A SDOF system with a stick-slip nonlinearity, $k_d = 1 \cdot 10^7 \text{ N/m}$ and $F_d = 130 \text{ N}$.

The relation between the system response and feedback force from the stick-slip nonlinearity follows the curve shown in Figure 5b. Here $g(x)$ is the feedback force from the nonlinearity and F_d the force level at which the system starts to slip. While $|g(x)| < F_d$, the stick-slip model acts like a linear spring with stiffness k_d , and there is no damping produced. When the displacement reaches the level where, $g(x) = F_d$, the damper will be in its slip phase and the feedback force, $g(x)$, will remain at F_d until the motion changes direction. The damper will then act as a linear spring again until the condition $g(x) = -F_d$ is fulfilled. Thus, when the damper alternates between stick and slip conditions, the feedback force, $g(x)$, will have two possible solutions for every displacement, except for the points where the motion changes direction. Which of these two solutions that is valid depends on the displacement history of the damper. To

illustrate the effect that this nonlinearity has on the dynamics of the system in Figure 5, results from simulations using sinusoidal and random noise excitation at different force levels are shown in Figure 6.

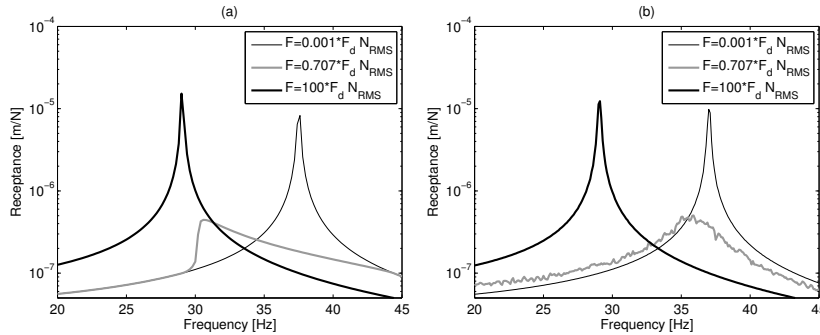


Figure 6: Effect on the FRF of a stick-slip nonlinearity obtained by excitation at different force levels. (a) upward sinusoidal sweep and (b) random noise excitation (The force is low-pass filtered using a Butterworth filter of order 3 and cutoff frequency 100 Hz).

As seen in Figure 6 the stick-slip nonlinearity shows a different dynamic behavior compared to the zero-memory nonlinearity in section 2.1. The stick-slip system exhibits two linear regions: One at low force levels, when the system never reaches the slip-level. The total stiffness is then $k + k_d$ N/m. And one at high force levels, large displacements, when the effect of the force feedback and damping caused by the stick-slip model are negligible compared to the excitation force and energy losses caused by the viscous damper in the underlying linear system. Therefore, as the level of the excitation force increases, the FRF of the stick-slip system approaches the FRF of the underlying linear system. In between these two regions there is a stick-slip region where the energy loss due to the hysteretic effect is very high. That the system behaves linearly at low force levels and approaches a linear behavior as the force level increases is confirmed by the FRFs obtained by harmonic and random excitation. At low and high force levels, the estimated FRFs of the system are similar, while the estimates differ noticeably when the system is in its stick-slip phase. The stick-slip system is a simple example of a hysteretic nonlinearity; more versatile hysteresis models are described in [28, 29, 30, 31, 32].

3 Time Domain Forced Response Simulation

Forced response simulation here refers to computing the motion (displacement, velocity or acceleration) of a system for a given force vector. The general approach is to use some method for time integration. Commonly used methods are, e.g., the Runge-Kutta method with variations [33] and Newmark's method [34]. In this chapter a method for forced response simulations based on digital filter theory is presented. This method is utilized throughout the thesis for forced response simulations with arbitrary sampled input signals. Consider a system with localized nonlinearities, described by:

$$\mathbf{M}\ddot{\mathbf{x}}(t) + \mathbf{C}\dot{\mathbf{x}}(t) + \mathbf{K}\mathbf{x}(t) + \mathbf{g}(\ddot{\mathbf{x}}(t), \dot{\mathbf{x}}(t), \mathbf{x}(t)) = \mathbf{f}(t) \quad (3)$$

where \mathbf{M} , \mathbf{C} and \mathbf{K} are the system's mass, damping and stiffness matrices, respectively. $\ddot{\mathbf{x}}(t)$, $\dot{\mathbf{x}}(t)$ and $\mathbf{x}(t)$ are the acceleration, velocity and displacement vectors, respectively. The vector $\mathbf{f}(t)$, describes the external forces acting on the system and the vector $\mathbf{g}(t)$, includes artificial external forces that represent the nonlinearities.

An arbitrary transfer function, $H_{pq}(s)$, of the linear (**MCK**) system in Equation (3) can be compactly represented by modal superposition of its residues, R_{pqr} , and poles, λ_r , [35]:

$$H_{pq}(s) = \sum_{r=1}^N \frac{R_{pqr}}{s - \lambda_r} + \frac{R_{pqr}^*}{s - \lambda_r^*} \quad (4)$$

where p refers to the response/output degree-of-freedom (DOF) and q refers to the DOF of excitation/input. r refers to the current mode and N denotes the total number of modes included and s is the Laplace variable. Equation (4) can be transformed into a discrete IIR-filter [36], and expressed as a difference equation where the current output, $x_p[n]$, is expressed as a weighted sum of previous inputs and outputs as:

$$x_p[n] = \sum_{r=1}^N \left(\sum_{i=0}^{N_B} B_{pqr}^i f_q[n-i] - \sum_{i=1}^{N_A} A_{pqr}^i x_{pr}[n-i] \right) \quad (5)$$

where N_B and N_A are the number of zeros and poles, respectively, in the filter. As seen in Equation (5), one set of filter coefficients, B and A , is needed for each mode included. The total response is calculated by modal superposition

as the sum of the responses from each individual mode.

The method can be extended to forced response simulations of nonlinear systems by modeling the nonlinearities as additional inputs (artificial forces). As an example, the difference equation for the system's response in DOF p due to force input in DOF $q = p$ and a displacement dependent nonlinearity connected between DOF p and ground becomes:

$$x_p[n] = \sum_{r=1}^N \left(\sum_{i=0}^{N_B} B_{pqr}^i (f_q[n-i] - g_p[n-i]) - \sum_{i=1}^{N_A} A_{pqr}^i x_p[n-i] \right) \quad (6)$$

Moving all unknown variables to the left side, putting the known variables equal to $C_n[n]$ and putting the sum of the known filter coefficients multiplied with $g_p[n]$ equal to a constant E_n yields:

$$x_p[n] + g_p[n]E_n = C_n[n] \quad (7)$$

$C_n[n]$ is dependent on the force and displacement history of the system and is therefore updated in each time step, hence the dependence on n , while E_n is a summation of the filter coefficients multiplied with $g_p[n]$ and is therefore independent of the system's history. Since the nonlinear restoring force, $g_p[n]$, is a function of the current displacement, $x_p[n]$, Equation (7) needs to be solved iteratively at each time step. Once the nonlinear restoring force is known, the system can be treated as a linear multiple-input/multiple-output system and the response in other DOFs solved for by utilizing linear filter operations, according to Equation (5). Since only the DOFs directly connected to the excitation force and nonlinearities needs to be considered in the nonlinear iteration process and the remaining responses can be calculated using linear filtering techniques, these forced response simulation routines can be made very fast. A graphical illustration of the simulation routine is shown in Figure 7.

The residues and poles constitutes the basis in the simulation routines, these can be obtained analytically, from finite element models (FEM), from lumped mass-damping-stiffness models (MCK) and from experimental modal analysis (EMA), which makes the simulation routines very versatile and useful in a wide application area. More details on how to calculate the filter coefficients and the errors involved in the simulations are given in Paper E and [37, 38].

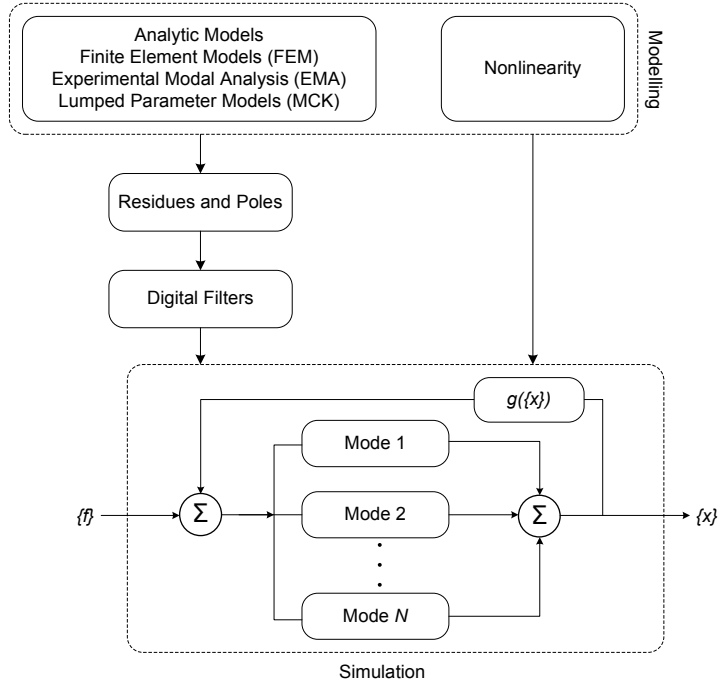


Figure 7: Illustration of the forced response simulation method. The underlying linear system is described by its residues and poles and the nonlinearities are modeled as additional external forces.

4 Experimental Testing

Due to the nature of the nonlinearities studied in this thesis, a single approach to characterize the theoretical and experimental systems investigated has not been possible to use. Therefore different characterization methods have been utilized, improved and developed. These methods are often based on an assumption regarding the characteristics of the excitation signal used, e.g., broad-banded or harmonic excitation. In the experimental investigations, the forces are applied on the structures using an electro-dynamic shaker. Due to the characteristics of the shaker and the shaker-structure interaction, realization of the needed excitation forces can be complicated. The types of excitation signals utilized in this research work, and how these signals can be applied on nonlinear systems are described in the following two sections.

4.1 Random Excitation

Random excitation is usually accomplished using an electrodynamic or hydraulic shaker. Due to the randomness of the amplitude and phase of the excitation signal, random excitation creates a "linearized" FRF; this linearization can make it difficult to detect if a system behaves nonlinearly [15, 16]. Also, random excitation is broad-banded, meaning that the energy associated with every single frequency is small, which can make it difficult to get enough energy into a system to excite structural nonlinearities. This issue is further enhanced by the fact that the shaker-structure interaction may lead to force dropouts around the resonances, where the nonlinear effects commonly are most evident, making it even harder to excite the nonlinearities [19]. Often, additional energy need to be added into the excitation signal around the resonance frequencies of the system under test, thereby facilitating excitation of the structural nonlinearities. Thus, detailed inspections of both the FRFs and the force spectrum is often necessary to determine if the nonlinearities are excited as intended. Two different test-structures are characterized based on random excitation in Papers C and D.

4.2 Harmonic Excitation

When using harmonic excitation, usually only one frequency is excited at a time. As a result all the energy in the force signal is associated with a single frequency, making harmonic input suitable for excitation of structural nonlin-

earities. Also, using harmonic input, it is possible to measure the steady-state response of the structure under test, facilitating analysis of specific details of the systems characteristics, such as the presence of additional harmonics related to nonlinear effects or steady-state hysteresis loops.

Harmonic excitation can be accomplished by, e.g., stepped-sine or sine-sweep. Using stepped-sine the system is excited with one frequency at a time and the measurement is taken when the system has reached its steady-state response. Sine-sweep is done by slowly and continuously varying the frequency of the excitation signal over a specified interval. The benefit with sine-sweep is its speed compared to stepped-sine excitation. However, stepped-sine allows for better possibilities to control the excitation signal since measurements are performed under steady-state conditions. This facilitates precise tuning by iterative off-line adjustment of the excitation signal. This is an important factor when measurements are performed on nonlinear systems.

Several methods developed in relation to harmonic excitation of nonlinear systems assume that the system is excited with a pure sinusoidal signal [26, 29, 39] which is simple to realize in simulations. In real applications, however, the actual force applied to the structure is the reaction force between the shaker and the structure under test [29, 40, 41]; see Figure 8.

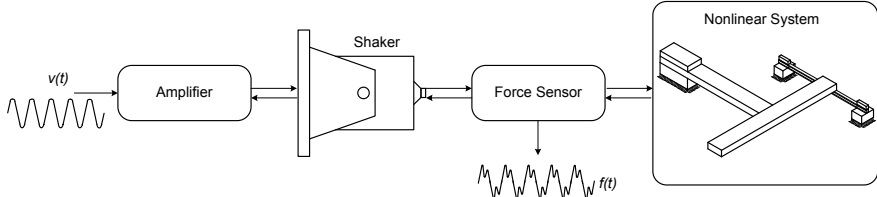


Figure 8: Reaction forces in the measurement chain; a pure sinusoidal voltage signal is the input to the amplifier, but due to the shaker-structure interaction, the excitation force becomes distorted.

The response from nonlinear systems generally contains additional frequency components. These are transferred to the excitation signal and result in a distorted input force. This effect is usually most evident around the resonances

where the system exhibits large deflections. The problem is further enhanced due to the fact that electro-dynamic shakers behave nonlinearly at large displacements [15]. Thus, excitation of a nonlinear system with a specified frequency at a desired amplitude requires precise tuning of the signal controlling the shaker movements. A control algorithm for pure sinusoidal excitation is developed in Paper A. The algorithm uses an off-line nonlinear iteration approach to find a suitable, multi harmonic, voltage signal as input to the shaker in order to obtain a pure sinusoidal force signal with a specified amplitude. Results from an experimental test [42] using this control algorithm is shown in Figure 9.

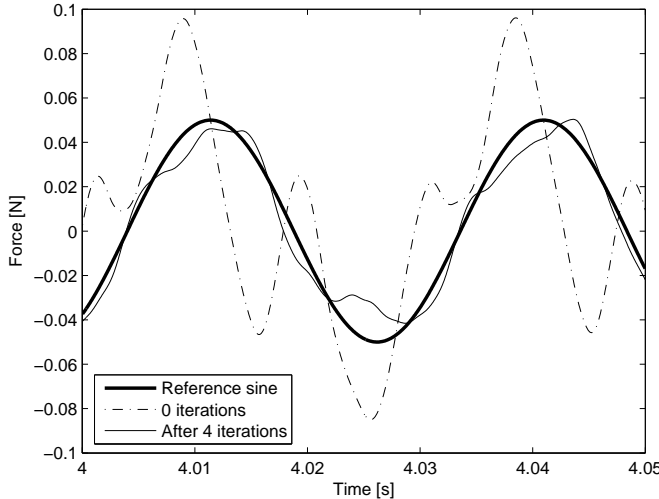


Figure 9: Result from an experimental test of the force control algorithm proposed in Paper A.

It is clear that the excitation force contains higher harmonics affecting the quality of the signal when only a sinusoidal signal is sent to the shaker (0 iterations). After a few iterations an input signal which noticeably reduces the distortion in the measured force is obtained.

5 Characterization of Nonlinear Systems

The overarching goal of parameter estimation is to find a mathematical model that describes the behavior of the observed system. For linear systems, modal analysis is commonly used to extract the modal parameters describing the studied system [2, 3, 43]. However, most methods developed for linear systems break down if applied to nonlinear systems. Thus, for nonlinear systems, alternative methods have to be utilized to estimate the studied system's parameters. For a summary of the most common characterization methods for nonlinear systems, the reader is referred to the following review articles [1, 10]. The characterization methods adopted in this research work are here divided into different groups dependent on the characteristics of the excitation force and whether the parameter estimation is performed in the frequency or in the time domain.

5.1 Frequency Domain

An important method for nonlinear parameter estimation, widely studied in recent years, is the *Reverse Path* method. This method is based on broadband excitation and was initially developed by Bendat et al. [44, 45] and Rice et al. [46, 47] and is thoroughly described in [21]. *Reverse Path* treats the nonlinearities as force feedback terms acting on an underlying linear system. The parameter estimation is performed in the frequency domain using conventional *Multiple-Input-Single-Output* (MISO) or *Multiple-Input-Multiple-Output* (MIMO) techniques and estimates of both the underlying linear properties and the nonlinear coefficients are obtained from a single analysis. The method is known as *Reverse Path* since the input and output quantities are reversed; see Figure 10a. *Reverse Path* has proven to work well in experimental tests and has been applied to various mechanical systems with zero-memory nonlinearities, which indicates that the method is robust and well suited for use in engineering applications [11, 12, 13, 48, 49].

In parallel with the development of *Reverse Path*, Adams et al. [50, 51] introduced an alternative variant known as *Nonlinear Identification through Feedback of Outputs* (NIFO), which removed the original reversal of the input and outputs; see Figure 10b.

The basic principle of the two methods described above can be explained by,

e.g., considering Duffing's equation:

$$m\ddot{x}(t) + c\dot{x}(t) + kx(t) + p(x(t))^3 = f(t) \quad (8)$$

which, in the frequency domain, can be expressed as:

$$B(\omega)X(\omega) + \mathcal{F}(p(x(t))^3) = F(\omega) \quad (9)$$

where $B(\omega)$ is the impedance of the underlying linear system and $\mathcal{F}(\cdot)$ denote the Fourier transform. If the nonlinearity is treated as an additional force acting on the underlying linear system, this problem can be solved according to either *Reverse Path* or NIFO by conventional MISO techniques.

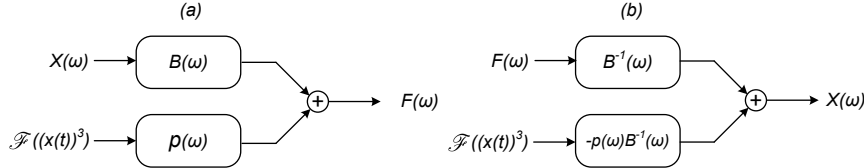


Figure 10: A SISO case transformed into a MISO case enabling nonlinear system identification with (a) *Reverse Path* and (b) NIFO.

As seen in Figure 10, using *Reverse Path*, Equation (9) is formulated as a MISO system with displacement and nonlinear feedback as inputs and force as output. Using NIFO, the inputs to the MISO model are force and nonlinear feedback, the output is displacement. An advantage with *Reverse Path* and NIFO is that estimates of both the underlying linear system and the nonlinear coefficient are obtained in one single analysis, which makes these methods fast and attractive to use. However, these characterization methods have not yet been successfully applied to systems with hysteresis.

5.2 Time/Frequency Domain

Frequently used methods for simulation of steady-state responses of nonlinear systems under harmonic excitation are *Harmonic-Balance* (HB) and *Multi-Harmonic-Balance* (MHB) [52, 53]. HB and MHB builds on the assumption of weak nonlinearity, i.e. if the studied system is excited with a harmonic input, the system's response will be harmonic. Thus, there exist a periodic solution

and the excitation force, the response and the nonlinear feedback forces can be expressed by Fourier series. A benefit with these methods is that the system's steady-state response is obtained directly. With time integration methods, which usually suffers from transient responses in the beginning, the integration needs to go on for a while to find the steady-state response, making time integration more computationally expensive.

Duffing's equation (Equation (8)) can, if excited by a sinusoidal signal, be expressed by a truncated one-term (HB) Fourier expansion:

$$(-m\omega_0^2 + j\omega_0 c + k)X(\omega_0)e^{j\omega_0 t} = (F(\omega_0) - G(\omega_0))e^{j\omega_0 t} \quad (10)$$

where:

$$G(\omega) = \mathcal{F}(p(x(t))^3) \quad (11)$$

Thus, $X(\omega_0)$, $F(\omega_0)$ and $G(\omega_0)$ are the complex Fourier coefficients of the systems displacement, excitation force and nonlinear feedback force, respectively, at the fundamental forcing frequency, ω_0 . Removing the time dependence, Equation (10) becomes:

$$B(\omega_0)X(\omega_0) - F(\omega_0) + G(\omega_0) = 0 \quad (12)$$

where $B(\omega)$ is the impedance of the underlying linear system. For a given excitation F at a specified frequency ω_0 , the system's response, $X(\omega_0)$, is estimated by balancing the Fourier coefficients in Equation (12) by each other. This "harmonic balance" procedure needs to be repeated for each frequency of interest, and the solutions represent the frequency response of the system. To extend HB to MHB, additional harmonics need to be considered [15, 29], which means that additional equations are added and instead a nonlinear system of equations need to be solved at every frequency step. MHB generally provides a more accurate estimate of the systems frequency response on the expense of a higher computational cost. By solving the system's frequency response over a specified interval, it is possible to calculate an FRF. The FRF obtained by HB and MHB are often regarded as the analytical analogue to the FRF obtained by stepped sine testing [15].

These methods have been used in applications for both simulation and system characterization with zero-memory and hysteretic nonlinearities [26, 29, 54, 23,

55, 52]. System characterization can be performed both in the time domain by comparing simulated and experimentally acquired steady-state responses and in the frequency domain by comparing FRFs obtained from stepped-sine measurements with FRFs calculated using HB or MHB. A procedure for system characterization in the frequency domain, utilizing MHB, is proposed in Paper B.

When setting up the HB and MHB equations it is usually assumed that the system is excited with a pure harmonic excitation, i.e. one single frequency. As explained previously, a single harmonic excitation can be difficult to realize in experimental measurements, due to the shaker characteristics and shaker-structure interaction, which can make comparisons between simulated and experimental data difficult. There exist methods which extends MHB to systems with multiple excitation frequencies [56, 57]. However, the complexity of the problem formulation and the total number of harmonics needed increases substantially [57], resulting in a less robust and less computationally efficient method.

An alternative approach, as suggested in Paper E, when a pure sinusoidal excitation cannot be realized or when non-periodic excitation forces are used (i.e. random or transient excitation [58, 59]), is to perform the characterization in the time domain using the measured force as excitation signal and compare simulated and experimentally acquired responses.

6 Summary of Papers

Paper A

This paper presents an algorithm for reducing harmonic distortion in the force signal during experimental tests on nonlinear systems with sinusoidal excitation. The distortions are attenuated by sending a multi-harmonic voltage signal with optimized amplitudes and phases to the shaker. Since the relation between the input voltage signal and the measured force is nonlinear, an iterative approach is required to find the correct set of harmonic components of the input voltage signal. The control algorithm uses the Newton-Raphson and Broyden's method as nonlinear solvers. Simulations show that the control algorithm is capable of obtaining a non-distorted force signal even in the presence of a significant nonlinearity.

Paper B

Two parameter estimation methods are studied; one based on random noise input and another based on sinusoidal excitation. The method based on random excitation treats the nonlinearities as force feedback terms acting on an underlying linear system. The parameter estimation is performed in the frequency domain by using conventional MIMO/MISO techniques known from linear theory. The studied method is applied in simulations on single-degree and multi-degree-of-freedom-systems and shows great potential. Building on Paper A, where a control algorithm for harmonic excitation was developed, a method for characterization of nonlinear systems based on sinusoidal input is also investigated. The method uses a combination of *multi-harmonic-balance* (MHB) and stepped-sine excitation. The parameter estimation is performed in the frequency domain by matching the measured and simulated frequency response functions with each other. The benefit of the MHB/stepped-sine method is its versatility. It can handle both zero-memory nonlinearities and nonlinearities with memory, such as systems with hysteresis.

Paper C

Building on the previous investigation concerning random excitation from Paper B, this paper presents a more detailed analysis together with experimental results. The method requires initial knowledge about the nonlinearity, i.e. the

physical location and the nonlinear functional form. A strategy is proposed to identify the nonlinear nodes and the type of nonlinearity that is present in the system. A validation with a simulation model indicate that this approach can be useful. Finally, an experimental system with a geometric (hardening-spring) nonlinearity is studied. The analysis of the experimental data indicates that the estimate of the underlying linear system around the resonance is very sensitive to how the parameter estimation model is formulated. In general, the experimental result shows that the analysis is significantly improved when using the nonlinear identification method compared to traditional linear techniques.

Paper D

Building on the results from Papers B and C, a generalized approach to apply the method of *Reverse Path* on continuous mechanical systems with several nonlinearities is developed. This approach uses unconditioned inputs and assumes that the locations of the nonlinearities are known beforehand and that response measurements can be obtained in the nonlinear nodes. Excitation is only needed in one location, which can be located away from the nonlinearities. The method provides the means to estimate both the underlying linear system and the nonlinear parameters of complex structures in a straightforward way. The method was applied in both simulations and experimental tests. The results from the experimental tests was compared to a static measurement of the nonlinear force and showed a very good agreement.

Paper E

For experimental testing, pure sinusoidal excitation can be both difficult and time consuming to realize. Therefore, complementing the results from Papers A and B, a method for characterizing systems with hysteresis based on discrete time records is presented. A new forced response routine for a general mechanical structure with a localized hysteretic mass damper is developed. The hysteresis effect of the damper is described by the Bouc-Wen equation and the intended industrial application is simulation of passive vibration attenuation in metal machining. This simulation method is then used as a basis in a two stage parameter estimation routine performed in the time domain. The nonlinear parameter estimation is performed by a real coded genetic algorithm, and applied in both simulations and experimental tests on a dry-friction damper.

Paper F

Simulating the dynamic behavior of different cutting tools used in metal machining requires knowledge about the forces acting on the tool. Therefore, accurate estimates of cutting forces are important. However, dynamic influences from the measurement system affect the result which can make the obtained cutting force data erroneous and misleading. This paper develops a method for off-line inverse filtering of the measured data which removes unwanted dynamic effects originating from the measurement system and improves the estimation of the cutting forces. The method is successfully tested in both simulations and in experimental test using different cutting conditions.

7 Concluding Discussion

This thesis focuses on the development and validation of methods for simulation, experimental testing and characterization of nonlinear mechanical systems. This research has evolved in collaboration with industrial partners through participatory action research in ongoing product development and research projects. The systems studied are considered to be predominantly linear but with local significant nonlinearities, giving the total system a weak nonlinear behavior. A fundamental strategy employed is to use already established and validated methods from linear analysis as a basis for the development of new and improved simulation and characterization methods for nonlinear mechanical systems.

The large amount of data needed for accurate assessment of developed nonlinear characterization methods puts a high demand on the simulation routines utilized. Using random noise, the combination of a requirement for high spectral resolution and a requirement for several averages to accurately estimate the statistical properties of the system's response, results in a need for long data sequences. The amount of data required further increases considering that *(i)* performing simulations based on sampled data requires a fine time resolution to keep the errors small and *(ii)* the response from nonlinear systems often contains higher harmonics which further increases the demand on a fine time resolution to accurately capture the systems dynamics. Additionally, characterization methods based on nonlinear optimization schemes often requires a large number of repeated simulations in order to converge toward a specified criterion. A result of this thesis is computationally efficient forced response simulation routines, facilitating extensive investigation of systems with zero-memory or hysteretic nonlinearities.

Two methods for nonlinear parameter estimation utilizing random input, *Reverse Path* and *Nonlinear Identification through Feedback of Outputs* (NIFO) are investigated both in simulations and experimental applications on mechanical systems with zero-memory nonlinearities. The methods provide an attractive solution methodology due to the formulation where additional inputs are created based on measured responses and that estimates of both the underlying linear system and nonlinear coefficients are obtained, by least square fits based on averaged spectral data. The modal parameters can then be extracted from the estimates of the underlying linear system and used in conjunction

with the nonlinear coefficients to build a theoretical model of the studied system. A specific result from this thesis is a generalization of the *Reverse Path* method which allows for characterization of systems with an arbitrary number of localized zero-memory nonlinearities in a structured way. The experimental tests indicate that the methods are robust, efficient and well suited for use with measurement data. The tests also show a discrepancy between *Reverse Path* and NIFO, indicating that the presence of contaminating noise has a significant effect on the result, which pose an interesting question for future research.

A significant part of this thesis treats simulation and characterization of systems with hysteresis effects. The characterization methods proposed are: (i) a frequency domain approach which requires a pure harmonic excitation force and (ii) a time domain approach which does not put any constraints on the characteristics of the excitation signal. Interesting for future work is to continue to develop and improve the suggested methods regarding characterization and modeling of hysteretically-damped tools for metal cutting. Examples of interesting topics within this field are characterization of different types of damping materials and simulation of the damper effect on machining productivity. Another important question for future research is how to apply *Reverse Path* and NIFO on systems with hysteresis effects.

An essential part of the research work has been experimental validation of the developed methods for characterization of nonlinear systems. This, in turn, has led to a need for methods which can facilitate experimental testing. Experimental validation of the nonlinear characterization methods was successfully completed on continuous mechanical systems with localized nonlinearities, confirming the robustness of the proposed methods concerning use with experimental data. The results from these tests provide a basis for further experimental validation on more complex mechanical systems than studied in this thesis.

The general contribution to science and technology of this thesis is the development and improvement of analysis tools for simulation, experimental testing and characterization of nonlinear mechanical systems with localized nonlinearities.

On a more specific level this thesis:

- Presents a method for improved harmonic excitation of nonlinear systems using numerically optimized input signals.
- Provides a simplified analysis procedure for continuous mechanical systems with an arbitrary number of localized zero-memory nonlinearities by a generalization of the *Reverse Path* method using partially correlated inputs.
- Presents a method to remove unwanted dynamic effects in cutting force measurements using inverse filtering. The method increases the usable frequency range of the dynamometer and significantly improves the measurement results compared to traditional techniques.
- Contributes to the experimental validation of the nonlinear characterization methods: *Reverse Path* and *Nonlinear Identification Through Feedback of Outputs*.
- Presents an efficient time domain simulation and characterization method for use with hysteretically-damped systems described by the Bouc-Wen hysteresis model.

References

- [1] Gaetan Kerschen, Keith Worden, Alexander F. Vakakis, and Jean-Claude Golinval. Past, present and future of nonlinear system identification in structural dynamics. *Mechanical Systems and Signal Processing*, 20(3):505 – 592, 2006.
- [2] David John Ewins. *Modal testing : theory, practice and application*. Research Studies Press, Baldock, 2. ed. edition, 2000.
- [3] Randall J. Allemand. *Analytical and experimental modal analysis*. Structural Dynamics Research Laboratory, University of Cincinnati, Cincinnati, Ohio 45221-0072, 1994. UC-SDRL-CN-20-263-662.
- [4] H. R. E. Siller. *Non-linear modal analysis methods for engineering structures*. PhD Thesis, Imperial College, London, 2004.
- [5] A. Jönsson. *Lean Prototyping of multi-body and mechatronic systems*. PhD Thesis, Blekinge Institute of Technology, 2004.
- [6] J. Wall. *Dynamic study of an automobile exhaust system*. Licentiate Thesis, Blekinge Institute of Technology, 2003.
- [7] T. Englund. *Dynamic characteristics of automobile exhaust system components*. Licentiate Thesis, Blekinge Institute of Technology, 2003.
- [8] J. Wall. *Simulation-driven design of complex mechanical and mechatronic systems*. PhD Thesis, Blekinge Institute of Technology, 2007.
- [9] J. Fredin. *Modelling, simulation and optimisation of a machine tool*. Licentiate Thesis, Blekinge Institute of Technology, 2009.
- [10] Douglas E. Adams and Randall J. Allemand. Survey of nonlinear detection and identification techniques for experimental vibrations. In *Proceedings of the 23rd International Conference on Noise and Vibration Engineering, ISMA*, pages 517 – 529, Leuven, Belgium, 1998.
- [11] L. Garibaldi. Application of the conditioned reverse path method. *Mechanical Systems and Signal Processing*, 17(1):227 – 235, 2003. Conditioned reverse path (CRP) method;

- [12] S. Marchesiello. Application of the conditioned reverse path method. *Mechanical Systems and Signal Processing*, 17(1):183 – 188, 2003. Dampers;.
- [13] G. Kerschen, V. Lenaerts, and J.-C. Golinval. Identification of a continuous structure with a geometrical non-linearity. part i: Conditioned reverse path method. *Journal of Sound and Vibration*, 262(4):889 – 906, 2003.
- [14] K.Y. Sanliturk, D.J. Ewins, and A.B. Stanbridge. Underplatform dampers for turbine blades: Theoretical modeling, analysis, and comparison with experimental data. *Journal of Engineering for Gas Turbines and Power*, 123(4):919 – 929, 2001.
- [15] K. Worden and G. R. Tomlinson. *Nonlinearity in Structural Dynamics: Detection, Identification and Modelling*. IOP Publishing Ltd, Bristol, UK, 2001.
- [16] A.F. Vakakis and D.J. Ewins. Effects of weak non-linearities on modal analysis. *Mechanical Systems and Signal Processing*, 8(2):175 – 98, 1994/03/.
- [17] Influence and characterisation of weak non-linearities in swept-sine modal testing. *Aerospace Science and Technology*, 8(2):111 – 120, 2004.
- [18] Ulrich Fuellekrug and Dennis Goege. Identification of weak non-linearities within complex aerospace structures. *Aerospace Science and Technology*, 2011.
- [19] A. Josefsson. *Identification and Simulation Methods for Nonlinear Mechanical Systems Subjected to Stochastic Excitation*. PhD Thesis, Blekinge Institute of Technology, 2011.
- [20] Julius S. Bendat and Allan G. Piersol. *Engineering applications of correlation and spectral analysis*. Wiley, New York, 2. ed. edition, 1993.
- [21] Julius S. Bendat. *Nonlinear system analysis and identification from random data*. Wiley, New York, 1990.
- [22] A. Al Majid and R. Dufour. Harmonic response of a structure mounted on an isolator modelled with a hysteretic operator: Experiments and prediction. *Journal of Sound and Vibration*, 277(1-2):391 – 403, 2004.

- [23] Y.Q. Ni, J.M. Ko, and C.W. Wong. Identification of non-linear hysteretic isolators from periodic vibration tests. *Journal of Sound and Vibration*, 217(4):737 – 756, 1998.
- [24] K. H. Hornig. Parameters characterization of the bouc/wen mechanical hysteresis model for sandwich composite materials by using real coded genetic algorithms. Technical report, Mechanical Engineering Department, Ross Hall, Auburn, Alabama, 2000.
- [25] D Smallwood, D Gregory, and R Coleman. Damping investigations of a simplified frictional shear joint. In *Proceedings of Shock and Vibration Symposium*, 2000.
- [26] Giovanna Girini and Stefano Zucca. Multi-harmonic analysis of a sdof friction damped system. In *Proceedings of 3rd Youth Symposium on Experimental Solid Mechanics*, Poreta Terme, Italy, 2004.
- [27] Francisco J. Marquina, Armando Coro, Alberto Gutierrez, Roberto Alonso, David J. Ewins, and Giovanna Girini. Friction damping modeling in high stress contact areas using microslip friction model. volume 5, pages 309 – 318, Berlin, Germany, 2008.
- [28] Jack W. Macki, Paolo Nistri, and Pietro Zecca. Mathematical models for hysteresis. *SIAM Review*, 35(1):94 – 123, 1993.
- [29] Janito V. Ferreira. *Dynamic Response Analysis of structures with non-linear components*. PhD Thesis, Imperial College, London, 1998.
- [30] Mohammed Ismail, Faycal Ikhouane, and Jose Rodellar. The hysteresis bouc-wen model, a survey. *Archives of Computational Methods in Engineering*, 16(2):161 – 188, 2009.
- [31] Yousef Iskandarani and Hamid Reza Karimi. Hysteresis modeling for the rotational magnetorheological damper. In *Proceedings of the 4th WSEAS international conference on Energy and development - environment - biomedicine*, GEMESED'11, pages 479–485. World Scientific and Engineering Academy and Society (WSEAS), 2011.
- [32] Fayçal Ikhouane and José Rodellar. *Systems with Hysteresis: Analysis, Identification and Control Using the Bouc-Wen Model*. John Wiley & Sons, 2007.

- [33] Erwin Kreyszig. *Advanced Engineering Mathematics*. Wiley, New York, 8th edition edition, 1999.
- [34] Nathan M. Newmark. Method of computation for structural dynamics. *AGARD Conference Proceedings*, 2:1235 – 1264, 1972.
- [35] Anders Brandt. *Noise and vibration analysis : signal analysis and experimental procedures*. Wiley, Chichester, 2011.
- [36] K. Ahlin, M. Magnevall, and A. Josefsson. Simulation of forced response in linear and nonlinear mechanical systems using digital filters. In *Proceedings of ISMA 2006*, 2006.
- [37] K Ahlin. On the use of digital filters for mechanical system simulation. In *Proceedings of 74th Shock and Vibration Symposium*, 2003.
- [38] K. Ahlin. Time history forced response in mechanical systems. *SVIB AU Symposium Riksgränsen*, 2005.
- [39] Hugo Ramon Elizalde Siller. *Non-linear modal analysis methods for engineering structures*. PhD Thesis, Imperial College, London, 2004.
- [40] S Rossmann. Development of force controlled modal testing on rotor supported by magnetic bearings. Master's thesis, Imperial College, London, 1999.
- [41] I. Bucher. Exact adjustment of dynamic forces in presence of non-linear feedback and singularity - theory and algorithm. *Journal of Sound and Vibration*, 218(1):1 – 27, 1998.
- [42] M. Magnevall, A. Josefsson, and K. Ahlin. Experimental verification of a control algorithm for nonlinear systems. In *Proceedings of IMAC XXIV*, 2006.
- [43] Nuno Manuel Mendes Maia and Júlio Martins Montalvão e Silva. *Theoretical and experimental modal analysis*. Research Studies Press, Taunton, 1997.
- [44] J. S. Bendat and A. G. Piersol. Spectral analysis of non-linear systems involving square-law operations. *Journal of Sound and Vibration*, 81(2):199 – 214, 1982.

- [45] J.S. Bendat and A.G. Piersol. Decomposition of wave forces into linear and non-linear components. *Journal of Sound and Vibration*, 106(3):391 – 408, 1986.
- [46] H.J. Rice and J.A. Fitzpatrick. A generalised technique for spectral analysis of non-linear systems. *Mechanical Systems and Signal Processing*, 2(2):195 – 207, 1988.
- [47] H.J. Rice and J.A. Fitzpatrick. A procedure for the identification of linear and non-linear multi-degree-of-freedom systems. *Journal of Sound and Vibration*, 149(3):397 – 411, 1991.
- [48] A. Josefsson, M. Magnevall, and K. Ahlin. On nonlinear parameter estimation with random noise signals. In *Proceedings of IMAC XXV*, 2007.
- [49] M. Magnevall, A. Josefsson, and K. Ahlin. On parameter estimation and simulation of zero memory nonlinear systems. In *Proceedings of IMAC XXVI*, 2008.
- [50] D.E. Adams and R.J. Allemand. Frequency domain method for estimating the parameters of a non-linear structural dynamic model through feedback. *Mechanical Systems & Signal Processing*, 14(4):637 – 656, 2000.
- [51] Muhammad Haroon and Douglas E. Adams. A modified h2 algorithm for improved frequency response function and nonlinear parameter estimation. *Journal of Sound and Vibration*, 320(4-5):822 – 837, 2009.
- [52] C. Pierre, A.A. Ferri, and E.H. Dowell. Multi-harmonic analysis of dry friction damped systems using an incremental harmonic balance method. pages ASME, New York, NY, USA –, Miami Beach, FL, USA, 1985.
- [53] A. Cardona, T. Coune, A. Lerusse, and M. Geradin. A multiharmonic method for non-linear vibration analysis. *International Journal for Numerical Methods in Engineering*, 37(9):1593 – 608, 1994/05/15.
- [54] S. L. Lau, Y. K. Cheung, and S. Y. Wu. Incremental harmonic balance method with multiple time scales for aperiodic vibration of nonlinear systems. *Journal of Applied Mechanics, Transactions ASME*, 50(4a):871 – 876, 1983.

- [55] K.Y. Sanliturk and D.J. Ewins. Modelling two-dimensional friction contact and its application using harmonic balance method. *Journal of Sound and Vibration*, 193(2):511 – 523, 1996.
- [56] A. Raghothama and S. Narayanan. Periodic response and chaos in nonlinear systems with parametric excitation and time delay. *Nonlinear Dynamics*, 27(4):341 – 65, 2002/03/.
- [57] J.F. Dunne and P. Hayward. A split-frequency harmonic balance method for nonlinear oscillators with multi-harmonic forcing. *Journal of Sound and Vibration*, 295(3-5):939 – 963, 2006.
- [58] A. Kyprianou, K. Worden, and M. Panet. Identification of hysteretic systems using the differential evolution algorithm. *Journal of Sound and Vibration*, 248(2):289 – 314, 2001.
- [59] Yin Qiang, Zhou Li, and Wang Xinming. Parameter identification of hysteretic model of rubber-bearing based on sequential nonlinear least-square estimation. *Earthquake Engineering and Engineering Vibration*, 9(3):375 – 83, Sept. 2010.

Paper A

Control Algorithm For Sine Excitation On Nonlinear Systems

Paper A is published as:

Josefsson, A., Magnevall, M. and Ahlin, K. Control Algorithm for Sine Excitation on Nonlinear Systems, In *Proceedings of IMAC-XXIV, Conference & Exposition on Structural Dynamics*, St. Louis, USA, 2006.

Control Algorithm For Sine Excitation On Nonlinear Systems

Andreas Josefsson
Martin Magnevall
Kjell Ahlin

Blekinge Institute of Technology, SE-371 79 Karlskrona, Sweden

Abstract

When using electrodynamic vibration excitors to excite structures, the actual force applied to the structure under test is the reaction force between the exciter and the structure. The magnitude and phase of the reaction force is dependent upon the characteristics of the structure and exciter. Therefore the quality of the reaction force i.e. the force applied on the structure depends on the relationship between the exciter and structure under test.

Looking at the signal from the force transducer when exciting a structure with a sine wave, the signal will appear harmonically distorted within the regions of the resonance frequencies. This phenomenon is easily observed when performing tests on lightly damped structures. The harmonic distortion is a result of nonlinearities produced by the shaker when undergoing large amplitude vibrations, at resonances.

When dealing with non-linear structures, it is of great importance to be able to keep a constant force level as well as a non-distorted sine wave in order to get reliable results within the regions of the resonance frequencies. This paper presents theoretical methods that can be used to create a non-distorted sinusoidal excitation signal with constant force level.

Nomenclature

A	Estimate of Jacobian
f	Frequency, [Hz]
F_M	Measured Force Vector with sine and cosine components for each harmonic
F_V	Difference between measured and desired Force vector
J	Jacobian included in partial derivatives
k	Number of harmonics to be controlled
n	Iteration counter
r_n	Sine and cosine components in response (force) signal
t	Time, [sec]
v_n	Sine and cosine components in input (volt) signal
V_n	Input voltage vector with sine and cosine components for each harmonic

1 Introduction

When performing measurements on nonlinear structures a stepped-sine excitation is a favorable method. Unlike random noise signals, a sine-excitation can be controlled to desired force amplitude as well as providing a better physical understanding of the actual problem.

Most of the theory developed for nonlinear systems [1] relies on the fact that the structure under test is excited with a pure sine wave. However, if the structure has a strong nonlinear behavior, the response signal will contain higher harmonics or sub-harmonics. This will also give distortion in the force signal since the force applied is the reaction force between the exciter and the structure.

This problem will be further amplified since the shaker in itself shows a non-linear behavior at larger displacements. This is due to the fact that the coil is moving in the non-linear parts of the magnetic field. Distortion in the force signal can therefore be observed even when exciting linear systems, particularly weakly damped structures with large vibrations at resonance frequencies.

A principal simulation model used when developing the control algorithm is shown in Figure 1. A pure sine signal is sent as a voltage signal through a non-

linear system and gives a distorted signal with higher harmonics as output. The system consists of an unknown nonlinear relationship depending on the shaker, the interaction between the shaker and the structure and the nonlinearity in the structure. Results from simulations with different types of nonlinearity for system in Figure 1 will be shown in chapter 5, where the black box is described as a lumped mass-model with added non-linear elements.

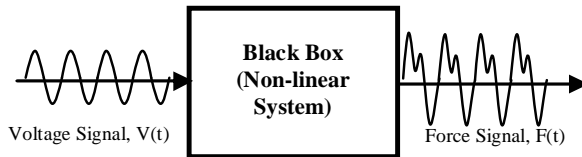


Figure 1: A black box used in simulations. A harmonic voltage signal gives a distorted force signal containing higher harmonics from an unknown non-linear system.

2 Development of a Control Algorithm

The essential concept used, based on methods developed by Bucher, Ewins et al [1, 2, 3], is to send a voltage signal including higher harmonics or sub-harmonics into the system. The phase and amplitude of the added signal content should be designed to decrease the distortion in the force signal. However, there is an unknown and nonlinear relationship between the input signal and the output force signal. Therefore an iterative procedure is required to find the correct voltage signal. This chapter describes the development of this procedure.

A general expression for the actual force measured can be written as a sum of sine and cosine components including k number of harmonics i.e.

$$F(t) = \sum_{n=1}^k (r_{2n-1} \sin(2\pi n ft) + r_{2n} \cos(2\pi n ft)) \quad (1)$$

where f is the fundamental harmonic. For each harmonic there is a sine and cosine component to describe the actual amplitude and phase.

Alternatively, Equation (1) can be written in matrix form for each time sample as:

$$\begin{bmatrix} \sin(2\pi ft_0) & \cos(2\pi ft_0) & \cdots & \cos(2\pi kft_0) \\ \sin(2\pi ft_1) & \cos(2\pi ft_1) & \cdots & \cos(2\pi kft_1) \\ \vdots & \vdots & \vdots & \vdots \\ \sin(2\pi ft_T) & \cos(2\pi ft_T) & \cdots & \cos(2\pi kft_T) \end{bmatrix} \begin{Bmatrix} r_1 \\ r_2 \\ \vdots \\ r_{2k} \end{Bmatrix} = \begin{Bmatrix} F(t_0) \\ F(t_2) \\ \vdots \\ F(t_T) \end{Bmatrix} \quad (2)$$

From Equation (2) it is clear that the force vector $\{r_1 \ r_2 \ r_3 \ \dots \ r_{2k}\}$ can be determined with a least-square-estimate using measurement data from time t_0 to t_T .

The actual amplitude and phase at the fundamental harmonic can be calculated as

$$Z_0 = \sqrt{r_1^2 + r_2^2} \quad (3)$$

$$\psi_0 = \tan^{-1}(r_2/r_1) \quad (4)$$

Using (3) and (4) we can define

$$\{F_M\} = \{Z_0, \psi_0, r_3, r_4, \dots, r_{2k}\} \quad (5)$$

$$\{F_D\} = \{Z_d, \psi_d, 0, 0, 0 \dots\} \quad (6)$$

Thus, $\{F_M\}$ is the force vector we actually measure, and $\{F_D\}$ is the desired force vector when tuning is completed.

Similarly as in Equation (1), the voltage signal with added higher harmonics can be defined as

$$V(t) = \sum_{n=1}^k (v_{2n-1} \sin(2\pi nft) + v_{2n} \cos(2\pi nft)) \quad (7)$$

$$\{V_N\} = \{v_1, v_2, v_3, \dots, v_{2k}\} \quad (8)$$

$\{V_N\}$ is vector containing all sine and cosine coefficients for the voltage signal. Here it is assumed that the voltage signal should initially contain the same harmonic components as observed in the force signal. Consequently, if we want to control k number of harmonics (including the fundamental), there are $2k$ numbers of unknowns.

The required voltage signal cannot be identified by simply studying the force signal since there is an unknown non-linear relationship between $\{V_N\}$ and $\{F_M\}$. Instead the problem is dealt with as a system of non-linear equations. Solving this type of problems can presents some major difficulties. Normally there are several roots and the selected algorithm can be unable to find a solution if the initial guess is too far away.

The method selected in this work is based on a multidimensional Newton-Raphson scheme [4, 5]. Unlike more general optimization routines tested, such as Powell and Nelder-Mead, this method has quadratic convergence. Unfortunately the method requires the derivates to actually be calculated which can present some difficulties when dealing with measurement data.

The Newton-Raphson method also has relatively large sensitivity against starting values. However, this may not become a large problem in real measurements. Since the force signal is most distorted at resonances, it is possible to start in an area where the number of harmonics are low and then slowly step towards the resonance.

During the frequency sweep the previous set of input voltage, which gave a non-distorted force signal, is always used as initial guess.

Next, the Newton-Raphson procedure and its application to our problem are described. A general $n \times n$ nonlinear problem can be formulated as

$$\left\{ \begin{array}{l} g_1(x_1, x_2, \dots, x_N) \\ g_2(x_1, x_2, \dots, x_N) \\ \vdots \\ g_N(x_1, x_2, \dots, x_N) \end{array} \right\} = \left\{ \begin{array}{l} 0 \\ 0 \\ \vdots \\ 0 \end{array} \right\} \quad (9)$$

where $\{g_1, g_2, \dots, g_N\}$ are the functions to minimize. For our case the functions will be the difference between measured force vector and desired force vector.

In vector form this can be written as

$$\{F_V\} = \{F_M\} - \{F_D\} \quad (10)$$

Each of the functions in (10) are then assumed to be dependent on the input voltage vector described in Equation (8) so that

$$\{F_V(v_1, v_2, \dots, v_N)\} = \{0\} \quad (11)$$

Once an initial guess is provided on $\{V_N\}^n$ we would now like to determine $\{V_N\}^{n+1}$ so that it is a step towards the right solution i.e.

$$\{F_V\}^{n+1} < \{F_V\}^n \quad (12)$$

In order to fulfill (12) we must calculate the partial derivatives between $\{F_V\}$ and $\{V_N\}$.

$$\begin{Bmatrix} \Delta F_V^1 \\ \Delta F_V^2 \\ \Delta F_V^3 \\ \Delta F_V^4 \\ \vdots \\ \Delta F_V^{2k} \end{Bmatrix} = \begin{bmatrix} j_{11} & j_{12} & j_{13} & j_{14} & \cdot & j_{1(2k)} \\ j_{21} & j_{22} & j_{23} & j_{24} & \cdot & j_{2(2k)} \\ j_{31} & j_{32} & j_{33} & j_{34} & \cdot & j_{3(2k)} \\ j_{41} & j_{42} & j_{43} & j_{44} & \cdot & j_{4(2k)} \\ \cdot & \cdot & \cdot & \cdot & \cdot & j_{5(2k)} \\ j_{(2k)1} & j_{(2k)2} & j_{(2k)3} & j_{(2k)4} & \cdot & j_{6(2k)} \end{bmatrix} \begin{Bmatrix} \Delta v_1 \\ \Delta v_2 \\ \Delta v_3 \\ \Delta v_4 \\ \vdots \\ \Delta v_{2k} \end{Bmatrix} \quad (13)$$

Equation (13) is actually a linearization and since we have a nonlinear problem this will only be valid for small Δ . It is therefore essential that the initial guess on $\{V_N\}$ is sufficiently close to the root. Furthermore, the functions must be relatively smooth without large discontinuities.

All j_{nm} components in Equation (13) are a shorter notation for the actual partial derivate and the complete matrix is defined as the systems Jacobian, i.e

$$[J_{nm}] = \frac{\partial F_V^n}{\partial v_m} \quad (14)$$

The partial derivate can be determined with a finite difference approach so that

$$[J_{nm}] = \frac{1}{2h} (\Delta F_V^n(v_m + h) - \Delta F_V^n(v_m - h)) \quad (15)$$

where h is the step length used to estimate the derivatives.

By using an appropriate value for h and change the m :th value in the voltage vector, we can observe all the differences between the measured force vector and the desired force vector. As a result, the complete m :th column in $[J]$ can be determined from two function evaluations i.e measurements. If k numbers of harmonics are controlled we have $2k$ unknown and thus $4k$ number of measurements are required to determine the complete Jacobian.

From Equation (13) a new guess on the input voltage vector can be formulated as

$$\{V_N\}^{n+1} = \{V_N\}^n - [J]^{-1} \{F_V\} \quad (16)$$

If the initial $\{V_N\}$ was sufficiently close to the root, $\{V_N\}^{n+1}$ should be one step closer to the correct solution. From here a new Jacobian can be calculated and a new step is taken. Rather than attempting to find the exact solution, the quantity

$$F_{crit} = \sum_{n=1}^{2k} \{F_V\}^n \quad (17)$$

is calculated and a global criteria on F_{crit} is used for when the new solution should be accepted.

Once (17) is fulfilled the force signal is said to be close to a non-distorted sine. The response at selected points on the structure can therefore be saved for FRF-calculation. Then the desired fundamental frequency on the force signal, Equation (1), can be incremented and the previous $\{V_N\}$ is used as initial guess. If new harmonic components become relevant in the force signal they are added to the controlled set of frequencies and new iterations are performed.

3 Broyden's Method

The Newton-Raphson technique described in chapter 2 is useful for solving small systems of equations but is not very practical when the number of unknowns becomes too large. As previously described k number of unknowns

yields $4k$ number of measurement to determine the jacobian. Therefore, a single iteration where four harmonics are controlled can take up to 200-300 seconds (depending on measurement time required to find a steady-state solution).

To deal with this problem and increase the speed of the control algorithm several quasi-newton methods have been tested. This class of methods avoids the direct calculation of partial derivates. In this work Broydens method [4, 5] is tested where a secant method is used to approximate the partial derivates.

In a one-dimensional case the secant method replaces the derivate as

$$g'(x) = \frac{g(x^n) - g(x^{n-1})}{x^n - x^{n-1}} \quad (18)$$

$$g'(x)(x^n - x^{n-1}) \approx g(x^n) - g(x^{n-1}) \quad (19)$$

Extended to higher dimensions and to our application we can define

$$J(\{V_N\}^n)(\{V_N\}^n - \{V_N\}^{n-1}) \approx F_V(\{V_N\}^n) - F_V(\{V_N\}^{n-1}) \quad (20)$$

Broyden then uses an approximation to the jacobian matrix

$$A(\{V_N\}^n) \approx J(\{V_N\}^n) \quad (21)$$

which after two successive iterations can be updated with Equation (20). To achieve an updating formula for $[A]$, as suggested by Broyden [4, 5], the following vectors are defined

$$\{y_k\} = \{F_V\}^n - \{F_V\}^{n-1} \quad (22)$$

and

$$\{s_k\} = \{V_N\}^n - \{V_N\}^{n-1} \quad (23)$$

Using Equation (22) and (23), the estimate of the Jacobian can be updated with

$$A^n = A^{n-1} + \frac{y_k - A^{n-1}s_k}{\|s_k\|_2^2}(s_k)^T \quad (24)$$

Where $\|\cdot\|_2$ denotes the euclidean norm.

Equation (24) requires the two initial values on the voltage vector. In practice the first Jacobian can be calculated and then using Equation (16) to determine $\{V_N\}^1$. Alternatively a scalar multiple of the unit matrix can be used as initial guess for the Jacobian.

Once the first two values on the voltage vector are given, Equation (24) are used and

$$\{V_I\}^{n+1} = \{V_I\}^n - [A^n]^{-1} \{F_V\} \quad (25)$$

until Equation (17) is fulfilled.

4 Extended Force Control Algorithm

Since the Jacobian (calculated as in chapter 2 or estimated with Broyden) can contain a lot of disturbance for measurement data it is necessary to have a built in strategy to keep the solution process stable. A global strategy method is therefore used. The idea is to not always take the full step, instead Equation (25) is rewritten as

$$\{V_I\}^{n+1} = \{V_I\}^n - u [A^n]^{-1} \{F_V\} \quad (26)$$

As suggested by [1,4] we find a value u that minimize

$$G_V = \frac{1}{2} F_V^T F_V \quad (27)$$

To find the exact minimum may require several function evaluations (measurements) so instead selected values between $\{0.1, \dots, 1\}$ is tested and using interpolation it is possible to find a satisfactory value. This will help the algorithm to converge even when the starting values are less good or the Jacobian contains noise. To achieve a good starting value the multidimensional solver does not start until the amplitude on the fundamental harmonic is correct as suggested in [1, 3, 6].

The complete force algorithm from chapter 2, 3 and 4 is illustrated with a flow chart in Figure 2. After the complete voltage vector $\{V_N\}$ is defined we can choose to either use Broyden's method or Newton-Raphson's method as indicated in the flow chart.

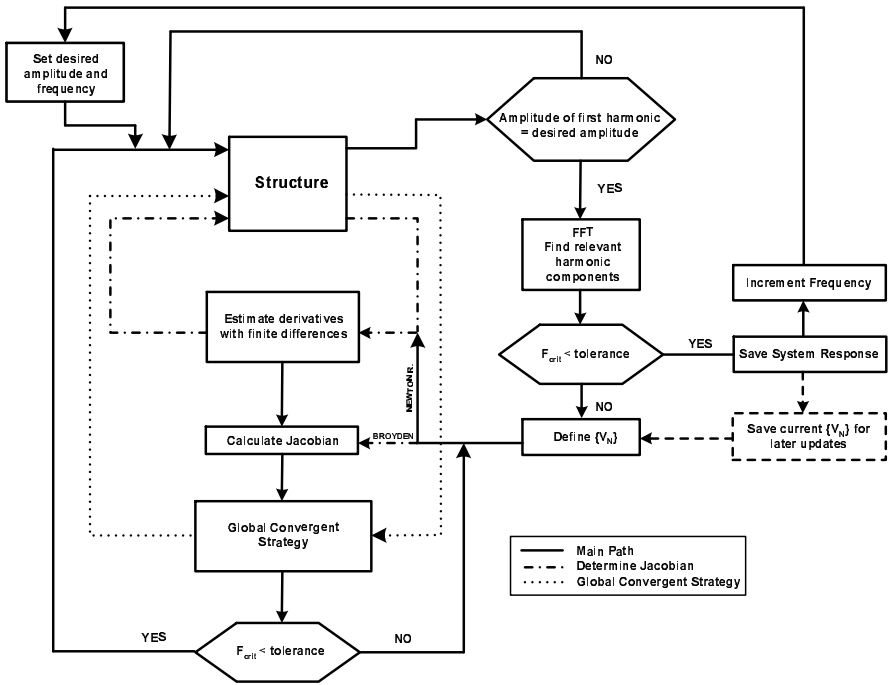


Figure 2: Flow chart of Force control algorithm. A voltage signal is sent to the amplifier and the resulting force signal can be measured with a force sensor. The control algorithm updates the voltage signal to achieve a non-distorted force signal.

5 Simulations and Results

A simulation model is created as explained in chapter 1. The shaker, the interaction between the shaker and the structure and the nonlinearity in the structure is here regarded as a black box and modeled as lumped mass model. This is a simplification since the true model between input voltage and output force is a non-linear electro-mechanic system. However, for simulations this provides a good way to actually test the algorithm. The values selected for m , c , k and P has no real physical meaning but are merely estimated from transfer

functions calculated between voltage/force. All calculations are performed in MATLAB [7].

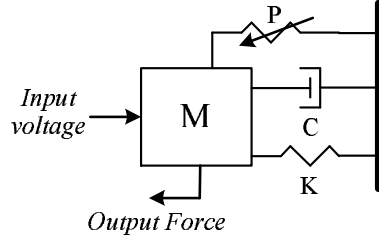


Figure 3: Simulation model used to test the algorithm. The values used are $m = 0.024 \text{ kg}$, $c = 1.5 \text{ Ns/m}$, $k = 1.6 \cdot 10^6 \text{ N/m}$ and $P = 1.6 \cdot 10^8 \text{ N/m}^3$.

The desired amplitude on the output signal is selected and the input signal is first adjusted to give an output signal with correct fundamental harmonic. Then, using the Newton-Raphson procedure, an input signal with higher harmonics is created as described in chapter 2.

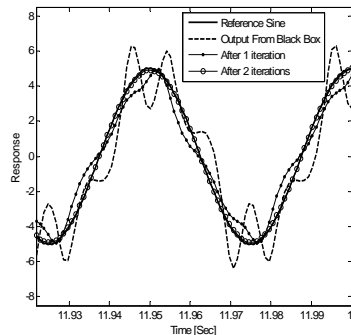


Figure 4: Simulation results where the algorithm is used to control the output signal from the non-linear system in Figure 3. In this case 40 simulated measurements were required to correct the signal.

The output from the system contains a significant third and fifth harmonic

component as shown in Figure 4. After two iterations the difference between the output signal and the reference signal is said to be acceptable and the algorithm can continue with a new frequency step. The initial input signal and the input signal after two iterations is shown in Figure 5. The actual amplitude on the final signal is larger to compensate for the loss to higher harmonics. Additionally, a slight change on phase of the main harmonic can be observed as well as a significant third harmonic in the final input signal.

Next, the modified control algorithm as described in chapter 3 is used to control the input signal. The first Jacobian is here calculated and used as initial guess for Broyden's method. The results can be studied in Figure 6. As observed this method requires an additional iteration before the solution is accepted since Broyden's method converges slower. However the amount of function evaluations (measurements) saved is still significant.

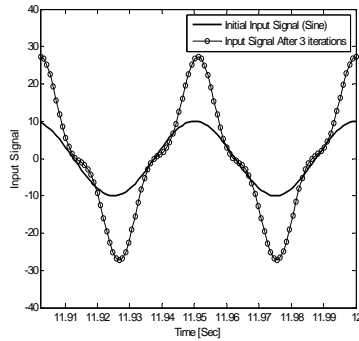


Figure 5: The higher harmonics in the input signal can be seen after 3 iterations.

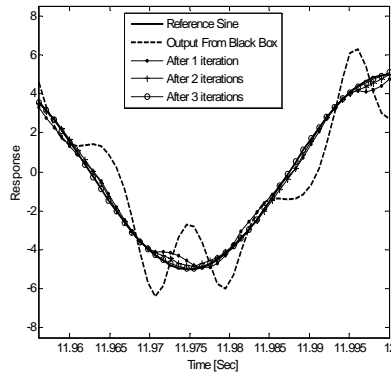


Figure 6: Broyden's method for the same system requires 28 simulated measurements to find the correct voltage signal.

6 Conclusions and Future Work

A non-distorted force signal can be difficult to obtain when measuring non-linear structures or weak linear structures at resonances and thus a control algorithm is necessary. This work has presented theoretical methods that can be used to reduce the distortion in the force signal. This can be achieved by creating a multi harmonic voltage signal with phase and amplitude designed to decrease all higher harmonics or sub-harmonics in the force signal. A control algorithm based on Newton-Raphson's method have been applied i.e. an iterative process is used to actually find the correct voltage signal. Further extensions have been made on the control algorithm by using Broyden's method to estimate the derivatives.

A complete control system is built in MATLAB where simulations have been performed on several arbitrary non-linear black box systems as described in chapter 1 and chapter 5. The result from simulations shows that the control algorithm can obtain a non-distorted output signal even when there is a significant nonlinearity. The potential of Broyden's method have been observed in simulations and further experiments is required to determine whether this method can be used in real measurements.

Additional work in the future will also be to create an improved electro-mechanic model of the shaker including the nonlinearities. From here a better understanding of the actual phenomena can be gained and the control algorithm can be further improved.

References

- [1] Janito V. Ferreira. *Dynamic Response Analysis of structures with non-linear components*. PhD thesis, Imperial College, London, 1998.
- [2] I. Bucher. Exact adjustment of dynamic forces in presence of non-linear feedback and singularity - theory and algorithm. *Journal of Sound and Vibration*, 218(1):1 – 27, 1998.
- [3] D.J. Ewins and S. Perinpanayagam. Testing technique for identifying and characterizing non-linear behaviour of an aero-engine structure. In *12th International Conference on Experimental Mechanics*, 2004.
- [4] William H. Press. *Numerical recipes in C : the art of scientific computing*. Cambridge Univ. Press, Cambridge, 2. ed. edition, 1992.
- [5] J. E. T. Penny and G. R. Lindfield. *Numerical methods using Matlab*. Prentice Hall, Upper Saddle River, N.J., 2. ed. edition, 2000.
- [6] Stephanie Rossmann. Development of force controlled modal testing on rotor supported by magnetic bearings. Master's thesis, Imperial College, London, 1999.
- [7] MATLAB Computing Software v 7.0 (R14), 2005.

Paper B

On Nonlinear Parameter Estimation

Paper B is published as:

Magnevall, M., Josefsson, A. and Ahlin, K. On Nonlinear Parameter Estimation, In *Proceedings of International Conference on Noise and Vibration Engineering (ISMA) 2006*, Leuven, Belgium, 2006.

On Nonlinear Parameter Estimation

Martin Magnevall
Andreas Josefsson
Kjell Ahlin

Blekinge Institute of Technology, SE-371 79 Karlskrona, Sweden

Abstract

The industrial demand on good dynamical simulation models is increasing. Since most structures show some form of nonlinear behavior, linear models are not good enough to predict the true dynamical behavior. Therefore nonlinear characterization, localization and parameter estimation becomes important issues when building simulation models. This paper presents identification techniques for nonlinear systems based on both random and harmonic excitation signals.

The identification technique based on random excitation builds on the well known reverse-path method developed by Julius S. Bendat. This method treats the nonlinearity as a feedback forcing term acting on an underlying linear system and the parameter estimation is performed in the frequency domain by using conventional MISO/MIMO techniques. Although this method provides a straightforward and systematic way of handling nonlinearities, it has been somewhat limited in use due to the complexity of creating uncorrelated inputs to the model. As is shown in this paper, the parameter estimation will not be improved with conditioned inputs and the nonlinear parameters and the underlying linear system can still be estimated with partially correlated inputs.

This paper will also describe a parameter estimation method to be used with harmonic input signals. By using the principle of harmonic balance and multi-harmonic balance it is possible to estimate an analytical frequency response function of the studied nonlinear system. This frequency

response function can, in conjunction with measured nonlinear transfer functions, be used to estimate the nonlinearity present in the system. This method is also applicable on nonlinear systems with memory, e.g. systems with hysteresis effects.

The above mentioned methods are applied to multi-degree-of-freedom and single-degree-of-freedom systems with different types of nonlinearities. Also, techniques for locating nonlinearities are discussed.

1 Introduction

The overall aim with parameter estimation is to find suitable parameters to a mathematical model, based on measurements of the inputs and outputs of a system. The mathematical model can, for instance, be based on a beforehand known model structure. This is known as parametric modeling, which will be studied in this paper. Furthermore, the systems studied contain significant nonlinearities that must be included when creating the model, hence nonlinear parameter estimation.

Systems used in engineering can generally be separated into two distinct groups; linear or nonlinear. A system, H , is said to be linear if it fulfills the principle of superposition:

$$H\{cx\} = cH\{x\} \quad (1)$$

$$H\{x_1 + x_2\} = H\{x_1\} + H\{x_2\} \quad (2)$$

A system which does not satisfy these properties is defined as nonlinear. Additionally, nonlinear systems can be classified into different groups as described in [1]. In this paper, two different types of non-linearities will be discussed; zero-memory nonlinear systems and nonlinear systems with memory. The next chapter will show how the frequency response functions can be used to identify and locate nonlinearities in a dynamic system. This will be followed by methods for parameter estimation with random noise signals in chapter 3, and next using sine excitation in chapter 4.

2 Nonlinear effects on the Frequency Response Functions

The frequency response functions can normally give sufficient information about a system. In structural dynamics it is often common to assume that there is an underlying linear system. By measuring the frequency response functions at different force amplitudes it is, in many cases, possible to identify the type of nonlinearity present as shown in Figure 1. For zero-memory nonlinear systems it is also possible to identify the type of nonlinearity with random noise signals as will be shown in Chapter 3.

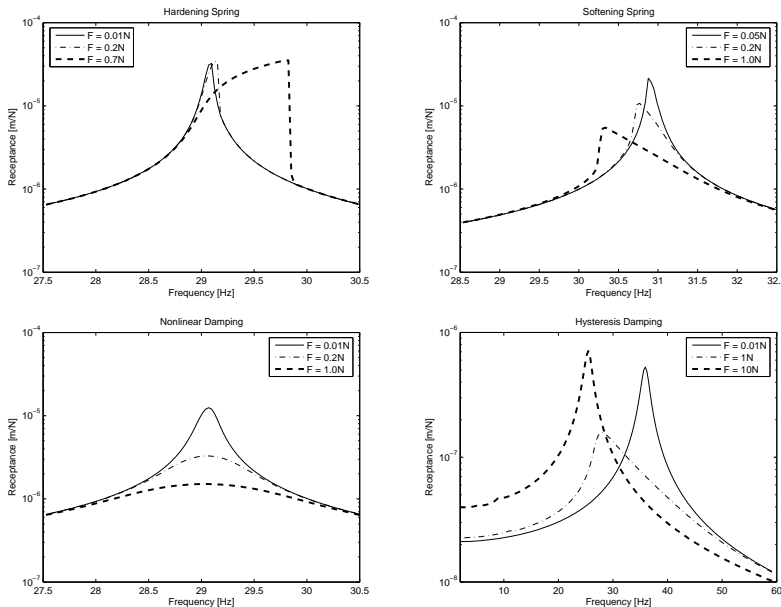


Figure 1: Frequency Response Functions measured with an upward sine sweep.

The nonlinear degree-of-freedoms can also be determined, from the frequency response functions, by using the fact that the nonlinearity usually only influence the system dynamics at high input amplitude. For example, consider a 2-dof system where a nonlinear element is connected from one dof to ground.

Figure 2 shows the point-receptance measured at each degree-of-freedom. Notice that, for H_{22} , the anti-resonance remains at the same position in frequency since the system is close to linear at this very low response amplitude. The same behavior can not be seen for H_{11} and thus, the nonlinear element must be connected to the second degree-of-freedom.

Hence, the frequency response function can be used to find the nonlinear degree of freedoms as well as identify the type of nonlinearity present. This information will be necessary in the following chapters, where a known model structure is assumed.

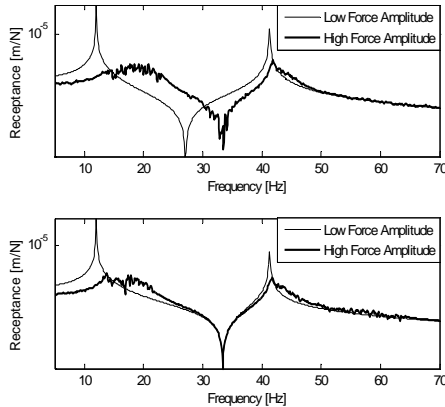


Figure 2: Simulated point receptance for a two-degree-of-freedom system with a nonlinear element connected to the second DOF. H_{11} above and H_{22} below. Notice that the anti-resonance is not moving for H_{22} since the nonlinear element is connected to the second DOF.

3 Parameter Estimation with Random Noise Signals

This chapter will study a method based on using random noise signals as initially developed by Bendat [1]. This method uses a least-square method in

the frequency domain to estimate parameters and is suitable to identify zero-memory nonlinear systems. The multiple-input-multiple-output theory, used in the method, will be initially reviewed in section 3.1, followed by an application to nonlinear systems in section 3.2 and finally two simulated examples in section 3.3.

3.1 The MIMO Identification Technique

Consider a general linear system, with N inputs and M outputs, and noise on the measured outputs, as shown in Figure 3.

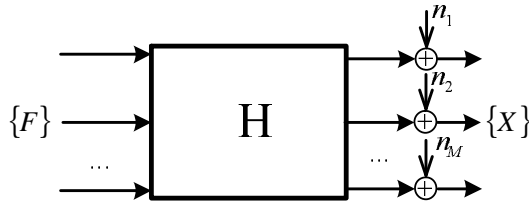


Figure 3: A Multiple-Input-Multiple-Output Model with noise on the outputs.

The H1-estimator for this system can be determined at each frequency as

$$\mathbf{H} = \mathbf{G}_{XF} \mathbf{G}_{FF}^{-1} \quad (3)$$

where \mathbf{G}_{XF} is the cross-spectral density matrix with size ($N \times N$), and \mathbf{G}_{FF} is the auto-spectral density matrix with size ($M \times N$).

Next, the coherence function is defined. Generally, the ordinary coherence function is defined as the linear relationship between any two signals. For a single-input-single-output model the use of the coherence function is straightforward but for a multiple input case, as shown in Figure 3, several ordinary coherence functions can be formulated, for instance the ordinary coherence between input p and output q :

$$\gamma_{pq}^2 = \frac{|\mathbf{G}_{X_p F_q}|^2}{\mathbf{G}_{F_q F_q} \mathbf{G}_{X_p X_p}} \quad (4)$$

Equation (4) yields a frequency dependent real-valued scalar equal to unity when perfect linear relationships exist between two spectra. However, for a

MIMO case, the ordinary coherence function between an output spectrum and an input spectrum can be misleading. Due to the influence of other inputs, this coherence function can be much less than unity even though a perfect linear relationship exists between all inputs and outputs. For this reason the multiple coherence function is more useful in a multiple input case.

A multiple coherence function can be calculated for each output as:

$$\gamma_m^2 = \frac{\mathbf{G}_{XF} \mathbf{G}_{FF}^{-1} \mathbf{G}_{XF}^H}{\mathbf{G}_{XX}} \quad (5)$$

The size of \mathbf{G}_{XF} will now be $(1 \times N)$ and \mathbf{G}_{XX} will be scalar since only one output is selected. Thus, M number of multiple coherence functions can be calculated for the system shown in Figure 3.

3.2 Using MIMO Identification for Nonlinear Systems

The MIMO identification technique can now be used to solve a nonlinear problem. Actually, there are several possible ways to formulate a nonlinear problem with MIMO-technique. For instance, consider Duffing's equation:

$$m\ddot{x} + c\dot{x} + kx + px^3 = f \quad (6)$$

In frequency domain this can be formulated as

$$B X + p\mathcal{F}(x^3) = F \quad (7)$$

where B is the impedance of the linear system and $\mathcal{F}(.)$ is the Fourier transform. Note that in Equation (7), p can be frequency dependent. Clearly, using the multiple input techniques from the previous section, this problem can be solved in, for instance, three different ways as shown in Figure 4 were $H = B^{-1}$.

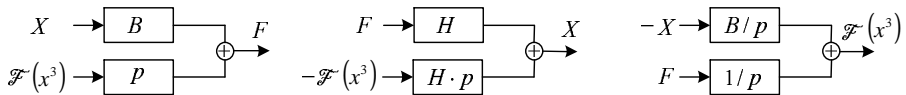


Figure 4: Three possible ways to solve Duffing's equation with multiple input techniques; Force as output (left), displacement as output (middle), nonlinear function as output (right).

In this paper, the applied force and the nonlinear feedback forces are used as input to the MIMO-model, since this formulation is easier to extend to a general nonlinear system as will be shown next. Various extensions to MDOF systems with several nonlinear elements have previously been done by, for instance, [2, 3, 4].

A general nonlinear system can be expressed as:

$$\mathbf{M}\{\ddot{x}\} + \mathbf{C}\{\dot{x}\} + \mathbf{K}\{x\} = \{f\} - N[\{x\}, \{\dot{x}\}] \quad (8)$$

where N is a set of nonlinear restoring forces depending on either x or \dot{x} . In more detail, the nonlinear operator can be written as

$$N[\{x\}, \{\dot{x}\}] = \sum_{m=1}^{N_{EL}} p_m \{w_m\} g_m(\{x\}, \{\dot{x}\}) \quad (9)$$

Thus, for each nonlinear component there is an unknown coefficient p_m , a position vector $\{w_m\}$ and a nonlinear function g_m . Typical nonlinear functions are shown in Equations (10)-(11). The position vector is here used in the formulation since the nonlinear function might act on the relative output between two degrees-of-freedom, as will be determined by the elements location, for instance:

$$g_m = (\{w_m\}^T \{x\})^3 \quad (\text{Cubic hardening spring}) \quad (10)$$

$$g_m = (\{w_m\}^T \{\dot{x}\})^2 \quad (\text{Quadratic damping}) \quad (11)$$

Equation (8) and (9) can be written in frequency domain as:

$$\{X\} = \mathbf{H}\{F\} - \mathbf{H} \sum_{i=1}^{N_{EL}} p_m \{w_m\} \mathcal{F}(g_m(\{x\}, \{\dot{x}\})) \quad (12)$$

From the expression above a new modified force vector can be defined which includes the nonlinear restoring forces as shown in Equation (13). This force vector is then used as input to a MIMO-model. To avoid confusion with the force vector used in the previous section this vector is notated as $\{R\}$.

$$\{R\} = \begin{Bmatrix} \{F\} \\ r_1 \\ \vdots \\ r_m \end{Bmatrix} \quad (13)$$

In (13) each r_m is the Fourier-transform of a nonlinear function, i.e.

$$r_m = -\mathcal{F}(g_m(\{x\}, \{\dot{x}\})) \quad (14)$$

As will be shown later, several nonlinear functions can be used for a single nonlinear element. For instance when several polynomials are used to estimate a gap- or clearance-nonlinearity.

Using this new modified force vector a set of transfer functions can be calculated using the equation for the $H1$ -estimator as:

$$\mathbf{H}_M = \mathbf{G}_{XR} \mathbf{G}_{RR}^{-1} \quad (15)$$

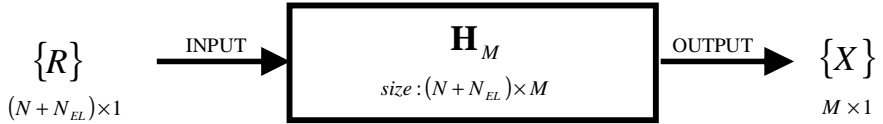


Figure 5: A force vector with applied force and the restoring nonlinear forces is used as input to a MIMO-model.

If the size of the matrices is defined as shown in Figure 5, the first column of the underlying linear system can be identified as the first column in \mathbf{H}_M . Thus, for a single force input the linear system can be extracted, $\{H_L\}$, and the nonlinear coefficients can, for each frequency, be calculated as:

$$p_i = \frac{1}{\{w_i\}^T \{H_L\}} \mathbf{H}_M^{(r, i+1)} \quad i \in \{1, 2, \dots, N_{EL}\} \quad (16)$$

$\mathbf{H}_M^{(r, i+1)}$ refer to a single element in matrix \mathbf{H}_M at row r (force input) and column $i + 1$.

Note that Equation (16) can easily be extended to a case where there is several force inputs. As can be seen in simulations, an applied force at each nonlinear DOF will reduce the necessary simulation time considerably.

With the method described above, the column that corresponds to the force input will always be estimated in the linear system. Thus, modal parameter estimation can be performed to determine the complete linear system. If two forces are applied, two columns in the linear system will be estimated and so forth.

The force input and the nonlinear restoring forces may be partially correlated with each other and, after averaging, the matrix \mathbf{G}_{RR} will be non-diagonal. This may introduce numerical instabilities when calculating the matrix inversion in Equation (15), particularly at the resonance. In general though, this error is very small and does not affect the result much.

The conditioning method, described in [1], where a set of uncorrelated inputs is created will not improve the parameter estimation in this case. For all simulated systems tested, it has not been possible to see any difference between using partially correlated inputs and the conditioned version with uncorrelated inputs. This is an important observation since it simplifies the calculations considerably.

The only advantage with using uncorrelated inputs is that the ordinary coherence can be calculated between the output and each input. These ordinary coherences will sum up to the multiple coherence and thus it is possible to see the significance of each nonlinear restoring force. This may be useful when searching for possible nonlinear functions and a method for calculating uncorrelated inputs is given below.

A new set of inputs can be defined by a transformation as:

$$\{U\} = \Phi \{R\} \quad (17)$$

Multiplying with the complex conjugate and averaging yields:

$$[G_{UU}] = \Phi \{R\} (\Phi \{R\})^H = \Phi \mathbf{G}_{RR} \Phi^H \quad (18)$$

Thus, if the matrix Φ is defined as described in [1], \mathbf{G}_{UU} will be a diagonal matrix.

Using this Φ -matrix the cross-correlation densities can also be calculated as

$$\mathbf{G}_{XU} = \mathbf{G}_{XR} \Phi^H \quad (19)$$

With \mathbf{G}_{UU} and \mathbf{G}_{XU} available the ordinary coherences between a selected output and each input can be calculated with Equation (4). Using the notations in Figure 5 there will be $N + N_{EL}$ ordinary coherences for each output.

3.3 Simulations

The method derived in section 3.2 is here demonstrated on two nonlinear systems. First, a single-degree-of-freedom with two nonlinear elements is used followed by a multi-degree-of-freedom system.

3.3.1 A SDOF-system with a nonlinear spring and damper

The test system used is shown in Figure 6 and consists of an underlying linear system with a cubic hardening spring and a quadratic damping element connected. The time response is simulated from this system using digital filters. Figure 7 shows several frequency response functions calculated with different force amplitudes.

With increasing force, the frequency response functions will decrease in amplitude as well as moving upward in frequency due to the presence of a damping nonlinearity and a cubic hardening spring. As mentioned in previous section it is possible to use several nonlinear functions as input and, with Equations (17)-(19), calculate a new set of uncorrelated inputs and then studying the ordinary coherences. However, this is not straightforward as the order in which the functions are defined and the amplitude of the response signal will affect the result. In this case, testing different combinations of Equation (20) will show that the cubic spring element and the quadratic damping element are most significant.

$$\{R\} = \{F \quad -x^2 \quad -x^3 \quad -x \operatorname{sgn}(x) \quad -v|v| \quad -v^3 \quad -v^5\}^T \quad (20)$$

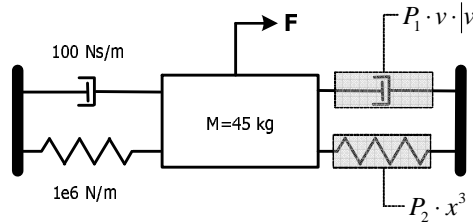


Figure 6: Test Case used in simulations. A single-degree of freedom system with two nonlinear elements, $P_1 = 2e5$ and $P_2 = 6e13$.

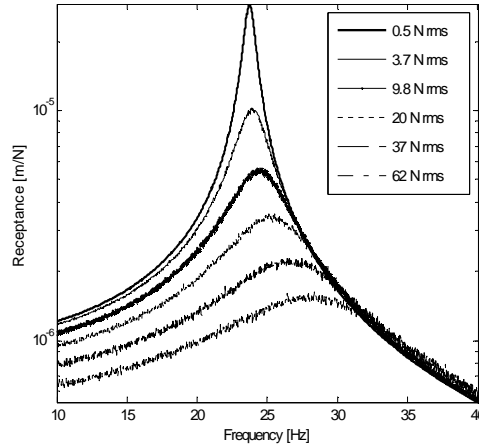


Figure 7: Several FRF's at different force amplitudes for the tested system.

The position vector and the nonlinear functions are therefore defined as:

$$w_{1,2} = \{1\} \quad r_1 = -\mathcal{F}((x_1)^3) \quad r_2 = -\mathcal{F}((v_1|v_1|)^3) \quad (21)$$

Using Equations (13)-(16), the nonlinear analysis can be performed and the result is shown in Figure 8. The linear system can be identified and the calculated average value of the nonlinear coefficients differ no more than $+/- 0.01\%$ from the theoretical value.

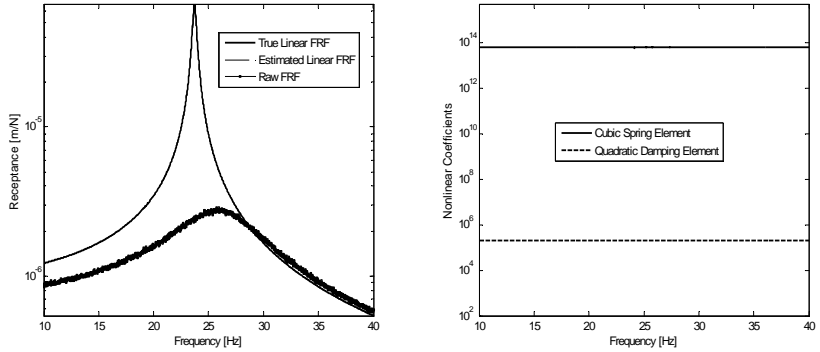


Figure 8: Estimate of the underlying linear system and the nonlinear coefficients.

3.3.2 A MDOF-system with a several nonlinear elements

The next example consists of a MDOF system with a cubic- and a quadratic-spring as shown below.

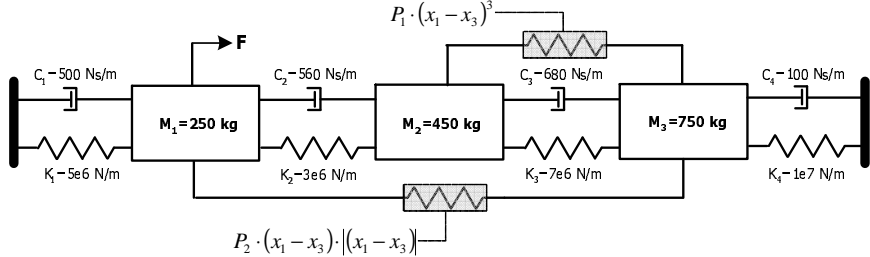


Figure 9: Test System used in Simulations, $P_1 = 4e16$ and $P_2 = 6e10$.

Using the same procedure as in section 3.3.1, the position vectors and the nonlinear functions for each nonlinear element is defined as

$$w_1 = \begin{pmatrix} 0 & -1 & 1 \end{pmatrix}^T, \quad w_2 = \begin{pmatrix} -1 & 0 & 1 \end{pmatrix}^T \quad (22)$$

$$r_1 = -\mathcal{F}\left(\left(\{w_1\}^T \{x\}\right)^3\right) \quad r_2 = -\mathcal{F}\left(\{w_2\}^T \{x\} | \{w_2\}^T \{x\}| \right) \quad (23)$$

The first column in the linear system and the nonlinear coefficients can then be solved with Equations (13)-(16), and the result is shown in Figure 10.

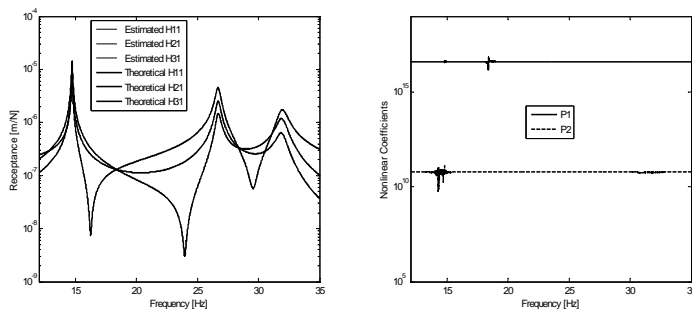


Figure 10: The first column in the linear system and the nonlinear coefficients.

Furthermore, the multiple coherence can be calculated for each output which is then compared with the multiple coherence function calculated for a conventional linear analysis (Figure 11). Notice that the multiple coherence is above 0.99 for all frequencies with the nonlinear analysis.

4 Parameter Estimation With Harmonic Input

The difference between broadband and narrow band excitation signals is the amount of energy associated with every single frequency point. In the case of a broadband signal, the energy associated with each specific frequency point is low. The result is a frequency response function which appears linearised around the resonance frequency. However, if sinusoidal excitation is used it is possible to obtain a good estimate of the frequency response function for the studied nonlinear system. This is illustrated in Figure 12.

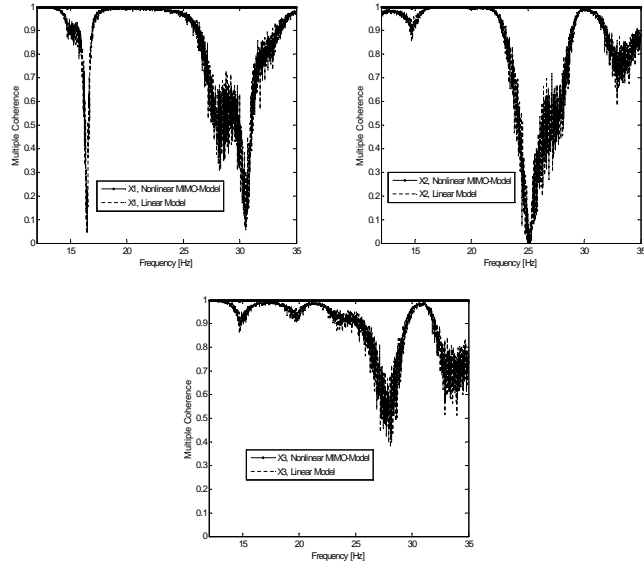


Figure 11: Multiple Coherence Functions.

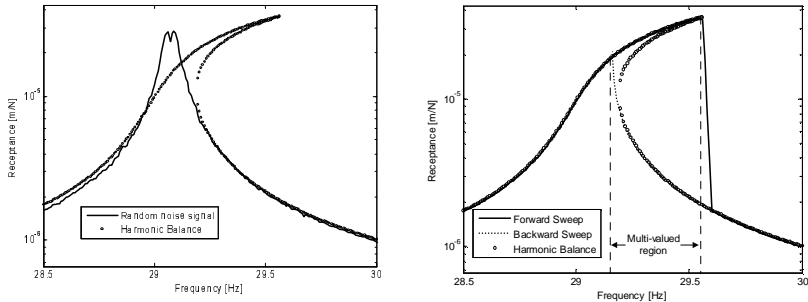


Figure 12: Transfer function of a nonlinear SDOF system obtained by random noise and sinusoidal excitation, compared with an analytical transfer function calculated by harmonic balance.

The frequency response function obtained by harmonic excitation can, in conjunction with an analytical frequency response function, be used to estimate the

nonlinearity present in the system. In this chapter, the principle and method of a parameter estimation procedure based on harmonic input will be discussed. The method is then tested on a nonlinear stick-slip system in section 4.2.

4.1 Theoretical Background

By exciting a nonlinear system with either a low or a high force, depending on the type of nonlinearity, the frequency response function of the underlying linear system can be estimated. This frequency response function can be used as basis to calculate an analytical nonlinear frequency response function of the studied system [5]. The basic principle of this will be described by using a nonlinear single degree of freedom system with an arbitrary nonlinearity, see Figure 13.

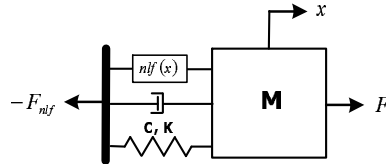


Figure 13: Single degree of freedom system with an arbitrary nonlinearity.

The equation of motion for this system is:

$$m\ddot{x} + c\dot{x} + kx = F - F_{nl}(x) \quad (24)$$

F_{nl} = displacement dependent force due to the nonlinearity.

$$F(t) = F_0 e^{j\omega t} \quad (25)$$

When the system above is excited with a pure sinusoidal force, according to Equation (25), the system response will contain higher harmonics due to the nonlinearity. This response can be expressed with a Fourier expansion.

$$x(t) = \sum_{k=1}^{\infty} x_k e^{jk\omega t} \quad (26)$$

Differentiation of this equation yields:

$$\dot{x}(t) = \sum_{k=1}^{\infty} jk\omega x_k e^{jk\omega t} \quad (27)$$

$$\ddot{x}(t) = - \sum_{k=1}^{\infty} k^2 \omega^2 x_k e^{jk\omega t} \quad (28)$$

The nonlinear force can be expressed in a similar fashion:

$$F_{nlf}(x) = \sum_{k=1}^{\infty} F_{nlk} e^{jk\omega t} \quad (29)$$

Putting Equations (25)-(29) into Equation (24) and considering for example three harmonics [1 3 5], the system of equations becomes:

$$\begin{aligned} -mx_1\omega^2 e^{j\omega t} + jcx_1\omega e^{j\omega t} + kx_1 e^{j\omega t} - F_0 e^{j\omega t} + F_{nl1} e^{j\omega t} &= 0 \\ -9mx_3\omega^2 e^{j3\omega t} + 3jcx_3\omega e^{j3\omega t} + kx_3 e^{j3\omega t} + F_{nl3} e^{j3\omega t} &= 0 \\ -25mx_5\omega^2 e^{j5\omega t} + 5jcx_5\omega e^{j5\omega t} + kx_5 e^{j5\omega t} + F_{nl5} e^{j5\omega t} &= 0 \end{aligned} \quad (30)$$

This system of equations can be rewritten in a more compact form:

$$\begin{aligned} (-m\omega^2 + jc\omega + k)x_1 - F_0 + F_{nl1} &= 0 \\ (-9m\omega^2 + 3jc\omega + k)x_3 + F_{nl3} &= 0 \\ (-25m\omega^2 + 5jc\omega + k)x_5 + F_{nl5} &= 0 \end{aligned} \quad (31)$$

As is evident, the bracketed expressions contain the impedance for each specific harmonic. So, the equation can be written as:

$$\begin{aligned} Z_1 x_1 - F_0 + F_{nl1} &= 0 \\ Z_3 x_3 + F_{nl3} &= 0 \\ Z_5 x_5 + F_{nl5} &= 0 \end{aligned} \quad (32)$$

By using the frequency response function of the underlying linear system mentioned previously, the impedance of the system is estimated and an analytical

frequency response function can be calculated using the method of harmonic balance. This presumes that the nonlinearity in the system is known. If the nonlinearity is not known, it can be estimated by fitting the analytical nonlinear frequency response function to a measured nonlinear frequency response function.

All nonlinear functions is defined by a set of parameters, the first step is to find out which type of nonlinearity is present in the current system and select a suitable model for this nonlinearity, some examples of how this can be done were described in chapter 2.

The parameters which define the nonlinear model can then be estimated by the method described in Figure 14. The cost function used as error estimate is defined as

$$\epsilon = \|H_{measurednonlinear} - H_{analyticnonlinear}\|_2 \quad (33)$$

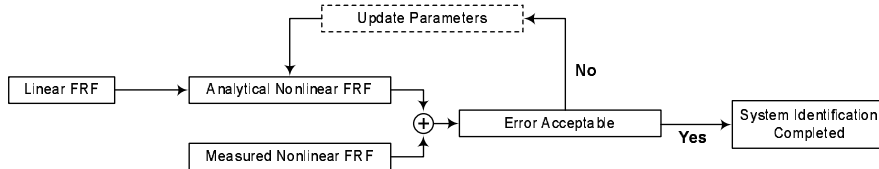


Figure 14: Flowchart of the parameter estimation procedure.

One benefit of this method, compared to random data based parameter estimation procedures, is the ability to use any nonlinear function, e.g. bilinear functions or functions with memory, instead of being forced to use only polynomial estimates.

4.2 Simulations

The method described previously will be illustrated by an example where parameter estimation is done on a nonlinear system with memory, a stick slip system. The nonlinear system used as a reference, i.e. the system the simulated measurements are performed on, is shown in Figure 15.

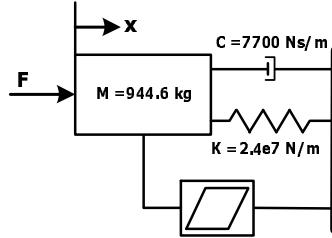


Figure 15: Nonlinear stick-slip system used as reference.

The nonlinearity in this system is defined by two parameters:

k_d - The stiffness during the stick-condition

F_d - The force level where the system starts to slip

Examples of frequency response functions obtained by swept-sine excitation at different force amplitudes are illustrated in Figure 16.

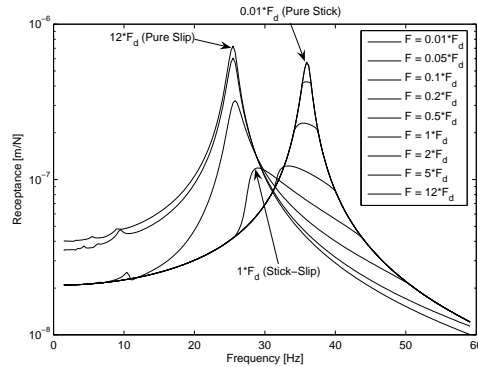


Figure 16: FRFs from different excitation amplitudes.

As shown in Figure 16, the system has two different resonance frequencies. One at low levels of excitation and one at high levels, between these excitation levels the hysteretic effect in the system gives the best damping. At high levels

of excitation the effects of the stick-slip nonlinearity is eliminated, due to the fact that the system is constantly in slip condition. Therefore the frequency response function at high levels of excitation can be used as an estimate of the underlying linear system and as input to the harmonic balance function.

Since the nonlinear function is supposed to be unknown a more general hysteresis function is used in the estimation. A system with this hysteresis function is shown in Figure 17.

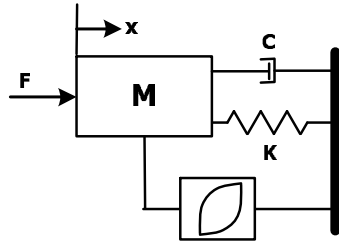


Figure 17: The assumed nonlinear system to be fitted to the reference system.

The virgin-curve of the hysteresis function in this system is governed by Equation (34).

$$F = \frac{xk_d}{\left(1 + \left(\frac{xk_d}{F_d}\right)^N\right)^{1/N}} \quad (34)$$

Where:

k_d - The stiffness during stick-condition

F_d - The force level where the system starts to slip

N - Determines the curvature

The exponent N in Equation (34) makes it far more flexible than a normal stick-slip function and thereby more adaptable to an arbitrary hysteresis func-

tion.

Ten percent noise was added to the response of all time signals and the harmonic balance calculations were carried out using four harmonics [1 3 5 7]. The non-gradient search algorithm *fminsearch* in MATLAB was used to find the desired parameters.

4.3 Results

The results from the simulation are displayed in Table 1:

Table 1: Reference and estimated parameters.

	F_d	k_d	N
Reference Parameters	246.048 N	$2.7e7$ N/m	
Estimated Parameters	242.05 N	$2.33e7$ N/m	22.55

Figure 18 shows a comparison between a reference hysteresis loop and the corresponding loop obtained by the estimated parameters of k_d , F_d and N .

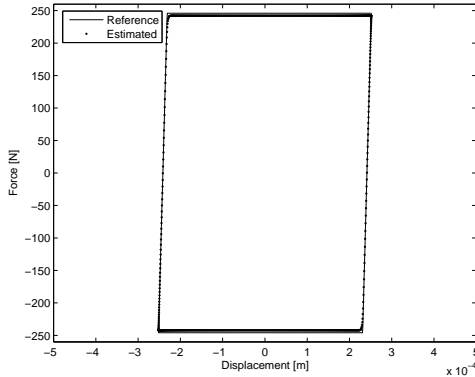


Figure 18: Comparison of the reference hysteresis loop and the loop obtained by the estimated parameters.

Figure 19 shows frequency response functions from sine-sweep measurements at different force amplitudes done on the estimated system and compared with the reference system.

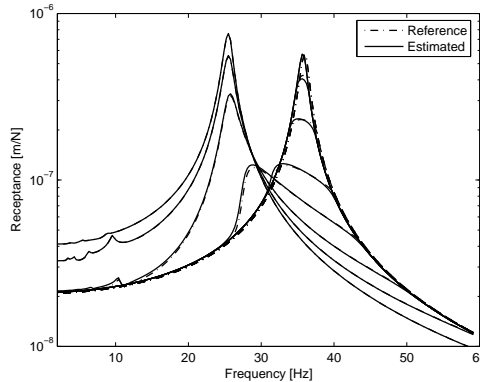


Figure 19: Comparison of frequency response functions from the reference and estimated system at different force amplitudes.

The match between the reference system and the estimated system is good but not perfect. Since the function used in the reference and estimated system are not the same and due to the fact that ten percent noise was added to all response signals, the result obtained looks promising. Also several different simulations have been carried out, not presented in this paper, both at different force amplitudes and with different initial guesses. They have all converged towards the same solution.

5 Discussions and Conclusions

Two methods of parameter estimation have been presented in this paper; with random noise and sinusoidal excitation. The method described in chapter 3 uses a least-square estimation in the frequency domain to find the parameters while the method in chapter 4 relies on the multi-harmonic-balance method and uses an optimizations routine to find suitable parameters.

A major benefit with using random noise signals is that conventional and already established methods for linear systems are used such as MIMO-technique. The method can also easily be extended to multiple-degree-of-freedoms with several nonlinear elements. However, with sine excitation and the harmonic-balance concept a wider range of nonlinear problems can be solved, including nonlinearities with memory as shown in section 4.2.

As demonstrated, both methods shows large potential in simulations and will therefore be further examined with experimental testing.

Acknowledgements

This work has been sponsored by The Knowledge Foundation in Stockholm, Sweden.

References

- [1] Julius S. Bendat. *Nonlinear system analysis and identification from random data*. Wiley, New York, 1990.
- [2] C.M. Richards and R. Singh. Identification of multi-degree-of-freedom non-linear systems under random excitations by the "reverse path" spectral method. *Journal of Sound and Vibration*, 213(4):673 – 707, 1998.
- [3] D.E. Adams and R.J. Allemand. Frequency domain method for estimating the parameters of a non-linear structural dynamic model through feedback. *Mechanical Systems & Signal Processing*, 14(4):637 – 656, 2000.
- [4] S. Marchesiello, L. Garibaldi, J.R. Wright, and J.E. Cooper. Applications of the conditioned reverse path method to structures with different types of non-linearities. In *Proceedings of the 25th International Conference on Noise and Vibration Engineering, ISMA*, pages 437 – 444, Leuven, Belgium, 2000.
- [5] Giovanna Girini and Stefano Zucca. Multi-harmonic analysis of a sdof friction damped system. In *Proceedings of 3d Youth Symposium on Experimental Solid Mechanics*, Poreta Terme, Italy, 2004.

Paper C

**On Nonlinear Parameter
Estimation with Random Noise
Signals**

Paper C is published as:

Josefsson, A., Magnevall, M. and Ahlin, K. On Nonlinear Parameter Estimation with Random Noise Signals, In *Proceedings of IMAC-XXV, Conference & Exposition on Structural Dynamics*, Orlando, USA, 2007.

On Nonlinear Parameter Estimation with Random Noise Signals

Andreas Josefsson
Martin Magnevall
Kjell Ahlin

Blekinge Institute of Technology, SE-371 79 Karlskrona, Sweden

Abstract

In the field of nonlinear dynamics it is essential to have well tested and reliable tools for estimating the nonlinear parameters from measurement data. This paper presents an identification technique based on using random noise signals, as initially developed by Julius S. Bendat. With this method the nonlinearity is treated as a feedback forcing term acting on an underlying linear system. The parameter estimation is then performed in the frequency domain by using conventional MISO/MIMO techniques. To apply this method successfully it is necessary to have some pre-information about the model structure and thus methods for nonlinear characterization and localization are studied. The paper also demonstrates the various ways the method can be formulated for multiple-degree-of-freedom systems. The implementation of the method is illustrated with simulated data as well as a practical application, where the method is used to create a dynamic model of a test-rig with a significant nonlinearity.

Nomenclature

H	Frequency Response Function
G_{xx}	Single sided, auto-spectrum of signal x
G_{xy}	Single sided, cross-spectrum of x with y
$\mathcal{F}(.)$	Fourier Transform
F, X	Force and displacement, frequency domain
f, x	Force and displacement, time domain
γ_m^2	Multiple Coherence Function

1 Introduction

The overall aim with parameter estimation is to find suitable parameters to a mathematical model, based on measurements of the inputs and outputs of a system. The mathematical model can, for instance, be based on a beforehand known model structure. This is known as parametric modelling, which will be studied in this paper. Furthermore, the systems studied contain significant nonlinearities that must be included when creating the model, hence nonlinear parameter estimation.

Systems used in engineering can generally be separated into two distinct groups; linear or nonlinear. A system, H , is said to be linear if it fulfills the principle of superposition:

$$H\{c \cdot x\} = c \cdot H\{x\} \quad (1)$$

$$H\{x_1 + x_2\} = H\{x_1\} + H\{x_2\} \quad (2)$$

A useful tool for detecting nonlinearities is the frequency response function. For a significant nonlinearity the amplitude and/or the resonance frequencies will be dependent on the excitation amplitude. Thus, the FRF's gives a linear approximation at the specific excitation amplitude and fails to fully describe the dynamics.

This work will study a method where random noise signals are used and the parameter estimation is done in the frequency domain. The methods are described in Chapter 2 and Chapter 3. This will be followed by a brief analysis of the errors introduced when doing the parameter estimation. Finally an experimental test is performed, in Chapter 5, where a nonlinear structure is studied.

2 Using Random Noise Signals for Nonlinear Systems

One of the most promising identification techniques for nonlinear parameter estimation was initially developed by Bendat [1]. The method estimates the parameters in the frequency domain with conventional Multiple-Input-Multiple/Single-Output (MIMO/MISO) procedures. The latter is often used in linear theory and is demonstrated below.

For a general linear system, with N inputs and M outputs, and noise on the measured outputs, as shown in Figure 1, a least-square solution that minimize the noise on the outputs (H_1 -estimator) can be determined at each frequency as

$$\mathbf{H}_1 = \mathbf{G}_{YX} \cdot \mathbf{G}_{XX}^{-1} \quad (3)$$

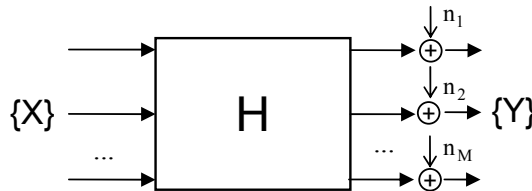


Figure 1: A Multiple-Input-Multiple-Output Model (MIMO) with noise on the outputs.

In Equation (3), \mathbf{G}_{YX} is the cross-spectral density matrix with size $(M \times N)$, \mathbf{G}_{XX} is the auto-spectral density matrix with size $(N \times N)$ and \mathbf{H}_1 is the estimated transfer matrix with size $(M \times N)$. Furthermore, a multiple coherence

function can be calculated for each output as

$$\gamma_m^2 = \frac{\mathbf{G}_{YX} \cdot \mathbf{G}_{XX}^{-1} \cdot \mathbf{G}_{YX}^H}{G_{YY}} \quad (4)$$

The size of \mathbf{G}_{YX} will be $(1 \times N)$ and G_{YY} will be a scalar since only one output is selected. Thus, M number of multiple coherence functions can be calculated for the system shown in Figure 1. A multiple coherence equal to one for all frequencies indicates that the measured response can be explained totally by the measured inputs, without the effect of extraneous noise.

The MIMO/MISO technique can also be suitable to model nonlinear mechanical systems. In many cases, a nonlinear problem can be viewed as several nonlinear feedback forces acting on an underlying linear system. Thus, artificial inputs are created and, together with the measured quantities, used as input to the MIMO/MISO model when doing the analysis. This can best be illustrated with a simple example.

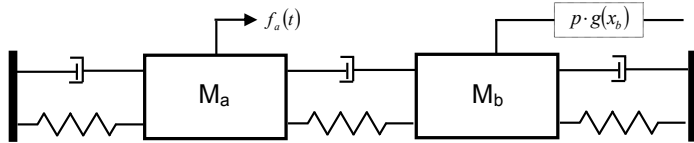


Figure 2: A nonlinear system with two degrees of freedom and a nonlinear element connected to the second dof. The nonlinearity is described with a nonlinear operator $g(\cdot)$ with a coefficient p .

The system shown in Figure 2 can be modeled in frequency domain as

$$\begin{bmatrix} H_{aa} & H_{ab} \\ H_{ba} & H_{bb} \end{bmatrix} \begin{Bmatrix} F_a \\ -P \cdot \mathcal{F}(g(x_b)) \end{Bmatrix} = \begin{Bmatrix} X_a \\ X_b \end{Bmatrix} \quad (5)$$

Alternatively, Equation (5) can be rewritten, for each row, as

$$X_a \cdot H_{aa}^{-1} + \frac{H_{ab}}{H_{aa}} \cdot P \cdot \mathcal{F}(g(x_b)) = F_a \quad (6)$$

$$X_b \cdot H_{ba}^{-1} + \frac{H_{bb}}{H_{ba}} \cdot P \cdot \mathcal{F}(g(x_b)) = F_a \quad (7)$$

There are several possible ways to formulate this problem with MIMO/MISO. With the original *Reverse-Path* technique (RP) [1], Equations (6)-(7) can be used and the analysis is accomplished as illustrated in Figure 3. With *Nonlinear-Identification-Through-Feedback-of-Outputs* (NIFO) [2], Equation (5) is used directly and the linear system and the nonlinear coefficients are estimated as shown in Figure 4.

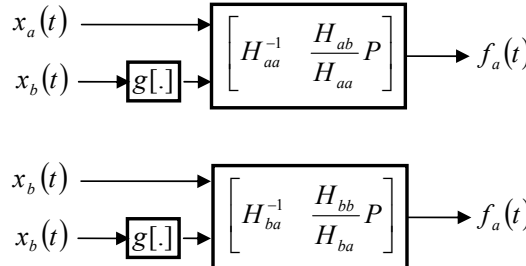


Figure 3: *Reverse-Path* (RP): Two MISO analyses are performed and using the reciprocity of the underlying linear system H_{aa}^{-1} , H_{ba}^{-1} and the nonlinear coefficient P can be identified. Here, $g(.)$ is a nonlinear operator.

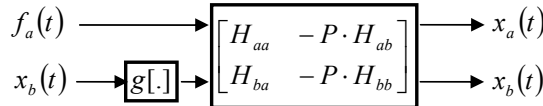


Figure 4: *Nonlinear Identification Through Feedback of Outputs* (NIFO): A single MIMO analysis is performed and using the reciprocity of the underlying linear system H_{aa} , H_{ba} and the nonlinear coefficient P can be identified. As in Figure 3, $g(.)$ is a nonlinear operator.

In the above figures, all inputs and outputs quantities are given in the time domain, to emphasize that the input signal $x_b(t)$ must pass through the nonlinear function, for instance $g(x) = x^3$, before the spectral densities can be calculated. The transfer functions are then given by Equation (3) and, in both cases, two multiple coherence functions can be calculated with Equation (4).

Notice that the transfer function $P(f)$ can be both frequency dependent and

complex. However, in this example $P(f)$ will be, after a sufficient number of averages, real-valued and constant throughout the frequency range. It is also possible to use several nonlinear inputs and obtain a polynomial fit to the true nonlinearity, as may be the case with a gap- or clearance-nonlinearity.

As shown in the above example, the NIFO-technique is more compact and easier to work with - especially for larger systems with several nonlinear elements - since MIMO is used as shown in [2, 3]. With the reverse-path technique the system must always be rewritten with force as output as in Equations (6)-(7).

In an ideal case, without any noise, both methods will give the same estimates since they are mathematically identical. However, in the presence of leakage errors and - for a real measurement - external noise, the estimates are not identical as will be discussed in chapter 4.

3 Classify Nonlinearities and Finding Nonlinear Nodes

With the method studied in previous chapter the type of nonlinearity and its location in the system must be known for the analysis to work which may seem like a major drawback. However, as will be shown in this chapter, the MIMO/MISO analysis can actually be a good tool to determine the model structure.

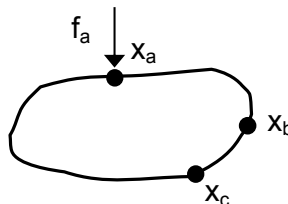


Figure 5: A blackbox system used in simulations with three degree of freedoms. A nonlinear element is connected either to a single node, or is dependent on the relative motion between two nodes.

A simulated blackbox system with three degrees-of-freedom is studied, as shown in Figure 5. The system does not fulfill the properties given by Equations (1)-

(2) since a nonlinear element is connected somewhere. By studying the FRF data it was possible to see the presence of a hardening spring nonlinearity.

Random data was simulated at all three dofs and, for the analysis, a reverse-path model was created for the system as illustrated in Figure 6. Here, a polynomial with three terms is used to describe the nonlinearity but the input signal $q(t)$ is unknown. The nonlinear element may be connected to ground from any dof or may depend on the relative motion between two dofs.

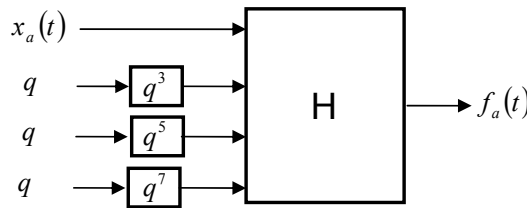


Figure 6: A reverse-path model created for the unknown system shown in Figure 5. The input signal $q(t)$ is unknown and depends on the nonlinearity.

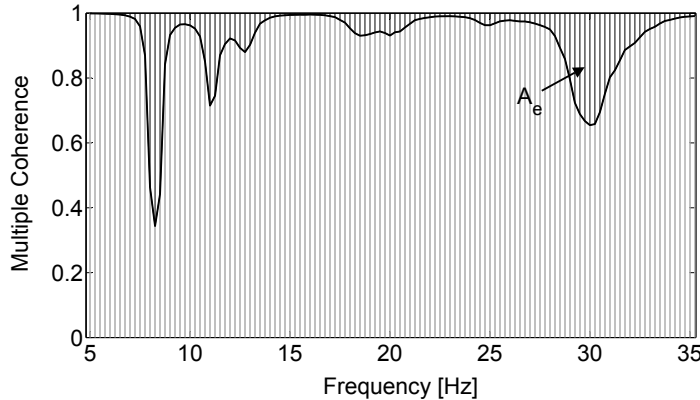


Figure 7: Multiple Coherence Function. The area shown in the figure was calculated for each combination of inputs and an error function was defined as $1/(A_e)$.

To solve this problem all possible combinations of inputs was tested and the

multiple coherence function was used to evaluate each combination. If the model is correct the multiple coherence function should be close to one for all frequency. The area, A_e , shown in Figure 7, was therefore calculated for each combination of inputs. The error function is then defined as $1/A_e$, i.e the highest value for the overall best multiple coherence.

As shown in Figure 8, this method correctly detects that the nonlinear element is connected between x_b and x_c . With the nonlinear nodes identified the test was repeated but with different nonlinear functions as shown in Figure 9. Nonlinear functions that depend on the velocity, as well as x^2 , were included for comparison. The true nonlinearity in the black-box system was a cubic function that depends on the relative motion between x_b and x_c . As illustrated with this example, random data can in many cases be used to classify nonlinearities and finding nonlinear nodes.

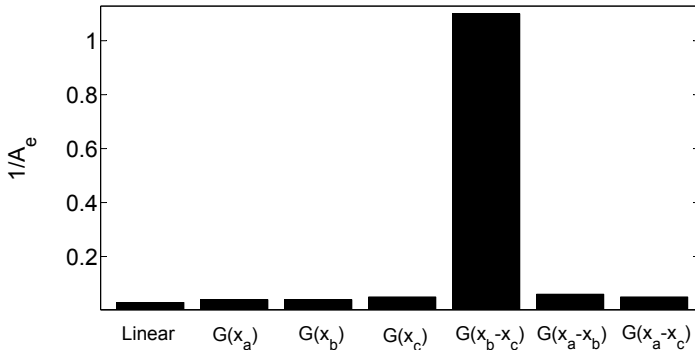


Figure 8: The method correctly detects that the nonlinear element is connected between x_b and x_c . The true nonlinearity in the black-box system was a cubic function that depends on the relative motion between x_b and x_c .

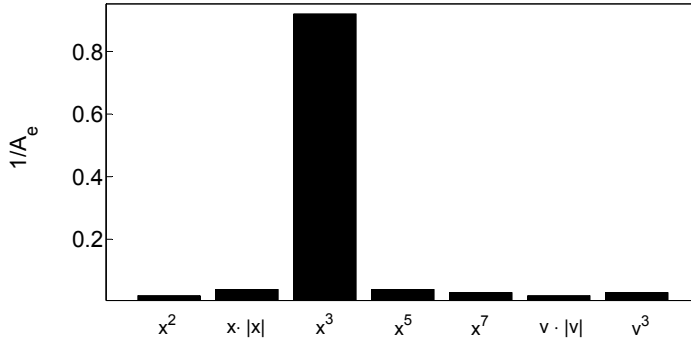


Figure 9: The presence of a cubic stiffness could clearly be seen. Nonlinear functions that depend on the velocity, as well as x^2 , were included for comparison.

4 Errors in the Analysis

When using random noise signals the estimated spectral densities will contain random and bias (systematic) errors. The effect from random errors can be controlled with a sufficient number of averages and normally, overlap processing is applied for more effective use of data. The bias error, on the other hand, does not necessarily decrease with averaging since this error comes from consistently estimating an incorrect spectrum, for instance due to aliasing or leakage.

The time-leakage effect can give a considerable random error. This error occurs when the signal is truncated and an output signal is measured which is not totally correlated with the input signal. In the beginning of the output signal, for a certain time block, there is data which depends on the input signal from the previous time block. This effect will be even more significant for lightly damped structure. The leakage error can be reduced by increasing the block length. The bias error is a function of the truncation and the window used and may also be reduced by increasing the block length.

When using MIMO/MISO to identify nonlinear systems it is essential to use a sufficient amount of data due to a relatively high sensitivity to these errors, as can clearly be seen in simulations.

Bias errors can also be introduced by contaminating noise in the measure-

ment. The H_1 -estimator, Equation (3), assumes that the noise on the input channels in the MIMO/MISO model is small and can be neglected, while the H_2 -estimator, Equation (8), neglects the noise on the output channels.

$$\mathbf{H}_2 = \mathbf{G}_{YY} \cdot \mathbf{G}_{XY}^{-1} \quad (8)$$

However, the H_2 -algorithm is less useful for multiple-input models since it is necessary to calculate an inverse to a non-square matrix if the number of inputs and outputs are not equal. For this reason, the H_1 -estimator must be used instead. The effect this will have on the parameter estimation can be demonstrated with a simulated example.

A duffing system is used with the following parameters: $M = 150$ Kg, $C = 800$ Ns/m, $K = 4 \cdot 10^6$ N/m and a cubic term $P = 2 \cdot 10^{12}$ N/m³. The excitation force was set to an amplitude were the resonance would increase approximately 15-20 percent relative to the underlying linear system.

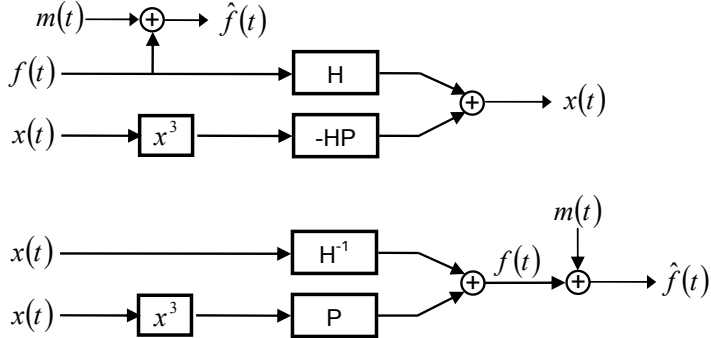


Figure 10: Analysis of a duffing system with a NIFO model (above) and the reverse-path technique (below). A small amount of noise is added to the force channel as shown in the figure.

Two possible MISO-models (NIFO and Reverse-Path) are shown in Figure 10. When doing the analysis a small amount of noise was added to the force channel as shown in the figure. The noise was designed with an RMS-value equal to approximately 5-10 percent of the RMS-value of the force signal.

The simulation was done with a sampling frequency of 512 Hz and enough data was simulated so that the analysis could be done with 2^{16} in blocksize (fft) and 200 averages with 50 percent overlap.

As shown in Figure 11, the reverse-path formulation performs better while the NIFO formulation gives a relatively large bias error since the H_1 -estimator minimizes the effect from noise at the output. This is an undesirable effect since in reality the dominating noise may be on the force signal due to force-dropouts and a very weak force signal at the resonance.

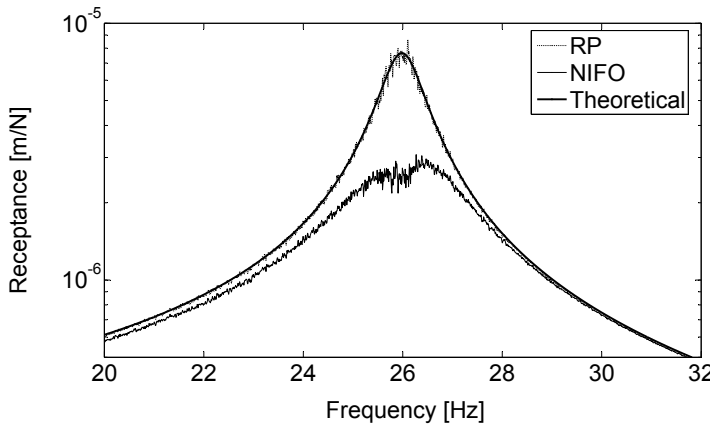


Figure 11: Estimated linear system - comparison between the two models shown in Figure 10. After averaging a large bias error is left with NIFO while the reverse-path formulation performs better since the H_1 -estimator minimizes the effect from noise at the output.

5 Experimental Test

In this chapter the methods described previously is used to model a real structure with a small but significant nonlinearity. The test structure is described in section 5.1 and the experimental setup is explained in Section 5.2 followed by results from the nonlinear analysis in Section 5.3.

5.1 The Nonlinear Testrig

The structure under test consists of a clamped beam supported at point A with two clamped thin beams as shown in Figure 12. The design comes from a similar test-rig that was developed by J. Ferreira [4] and has since then been used to verify various identification methods [4, 5].

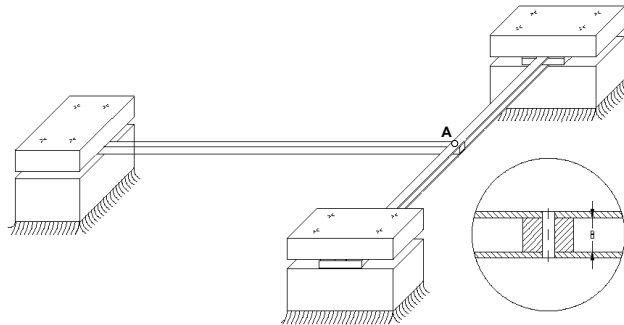


Figure 12: The structure used in the experiment consists of a clamped beam with two fixed transversal beams connected at point A. The clamped beam has a cross section of (15x8) mm with a free length of 420 mm and the two transversal beams has a cross section of (13x1.4) mm and free length 242 mm.

The properties of the beam are interesting since it can be described as a linear system (the clamped beam) with a local nonlinearity at the free end. Due to the thin geometry of the transversal beams the linear assumption is no longer valid. As illustrated in Figure 13, the geometry is changed as the beams deflect and the length along the center line of the beams (L') becomes longer than the original length L . This will introduce axial forces (N) which will increase the stiffness of the beam [6]. However, the material is still elastic and when the force is removed, the system will return to its initial position without any change in material properties. Hence, this effect is known as geometric nonlinearity since the nonlinearity is only related to changes in geometry.

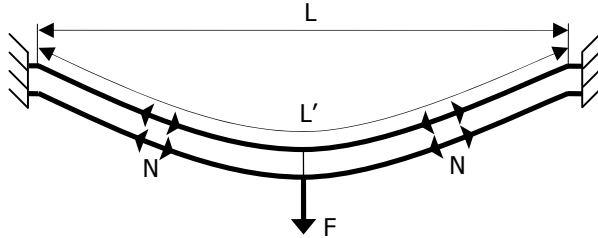


Figure 13: The transversal beams will behave nonlinearly at higher displacements. As the force is increased the beams becomes longer than the original length L , and an axial force is introduced along the beams. The stiffness will therefore increase. This effect is known as geometric nonlinearity.

Using ABAQUS® a nonlinear static model could be created. ABAQUS uses an iterative scheme where the force is applied incrementally and a Newton-Raphson solver is used to balance the nonlinear equations. Using this solver, the theoretical nonlinear force-displacement relationship at point A could be calculated as

$$F_s(x) = 1.76 \cdot 10^4 \cdot x + 2.97 \cdot 10^9 \cdot x^3 \quad (9)$$

5.2 Experimental Setup

The complete setup for the experimental test is shown in Figure 14. The structure is firmly fixed to a rigid table and a rigid steel module is used to fix the shaker. The free end of the cantilever beam was selected as a response point since the nonlinear element is connected to this point. With the identification method described previously it is necessary to measure the response at the nonlinear degree of freedoms. However, the reference point (force) can be selected at any point along the cantilever. For practical reasons the shaker is fixed to the same point and thus the linear point-flexibility and the nonlinear coefficients will be estimated.

A force transducer was mounted on the top of the beam and the accelerometer was mounted under the bottom beam as shown in Figure 15. The force signals were created in MATLAB® and Signal Calc Mobilyzer® was used to acquire the raw time data. All data analysis was done in MATLAB.

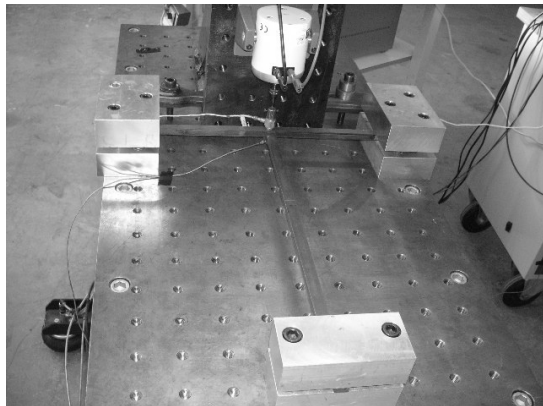


Figure 14: The complete setup for the experimental test. The structure is fixed to a rigid table and a shaker is used to excite the structure.

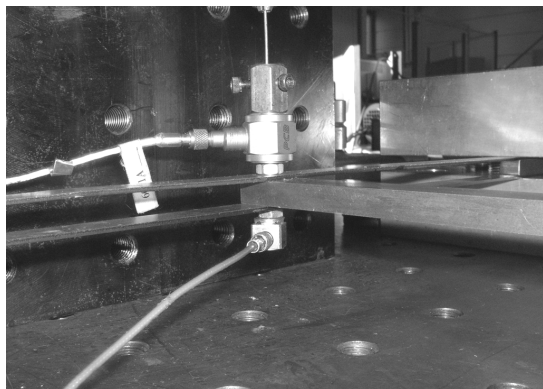


Figure 15: A detail view of the experimental setup. A force transducer and an accelerometer are used at the selected measurement point.

Initially, no evident nonlinear phenomena could be seen in the measurements due to force dropouts which only increased with higher excitation amplitude and thus avoiding the high displacement at the resonance. It was therefore necessary to create voltage signals which added more power at the resonances and carefully make sure that the force spectrum obtained was constant over

the desired frequency range.

5.3 Analysis of Experimental Data

The structure behaves linearly at low excitations and it was therefore necessary to find level of the excitation where the nonlinear effects are clear. A force amplitude which made the resonance move approximately 15% was selected for nonlinear analysis.

In the following two figures, two nonlinear analyses are compared with the raw FRF. The latter is the FRF obtained with conventional linear theory (SISO). Thus, the raw FRF is calculated without any compensation for nonlinear effects.

The nonlinear effects can clearly be seen in the raw measured FRF. A disturbance occurs at approximately $2f_0$ and $3f_0$. This disturbance can also be seen in the coherence function. A part of the response that is obtained at the resonance frequency will, due to the nonlinearity, create higher frequency response which the linear model fails to describe.

Two reverse-path models were created. First, a cubic function was used to describe the nonlinearity and the result can be studied in Figure 16. In the second model, shown in Figure 17, a cubic- and a square are used to describe the nonlinearity. It could be seen that the true nonlinearity was a non-symmetric function and thus a cubic function was not enough to describe this behavior. Figure 18 shows the estimated linear system with different methods. The true linear FRF was measured at very low excitation where the stiffness nonlinearity is unaffected. As shown in the figure, the estimated linear system with NIFO techniques gives larger amplitude errors. One possible explanation for this was given in chapter 4; if the force signal is contaminated with noise, the reverse-path technique will perform better.

The real parts of the nonlinear coefficients are shown in Figure 19. By definition, for a zero-memory nonlinear system, the imaginary parts of the nonlinear coefficients should be relatively small after a sufficient number of averages. For this experiment, the imaginary part was approximately ten times smaller than the real part after averaging. This may indicate a small amount of nonlinear damping which was not considered in the modeling.

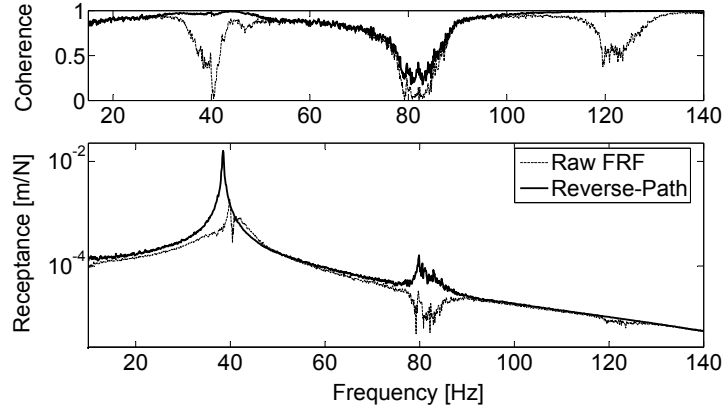


Figure 16: The Raw FRF (linear theory) compared with the linear system estimated with reverse-path technique. A cubic function is used to describe the nonlinearity. As shown, the FRF and the coherence are improved at the resonance and at three times the resonance frequency.

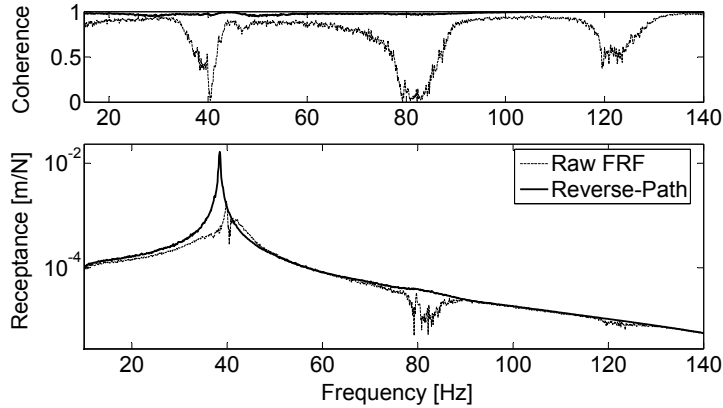


Figure 17: The Raw FRF (linear theory) compared with the linear system estimated with reverse-path technique. A cubic- and a square- function are used to describe the nonlinearity. As shown, the FRF and the coherence are considerably improved over the frequency range.

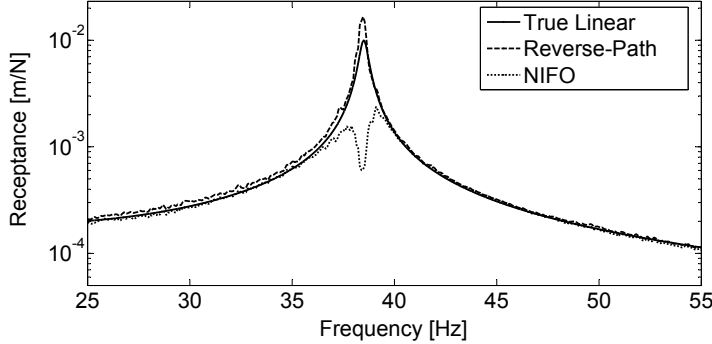


Figure 18: The estimated linear system with different methods. The true linear FRF, used as reference, was measured at very low excitation. As shown, the estimated linear system with NIFO techniques gives larger amplitude errors.

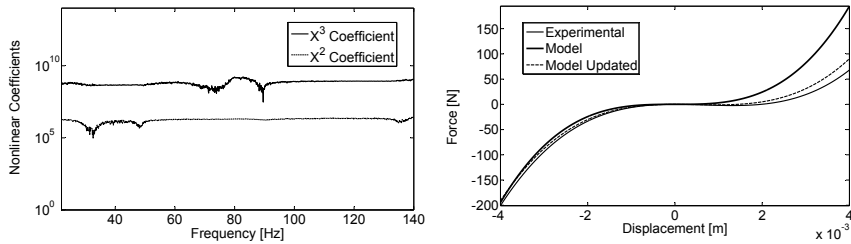


Figure 19: The nonlinear coefficients (left) and the estimated nonlinearity compared with the model (right). The nonlinear static model could be updated with the experimental parameters.

The estimated cubic coefficient was $2.2 \cdot 10^9 \text{ N/m}^3$, which was considered to be reasonable in comparison with the theoretical value from section 5.1. Due to the non-symmetric force, a square coefficient was identified as $4 \cdot 10^6 \text{ N/m}^2$. When studying the test rig it could be seen that the slender beams were not perfectly aligned with the cantilever beam, and thus creating a non-symmetric force. When this effect was included in the nonlinear static model, a better correlation between the experimental results and the simulated results could be obtained.

6 Conclusion

Nonlinear parameter estimation can be performed with random noise signals by using conventional MIMO/MISO techniques. The methods described in this work treat the nonlinearity as a feedback forcing term acting on an underlying linear system. Thus, the true linear system and the nonlinear coefficients can be estimated by measuring the input and output quantities.

The approach that is used in this work requires some pre-information about the type of nonlinearity present, and its location in the system. If this information cannot be obtained before the analysis it may be possible to try a set of different combinations and then utilize the multiple coherence function as shown in Chapter 3.

When using MIMO/MISO there are several possible ways to formulate a nonlinear problem. Two methods have been studied in simulations and experiments - referred to as NIFO and Reverse-Path. As shown in this work, it is essential to create nonlinear models which best compensate for the errors introduced with contaminating noise.

An experimental test was done on a structure with a significant nonlinearity and the results, presented in section 5.3, shows that the underlying linear system and the coefficients describing the nonlinearity could be identified. When comparing the results with linear theory a clear improvement could be seen: The estimated linear system is free from disturbance and with a correct resonance frequency. Thus, a simple but very useful application of the methods may be to make a better estimate of the linear system, for instance when comparison are made to a numerical linear model.

Acknowledgment

Financial support from the Swedish Knowledge Foundation is gratefully acknowledged

References

- [1] Julius S. Bendat. *Nonlinear System Analysis and Identification from Random Data*. John Wiley Sons, Inc., first edition, 1990.
- [2] D.E. Adams and R.J. Allemand. A frequency domain method for estimating the parameters of a non-linear structural dynamic model through feedback. *Mechanical systems and Signal Processing*, 14(4), 2000.
- [3] Martin Magnevall, Andreas Josefsson, and Kjell Ahlin. On nonlinear parameter estimation. *International Conference on Noise and Vibration Engineering (ISMA2006)*, s. 3817-3831, 2006.
- [4] J.V. Ferreira. *Dynamic Response Analysis of Structures with Nonlinear Components*. PhD thesis, Imperial College, London, 1998.
- [5] H. R. E. Siller. *Non-linear modal analysis methods for engineering structures*. PhD thesis, Imperial College, London, 2004.
- [6] Q. Jing, T. Mukherjee, and G.K Fedder. Large-deflection beam model for schematic-based behavioral simulations in nodas. *Proceedings of the International Conference on Modeling and Simulation of Microsystems*, 2002.

Paper D

**Nonlinear Structural
Identification by the “Reverse
Path” Spectral Method**

Paper D is published as:

Magnevall, M., Josefsson, A., Ahlin, K., Broman, G. Nonlinear Structural Identification by the “Reverse Path” Spectral Method, *Journal of Sound and Vibration*, vol. 331, no. 4, pp. 938-946, 2012.

Nonlinear Structural Identification by the “Reverse Path” Spectral Method

Martin Magnevall^{1,2}
Andreas Josefsson²
Kjell Ahlin²
Göran Broman^{2,3}

¹ AB Sandvik Coromant, SE-811 81 Sandviken, Sweden

² Blekinge Institute of Technology, SE-371 79 Karlskrona, Sweden

³ Luleå University of Technology, SE-971 87 Luleå, Sweden

Abstract

When dealing with nonlinear dynamical systems, it is important to have efficient, accurate and reliable tools for estimating both the linear and nonlinear system parameters from measured data. An approach for nonlinear system identification widely studied in recent years is "Reverse Path". This method is based on broad-band excitation and treats the nonlinear terms as feedback forces acting on an underlying linear system. Parameter estimation is performed in the frequency domain using conventional multiple-input-multiple-output or multiple-input-single-output techniques. This paper presents a generalized approach to apply the method of "Reverse Path" on continuous mechanical systems with multiple nonlinearities. The method requires few spectral calculations and is therefore suitable for use in iterative processes to locate and estimate structural nonlinearities. The proposed method is demonstrated in both simulations and experiments on continuous nonlinear mechanical structures. The results show that the method is effective on both simulated as well as experimental data.

1 Introduction

In the past years much effort has been put into the field of parameter estimation of nonlinear dynamical systems. A large number of methods have been developed, but there is still no method applicable to a general structure with an arbitrary nonlinearity. A survey of the most common current methods is found in [1]. An important method, widely studied in recent years, is the "Reverse Path" method. This is based on broad-band excitation and was initially developed by Bendat et al. [2, 3] and Rice et al. [4, 5] and is thoroughly described in [6]. "Reverse Path" treats the nonlinearities as force feedback terms acting on an underlying linear system. The parameter estimation is performed in the frequency domain using conventional multiple-input-multiple-output (MIMO) or multiple-input-single-output (MISO) techniques and estimates of both the underlying linear properties and the nonlinear coefficients are obtained. "Reverse Path" has proven to work well both in simulations and in experimental tests on various mechanical systems with local nonlinearities [7, 8, 9, 10, 11], which indicates that the method is robust and well suited to use in engineering applications within nonlinear structural identification. Applications of the "Reverse-Path" method in other fields are, e.g. Esmonde et al. [12] who successfully applied the method for parameter estimation of nonlinear squeeze film dynamics, and Liagre et al. [13] who applied the "Reverse-Path" method in offshore engineering.

The method of "Reverse Path" requires the form of the nonlinearities as well as their locations to be known beforehand in order to provide accurate estimates. Otherwise an iterative approach is required for estimating the location [14] and/or the nonlinear functional form [7, 11]. For this to be performed in an efficient way, a method that can apply "Reverse Path" on a general nonlinear system is needed. Rice et al. [5] developed a method for arbitrary multi-degree-of-freedom (MDOF) systems with localized nonlinearities using unconditioned (partially correlated) inputs. However, the method requires that the system is excited in all measurement points, which can be impractical for complex nonlinear structures. Richards et al. [15] developed a general approach for MDOF systems based on conditioned (uncorrelated) inputs which only requires a single excitation point. A disadvantage with this method is the significant complication of the problem formulation due to the need for conditioned inputs.

This paper presents a method which applies the "Reverse Path" method on a

general MDOF system with localized nonlinearities. The approach uses unconditioned inputs and assumes that the location of the nonlinearities is known beforehand and that response measurements can be obtained at the nonlinear nodes. Excitation is only needed in one point which can be located away from the nonlinearities. The method is based on discretization of the continuous nonlinear structure by the measurement points. Then, using reciprocity and position vectors describing the location of the nonlinearities, both the underlying linear system and the nonlinear coefficients can be estimated in a straightforward way.

2 Problem Formulation

Consider a MDOF system with localized nonlinearities, described by:

$$\mathbf{M}\ddot{\mathbf{x}}(t) + \mathbf{C}\dot{\mathbf{x}}(t) + \mathbf{K}\mathbf{x}(t) + \mathbf{nl}(\mathbf{x}(t), \dot{\mathbf{x}}(t), \ddot{\mathbf{x}}(t)) = \mathbf{f}(t) \quad (1)$$

where \mathbf{M} , \mathbf{C} and \mathbf{K} are the system’s mass damping and stiffness matrices, respectively, all having the size $(N \times N)$. $\ddot{\mathbf{x}}(t)$, $\dot{\mathbf{x}}(t)$ and $\mathbf{x}(t)$ are the acceleration, velocity and displacement vectors, respectively, having the size $(N \times 1)$. The vector $\mathbf{f}(t)$, having the size $N \times 1$, contains the external forces acting on the system and $\mathbf{nl}(t)$, having the size $N \times 1$, is the nonlinear restoring force vector:

$$\mathbf{nl}(t) = \sum_{m=1}^M P_m \mathbf{w}_m y_m(\mathbf{x}(t), \dot{\mathbf{x}}(t), \ddot{\mathbf{x}}(t)) \quad (2)$$

P_m is the coefficient related to the nonlinear function y_m and \mathbf{w}_m , having the size $N \times 1$, is a vector describing the location of nonlinear element m . For an example see Equation (13a). M is the total number of nonlinear elements. Examples of nonlinear functions are given in Equations (3) and (4).

$$y_m(t) = \mathbf{w}_m^T \mathbf{x}(t) |\mathbf{w}_m^T \mathbf{x}(t)| \quad \text{Square hardening spring} \quad (3)$$

$$y_m(t) = ((\mathbf{w}_m^T \dot{\mathbf{x}}(t))^3 \quad \text{Cubic damping} \quad (4)$$

It is possible to use polynomial estimates of the nonlinearities containing several terms, which is useful when modeling, for example, structural play, saturation effects or systems with unsymmetric nonlinear behavior. Then, each individual term in the polynomial approximation is treated as a separate nonlinearity

giving as many nonlinear elements and position vectors as there are terms in the polynomial.

Combining Equations (1) and (2) in the frequency domain yields:

$$\mathbf{X}(\omega) + \mathbf{H}(\omega) \sum_{m=1}^M P_m(\omega) \mathbf{w}_m Y_m(\omega) = \mathbf{H}(\omega) \mathbf{F}(\omega) \quad (5)$$

where $\mathbf{H}(\omega)$ is the frequency response function (FRF) matrix of the underlying linear system and $Y_m(\omega)$ is the Fourier transform of the nonlinear function $y_m(t)$, Equation (6). In order to preserve generality, the nonlinear coefficients P_m in Equation (5) are allowed to be frequency dependent.

$$Y_m(\omega) = \mathcal{F}\left(y_m(\mathbf{x}(t), \dot{\mathbf{x}}(t), \ddot{\mathbf{x}}(t))\right) \quad (6)$$

The “Reverse Path” formulation requires the measured displacements and the nonlinear feedback forces to be used as inputs, and the measured forces as output. Now, based on Equation (5) and the assumption that the system is only excited in one node, q , the following “Reverse Path” formulation can be obtained for every response node i :

$$\underbrace{\begin{bmatrix} \frac{1}{H_{i,q}(\omega)} & \frac{\mathbf{H}_{i,:}(\omega)P_1(\omega)\mathbf{w}_1}{H_{i,q}(\omega)} & \frac{\mathbf{H}_{i,:}(\omega)P_2(\omega)\mathbf{w}_2}{H_{i,q}(\omega)} & \dots & \frac{\mathbf{H}_{i,:}(\omega)P_M(\omega)\mathbf{w}_M}{H_{i,q}(\omega)} \end{bmatrix}}_{\mathbf{B}_i(\omega)} \underbrace{\begin{bmatrix} X_i(\omega) \\ Y_1(\omega) \\ Y_2(\omega) \\ \vdots \\ Y_M(\omega) \end{bmatrix}}_{\mathbf{R}_i(\omega)} = F_q(\omega) \quad (7)$$

$H_{i,q}(\omega)$ refers to the value in $\mathbf{H}(\omega)$ at row i in column q and $\mathbf{H}_{i,:}(\omega)$ is a vector containing all values in row i . Eq. (7) is represented by the MISO system in Figure 1,

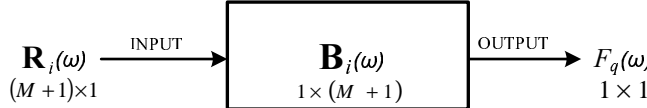


Figure 1: Displacement and nonlinear restoring forces are used as input and the force as output in a MISO model.

if the H_1 estimator is applied to this system, minimizing the noise on the measured force, $\mathbf{B}_i(\omega)$ is calculated as:

$$\mathbf{B}_i(\omega) = \mathbf{G}_{F_q \mathbf{R}_i}(\omega) \mathbf{G}_{\mathbf{R}_i \mathbf{R}_i}^{-1}(\omega) \quad i \in [1, 2, \dots, N] \quad (8)$$

where $\mathbf{G}_{F_q \mathbf{R}_i}(\omega)$ is the cross spectral density matrix between the measured force, $F_q(\omega)$, and the input vector, $\mathbf{R}_i(\omega)$. $\mathbf{G}_{\mathbf{R}_i \mathbf{R}_i}(\omega)$ is the auto spectral density matrix of the input vector $\mathbf{R}_i(\omega)$.

$$\mathbf{R}_i(\omega) = [X_i(\omega) \quad Y_m(\omega) \quad Y_{m+1}(\omega) \quad \dots \quad Y_M(\omega)]^T \quad (9)$$

As seen in Equation (9), the vector $\mathbf{R}_i(\omega)$ contains the displacement of node i in the frequency domain and the Fourier transforms of the nonlinear functions. The only difference between the vectors $\mathbf{R}_i(\omega)$ and $\mathbf{R}_{i+1}(\omega)$ is the linear displacements $X_i(\omega)$ and $X_{i+1}(\omega)$. Thus, it is possible to calculate as many FRFs $\mathbf{B}_i(\omega)$ as there are measured responses.

When all the FRFs $\mathbf{B}_i(\omega)$ are calculated the nonlinear coefficients $P_m(\omega)$ are estimated by:

$$P_m(\omega) = \frac{B_q^{m+1}(\omega)}{B_q^1(\omega)} \sum_{i=1}^N w_m^i B_i^1(\omega) \quad (10)$$

The subscript refers to the vector used and the superscript tells the specific position in that vector. q refers to the input, i.e. the driving point. A complete column, $H_{:,q}(\omega)$, in the FRF matrix of the underlying linear system can also be estimated by:

$$H_{i,q}(\omega) = \frac{1}{B_i^1(\omega)} \quad (11)$$

Applying Equations (8)-(11), both the nonlinear coefficients and the column and row (reciprocity) of the underlying linear system corresponding to the excitation node, q , are obtained. By modal parameter estimation the complete FRF matrix of the underlying linear system can be estimated and used to build a nonlinear model of the studied system.

The presented method provides a structured approach to apply the method of “Reverse Path” to general nonlinear MDOF systems. The method requires that the location of the nonlinearities is known and that response measurements can be obtained in the nonlinear nodes and at the node of excitation. There are, however, no restrictions on either the number of nonlinear elements or the number of terms in the polynomials or power series used to estimate the structural nonlinearities. Additionally, the method only requires excitation in one node and there is no restriction on the force location.

3 Simulations

A cantilever beam with two cubic nonlinearities is used in the simulation, Figure 2. One nonlinearity is located between node 1 and ground and one is located between nodes 2 and 3. The excitation force is applied in node 4 (Gaussian random noise), away from the nonlinearities. The first five modes of the beam are taken into account in the simulation. To further explain the method derived in section 2, a few steps in the identification is shown by specific equations, only valid for this model, which are then related to the corresponding general equation in section 2. For the sake of brevity, the frequency dependence (ω) is dropped in the following sections.

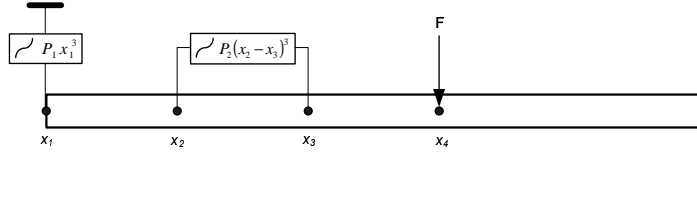


Figure 2: The cantilever beam with two nonlinearities used in the simulation. The specifications of the beam are: Density: $\rho = 2700 \text{ kgm}^{-3}$; Youngs Modulus: $E = 70 \text{ GPa}$; Length: $L = 1 \text{ m}$; Mass: $m = 1.1 \text{ kg}$; Area moment of inertia: $I = 7.34 \cdot 10^{-9} \text{ m}^4$. The nodes 1 – 4 are located at $l = 1.0, 0.8, 0.6$ and 0.4 m . The nonlinear parameters are: $P_1 = 7 \cdot 10^6 \text{ Nm}^{-3}$ and $P_2 = 3 \cdot 10^8 \text{ Nm}^{-3}$

The system in Figure 2 can, in the frequency domain, be expressed as:

$$\underbrace{\begin{bmatrix} H_{11} & H_{12} & H_{13} & H_{14} \\ H_{21} & H_{22} & H_{23} & H_{24} \\ H_{31} & H_{32} & H_{33} & H_{34} \\ H_{41} & H_{42} & H_{43} & H_{44} \end{bmatrix}}_{\mathbf{H}} \begin{bmatrix} -P_1 \mathcal{F}(x_1^3) \\ -P_2 \mathcal{F}((x_2 - x_3)^3) \\ P_2 \mathcal{F}((x_2 - x_3)^3) \\ F_4 \end{bmatrix} = \begin{bmatrix} X_1 \\ X_2 \\ X_3 \\ X_4 \end{bmatrix} \quad (12)$$

where \mathbf{H} is the FRF matrix of the underlying linear system and all nonlinearities are expressed as external forces acting on that system. For this specific analysis, the position vectors \mathbf{w}_1 and \mathbf{w}_2 and nonlinear functions Y_1 and Y_2 becomes:

$$\mathbf{w}_1 = [1 \ 0 \ 0 \ 0]^T; \quad \mathbf{w}_2 = [0 \ 1 \ -1 \ 0]^T \quad (13a)$$

$$Y_1 = \mathcal{F}\left(\left(\mathbf{w}_1^T \mathbf{x}\right)^3\right); \quad Y_2 = \mathcal{F}\left(\left(\mathbf{w}_2^T \mathbf{x}\right)^3\right) \quad (13b)$$

From Equation (12), an expression for the displacement X_4 is derived:

$$F_4 H_{44} - P_1 H_{41} \mathcal{F}(x_1^3) - P_2 (H_{42} - H_{43}) \mathcal{F}((x_2 - x_3)^3) = X_4 \quad (14)$$

Solving for F_4 and putting the equation in matrix form yields:

$$\underbrace{\begin{bmatrix} \frac{1}{H_{44}} & P_1 \frac{H_{41}}{H_{44}} & P_2 \frac{(H_{42} - H_{43})}{H_{44}} \end{bmatrix}}_{\mathbf{B}_4 = \mathbf{G}_{F_4} \mathbf{R}_4 \mathbf{G}_{\mathbf{R}_4}^{-1} \mathbf{R}_4} \underbrace{\begin{bmatrix} X_4 \\ \mathcal{F}(x_1^3) \\ \mathcal{F}((x_2 - x_3)^3) \end{bmatrix}}_{\mathbf{R}_4} = F_4 \quad (15)$$

Eq. (15) contains the FRF \mathbf{B}_4 from Equation (8). By calculating the rest of the FRFs (\mathbf{B}_3 , \mathbf{B}_2 and \mathbf{B}_1) it is possible to estimate the nonlinear coefficients as well as the FRFs of the underlying linear system using Equations (10)-(11).

The FRFs of the underlying linear systems for all response locations were estimated as well as the two nonlinear coefficients. The estimated linear FRF in node 1 from the nonlinear analysis was then compared with the true FRF of the underlying linear system. The raw-FRF (estimated FRF when the system is considered linear) was also calculated and compared to the results from the nonlinear analysis. The frequency range used for the parameter estimation was [5 – 800] Hz. Results are shown in Figures 3-6 and the simulation parameters are listed in Table 1.

Table 1: Simulation parameters

Signal Length	Blocksize	Window	Overlap	f_s
2,097,152 samples	131,072 samples	Hanning	50 %	4096 Hz

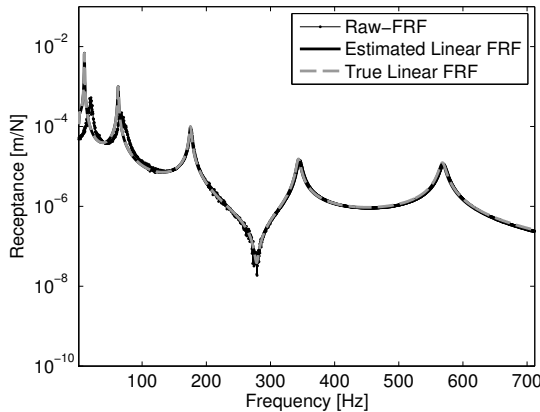


Figure 3: The underlying linear system obtained from “Reverse Path” compared to the raw-FRF obtained using linear analysis in node 1; Entire frequency range used in the nonlinear analysis.

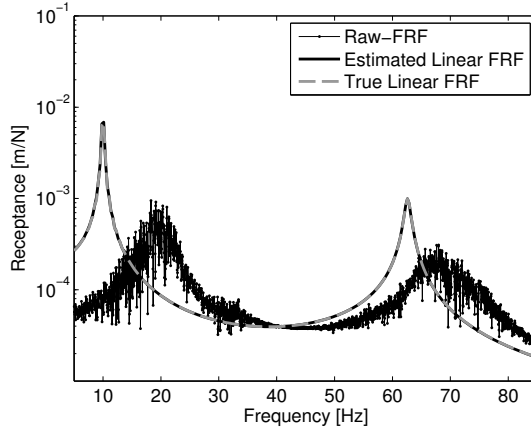


Figure 4: The underlying linear system obtained from “Reverse Path” compared to the raw-FRF obtained using linear analysis in node 1; The first two modes.

Figs. 3 and 4 clearly shows that the estimated underlying linear system is close to the true linear system. Also a big improvement between the raw-FRF and the FRF obtained from the nonlinear analysis can be seen.

As seen in Figure 5, the estimated nonlinear coefficients are constant over the entire frequency range. This is expected since the nonlinear functions used are displacement dependent. If the studied system only contains zero memory nonlinearities, i.e. nonlinear functions $nl(x, \dot{x}, \ddot{x})$ having output at any given time t that are nonlinear functions of $x(t), \dot{x}(t), \ddot{x}(t)$ at the same instant of time, the estimated coefficients should be real after averaging. Therefore, only the spectral mean value of the real parts are compared with the theoretical values. The estimated nonlinear coefficients are $P_1 = 7.02 \cdot 10^6 \text{ Nm}^{-3}$ and $P_2 = 3.07 \cdot 10^8 \text{ Nm}^{-3}$. The imaginary parts of the nonlinear coefficients are several orders of magnitude lower than the real parts.

For linear SISO systems the ordinary coherence function is often used as a goodness-of-fit measure. Generally the ordinary coherence function is defined as the linear relationship between any two signals. However, for MIMO and MISO systems the ordinary coherence can be misleading due to the influence

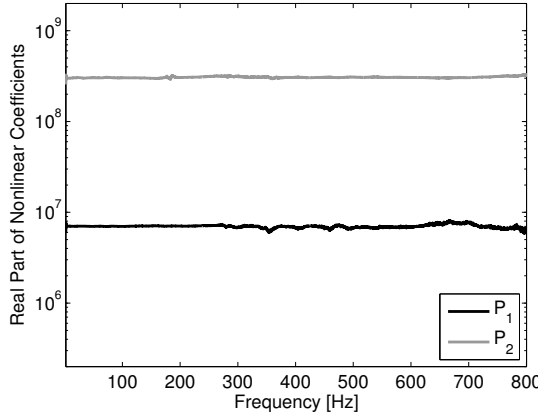


Figure 5: The real parts of the estimated nonlinear coefficients P_1 and P_2 .

of additional inputs not considered in the spectral estimation. For MIMO and MISO systems the multiple coherence is used instead. The multiple coherence gives the linear relationship between all the inputs and any given output. The “Reverse Path” formulation treats the nonlinearities as additional inputs acting on an underlying linear system and considering the case with excitation in only one node, the result is a MISO formulation with linear relationships between the inputs and the output. Thus, the multiple coherence is useful as a goodness-of-fit measure even for nonlinear systems. The multiple coherence can be calculated as:

$$\gamma_i^2 = \frac{\mathbf{G}_{F\mathbf{R}_i} \mathbf{G}_{\mathbf{R}_i \mathbf{R}_i}^{-1} \mathbf{G}_{F\mathbf{R}_i}^H}{\mathbf{G}_{FF}} \quad (16)$$

where \mathbf{G}_{FF} is a scalar since there is only one output. Eq. (16) shows that there exist as many multiple coherence functions as there are measured nodes in the system. The subscript i refers to the node used. It should be noted that both the real and imaginary parts of the nonlinear coefficients P_m will affect the multiple coherence. Usually only the spectral mean of the real part of P_m is used in the identification and therefore the multiple coherence can be misleading if the imaginary part of P_m is significant.

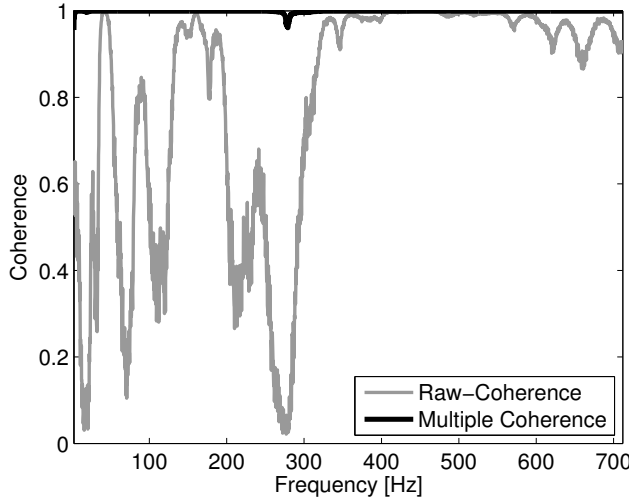


Figure 6: Raw-coherence (linear analysis) compared with the multiple coherence (nonlinear analysis) based on the structure’s response in node 1.

The multiple coherence from node 1, Figure 6, is almost equal to unity for all frequencies. Since the imaginary parts of the estimated coefficients P_m are very small compared to the real parts, this is an indication of a good model. The improvement compared with the raw-coherence (ordinary coherence) obtained from linear analysis is evident.

4 Experimental Tests

Successful applications of “Reverse Path”, on mechanical structures, using experimental data has been reported in e.g. [7, 8, 10]. The test-rigs used in these experiments consists of cantilever beams with a geometrical nonlinearity attached to the free end. These systems have well separated modes and the nonlinear element mainly affects the first bending mode. To investigate how the method behaves when the studied system has closely spaced modes which are affected by a nonlinear element, the set-up shown in Figure 7 is proposed. This test-rig consists of a T-beam with a local geometric nonlinearity. The setup has two closely spaced modes, the first bending and torsional mode, both strongly affected by the nonlinearity. Two slender beams fixed in their

end points and connected to the T-beam constitutes the nonlinearity, Figure 7. These beams will, when subjected to large displacements, behave nonlinearly due to geometrical effects. The system is modeled as a linear system with a local nonlinearity connected to ground. Consequently, the structure can be approximated as a linear system (the T-beam structure) with a local nonlinearity. The system is excited in node 5 and responses are measured in nodes 1 to 6, where node 5 is the nonlinear node. The position vector used for this analysis is $\mathbf{w} = [0 \ 0 \ 0 \ 0 \ 1 \ 0]^T$.

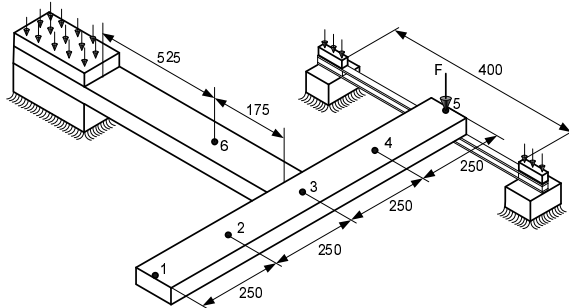


Figure 7: The T-Beam structure (made of aluminum) used in the experiment. A local nonlinearity is introduced in node 5 by two thin beams, 1.5 mm thick (steel). At large displacements, these thin beams will be affected by a geometric nonlinearity. Measurements are given in [mm].

The experimental setup is shown in Figure 8. The left picture show the entire setup with the shaker mounted in node 5, the right figure shows a detailed view of the shaker mounting and the attachment of the thin beams. The force transducer is firmly attached to the test structure using a bolted connection. Six accelerometers are used to measure the responses in all 6 nodes. The time data is collected with a SignalCalc® Mobilyzer unit and the post processing is performed in MATLAB®.

Since the nonlinear effects in the system are higher at large displacement levels, it is important to use a sufficiently high excitation force to get a clear nonlinear effect in the system's response. The RMS value of the force used in the measurement is 14.3 N. Due to force dropouts around the resonances, the nonlinear effects are reduced substantially if a flat force spectrum is supplied to the shaker. The force dropouts needs to be compensated for by adding extra

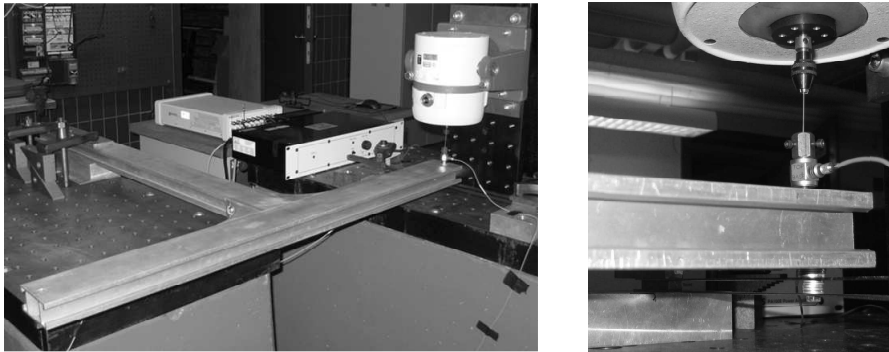


Figure 8: The experimental setup. The left picture shows the entire setup with the shaker mounted in node 5. To the right, a detailed picture of the shaker mounting and the attachment of the thin beams.

energy into the excitation signal around the resonances to sufficiently excite the nonlinearity. The ordinary coherence function is a useful indicator when determining a suitable excitation level. If the ordinary coherence (raw-coherence) deviates from unity this is an indication of nonlinear effects present in the system response. Also, inspecting the frequency spectrum of the measured force provides information about problems with force dropouts.

An uncertainty when analyzing the experimental data is the nonlinear functional form. Instead of using polynomial estimates with several terms to model a nonlinearity, power series with non-integer exponents can be used to reduce the number of nonlinear terms needed, [7, 8]. The exponents of the power series best describing the nonlinear functional form can, for example, be found by an iterative search routine. As shown previously, the multiple coherence function can be used as a measure of the goodness-of-fit of the estimated nonlinear system and is therefore useful as objective function when searching for an optimal description of the nonlinearity. In this case the area under the multiple coherence function was used as objective function and a simplex search algorithm was used to maximize this function. To make as good an estimate as possible, information regarding the studied system is needed. The ordinary coherence (raw-coherence) is a useful indicator of the nonlinear functional form. For example, in Figure 9 the ordinary coherence deviates from unity around the system resonances and at three times these frequencies. Also noticeable is that

there is no deviation at twice the resonance frequencies which indicates only odd harmonics in the nonlinear response. Since only odd harmonics are present, the nonlinear functional form can be assumed to have odd symmetry, i.e. the nonlinearity behaves the same for both positive and negative displacements, but with different sign. Further more, the nonlinearity is geometrical, which in theory has a cubic nonlinear form. Thus, the nonlinear functional form chosen for the optimization is $\text{sign}(x)|x^\alpha|$ with $\alpha = 3$ as initial value. The best fit was obtained with $\text{sign}(x)|x^{2.5872}|$ as the nonlinear function. The nonlinear parameter estimation was done with a sampling frequency $f_s = 2604.2$ Hz, block size 32768 samples, Hanning window, 50% overlap and 120 averages. These settings were enough to reach sufficient noise reduction and thus provide an accurate estimate of the system's frequency response. All responses were measured using accelerometers and the signals were numerically double integrated to displacement before the nonlinear analysis. After integration, a high-pass filter was applied to the signals in order to remove uncertainties caused by the low frequency characteristics in the numerical integration. A Butterworth filter of order 3 was used and the data were filtered in both directions to obtain a zero phase filter response. The cut-off frequency for the high pass filter was set to 2 Hz.

Fig. 9 shows the raw-coherence from the linear analysis (SISO) compared with the multiple coherence obtained from the nonlinear analysis (MISO). The nonlinear effect is clearly visible in the raw-coherence, especially around the resonances. It is clear that the raw-coherence is close to unity above 55 Hz with the exception for the region around 90 Hz. This indicates a perfect linear relationship between the input and output of the system. Due to the lack of nonlinear effects above 55 Hz, the frequency span [15 – 55] Hz was used when estimating the nonlinear coefficient. The real and imaginary part of the estimated coefficient are shown in Figure 10. Since the nonlinearity is expected to be of zero memory type, only the real part is used in the analysis. The real part of the estimated coefficient is constant over the entire frequency range and the spectral mean value is $1.2504 \cdot 10^8 \text{ Nm}^{-2.5872}$. The imaginary part changes with frequency and is on average 25 times smaller than the real part.

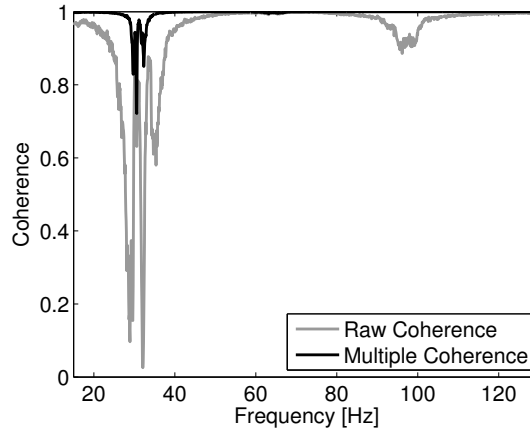


Figure 9: Raw-coherence (ordinary coherence) compared with multiple coherence.

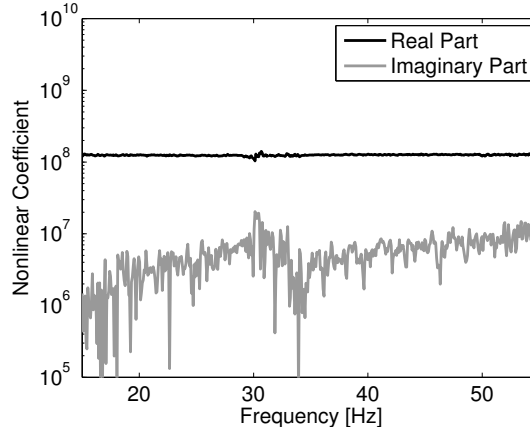


Figure 10: Estimated nonlinear coefficient

The estimated point FRF, H_{55} , of the underlying linear system obtained from nonlinear analysis is compared to the raw-FRF obtained by linear analysis, Figure 11. The nonlinear effect is clear in the heavily distorted raw-FRF.

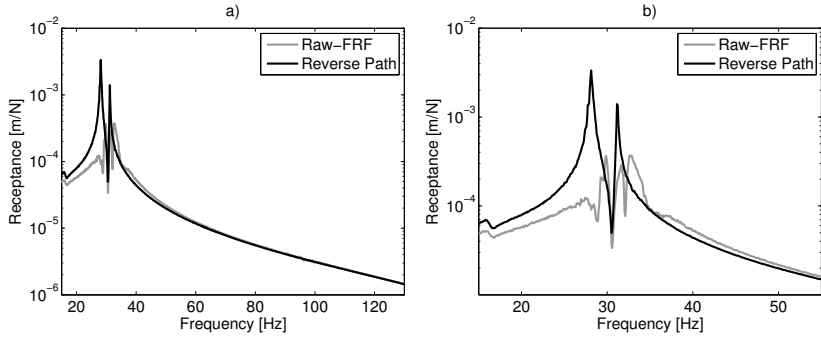


Figure 11: Estimated point FRF, H_{55} , from the nonlinear analysis compared with the FRF obtained using linear analysis, raw-FRF. a) effects over a wide frequency range b) effects around the resonance frequencies.

To verify the results from the dynamic tests, a static measurement of the structural stiffness was performed to get a second estimate of the nonlinearity. The nonlinear function obtained from this measurement is compared to the nonlinear function from the “Reverse Path” analysis in Figure 12. The estimated nonlinear coefficients are listed in Table 2.

Table 2: Estimated nonlinear coefficients

	“Reverse Path”	Static
Nonlinear Coefficient [$\text{Nm}^{-2.5872}$]	$1.2504 \cdot 10^8$	$1.2740 \cdot 10^8$

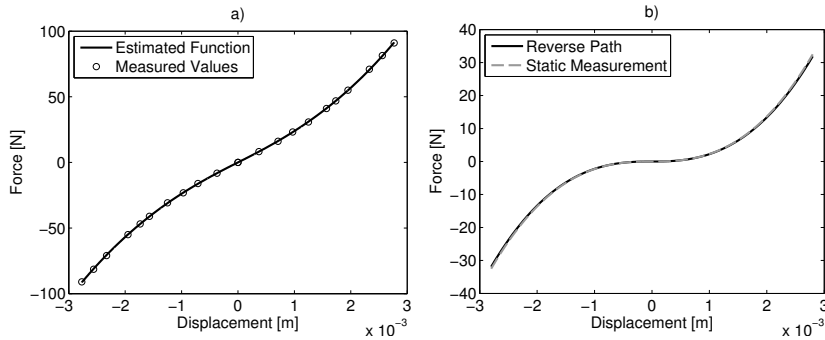


Figure 12: Statically measured forces vs. displacement. a) estimated function from the static measurement containing both linear and nonlinear stiffness, $f(x) = 2.1611 \cdot 10^4 \cdot x + 1.2740 \cdot 10^8 \cdot \text{sign}(x) \cdot |x^{2.5872}|$ b) nonlinear function estimated from the static measurement compared to the nonlinear function estimated by “Reverse Path”.

The estimated nonlinear functions agree well with the dynamic and static experiments, indicating reliable results. Also, good estimates of the underlying linear system was obtained for all measured nodes.

5 Conclusions

A general approach for analyzing multi-degree-of-freedom systems with several localized nonlinearities using the “Reverse Path” method has been presented. The suggested approach only requires the system to be excited in one location, which can be located away from the nonlinearities. Using this procedure, estimates of both the nonlinear coefficients as well as the frequency response functions of the underlying linear system in all response locations are obtained in a straightforward way. The method provides a structured way for solving complex nonlinear structures which makes it suitable for use in iterative processes when, for example, locating structural nonlinearities. The versatility and performance of the suggested method was demonstrated both by simulations and experimental tests.

References

- [1] G. Kerschen, K. Worden, A.F. Vakakis, and J.-C. Golinval. Past, present and future of nonlinear system identification in structural dynamics. *Mechanical Systems and Signal Processing*, 20(3):505 – 92, 2006/04/.
- [2] J. S. Bendat and A. G. Piersol. Spectral analysis of non-linear systems involving square-law operations. *Journal of Sound and Vibration*, 81(2):199 – 214, 1982.
- [3] J.S. Bendat and A.G. Piersol. Decomposition of wave forces into linear and non-linear components. *Journal of Sound and Vibration*, 106(3):391 – 408, 1986.
- [4] H.J. Rice and J.A. Fitzpatrick. A generalised technique for spectral analysis of non-linear systems. *Mechanical Systems and Signal Processing*, 2(2):195 – 207, 1988.
- [5] H.J. Rice and J.A. Fitzpatrick. A procedure for the identification of linear and non-linear multi-degree-of-freedom systems. *Journal of Sound and Vibration*, 149(3):397 – 411, 1991.
- [6] Julius S. Bendat. *Nonlinear system analysis and identification from random data*. Wiley, New York, 1990.
- [7] G. Kerschen, V. Lenaerts, and J.-C. Golinval. Identification of a continuous structure with a geometrical non-linearity. part i: Conditioned reverse path method. *Journal of Sound and Vibration*, 262(4):889 – 906, 2003.
- [8] L. Garibaldi. Application of the conditioned reverse path method. *Mechanical Systems and Signal Processing*, 17(1):227 – 235, 2003. Conditioned reverse path (CRP) method;.
- [9] S. Marchesiello. Application of the conditioned reverse path method. *Mechanical Systems and Signal Processing*, 17(1):183 – 188, 2003. Dampers;.
- [10] A Josefsson, M Magnevall, and K Ahlin. On nonlinear parameter estimation with random noise signals. In *Proceedings of IMAC XXV*, 2007.
- [11] M. Magnevall, A. Josefsson, and K. Ahlin. On parameter estimation and simulation of zero memory nonlinear systems. In *Proceedings of IMAC XXVI*, 2008.

- [12] H. Esmonde, J.A. Fitzpatrick, H.J. Rice, and F. Axisa. Modelling and identification of nonlinear squeeze film dynamics. *Journal of Fluids and Structures*, 6(2):223 – 248, 1992.
- [13] P.F. Liagre and J.M. Niedzwecki. Estimating nonlinear coupled frequency-dependent parameters in offshore engineering. *Applied Ocean Research*, 25(1):1 – 19, 2003.
- [14] A. Josefsson, M. Magnevall, and K. Ahlin. Estimating the location of structural nonlinearities from random data. In *Proceedings of IMAC XXVI*, 2008.
- [15] C.M. Richards and R. Singh. Identification of multi-degree-of-freedom nonlinear systems under random excitations by the ”reverse path” spectral method. *Journal of Sound and Vibration*, 213(4):673 – 707, 1998.

Paper E

**A Simulation and
Characterization Method for
Hysteretically Damped
Vibrations**

Paper E is published as:

Magnevall, M., Josefsson, A., Ahlin, K., Broman, G. A Simulation and Characterization Method for Hysteretically Damped Vibrations, *Submitted for publication*, 2011.

A Simulation and Characterization Method for Hysteretically Damped Vibrations

Martin Magnevall^{1,2}

Andreas Josefsson²

Kjell Ahlin²

Göran Broman²

¹ AB Sandvik Coromant, SE-811 81 Sandviken, Sweden

² Blekinge Institute of Technology, SE-371 79 Karlskrona, Sweden

Abstract

This paper presents a simulation and parameter estimation method for a general mechanical structure with a localized nonlinear damper. The intended industrial applications are simulation and characterization of passive dampers used for vibration attenuation in metal machining. A new forced response simulation routine for an arbitrary multi-degree-of-freedom system with a mass damper coupled via a Bouc-Wen hysteresis element is developed. The simulation method is used as a basis in a two stage parameter estimation routine performed in the time domain. The proposed method utilizes least square estimation in combination with nonlinear optimization by a real coded genetic algorithm. The methods are successfully used with both simulated and experimental data on a dry-friction damper.

Keywords: Bouc-Wen, Parameter estimation, Nonlinear, Genetic Algorithm, Dry-Friction

1 Introduction

Vibration problems in machine tooling are well documented. Excessive vibrations may limit the cutting speed and depth and thereby decrease the production rate. Vibrations also have a negative effect on the wear and tear of the tool, the surface finish of the completed work piece and the working environment [1]. A common vibration problem when using slender tools with long overhangs is regenerative vibrations (chatter) [1, 2, 3]. These vibrations can effectively be suppressed by increased damping. One way to increase the damping, in these applications, is to mount a hysteretic mass damper in the free end of the cutting tool; see Figure 1. A benefit with hysteretic dampers is that they attenuate vibrations over a broad frequency range, making them robust with respect to changes in machine tool dynamics. A theoretical model describing the tool-damper interaction in combination with efficient simulation and identification routines are of essence to predict and/or optimize the system's response during machining.

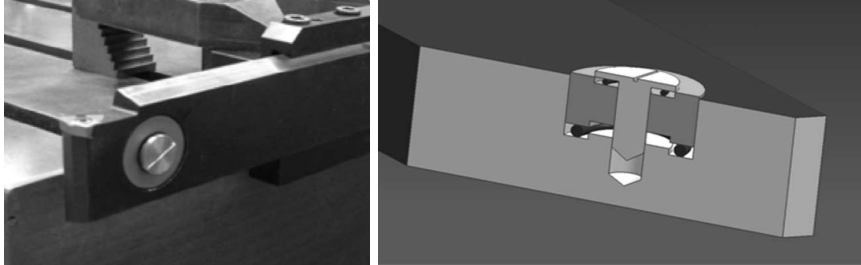


Figure 1: Example of a cutting tool with a damper mounted in the free end. The right figure shows the damper mass secured between two damping elements.

A model often used to describe hysteretic damping is the Bouc-Wen model [4]. This is capable of describing many different hysteresis shapes and has been used to describe both dry friction hysteresis and rubber damping elements. Ni et al. [5] used it to describe the dynamic behavior of a wire cable isolator, Qiang et al. [6] described the hysteretic behavior of a rubber bearing and Hornig [7] used the model to describe hysteresis damping in vibrating composite sandwich panels. These are examples of different areas where the Bouc-Wen model has been successfully applied. A detailed review can be found in [8]. The versatility of

A Simulation and Characterization Method for Hysteretically-Damped Vibrations

the Bouc-Wen model makes it suitable to use as a generic model for describing the hysteresis effects in a range of damping materials used for different cutting tool applications.

There are two commonly used approaches to solve the Bouc-Wen equation. One is to solve for the steady state response when the system is excited by a harmonic input signal. This is usually done by a multi-harmonic frequency/time domain alteration method [9, 10, 11]. The benefit of this method is its speed. The steady state solution of the system at a specific frequency is obtained instantly. A disadvantage is the fact that it usually requires pure sinusoidal excitation, which can be difficult and time consuming to accomplish in an experimental setup [12, 13]. Another approach is to use a time integration scheme [7, 14, 15, 16]. The benefit with time integration schemes are their versatility with respect to excitation signals. They are not limited to harmonic signals but can be used with transient, random and sine sweep excitation as well. This is beneficial since measured excitation forces can be used as input to a simulation model and thereby simplify comparisons between measured and simulated responses. A disadvantage is that they are usually rather time consuming.

Identification of the Bouc-Wen parameters is a highly nonlinear optimization problem and has been given much attention in recent years. A variety of system identification techniques have been developed for both time and frequency domain characterization, [8]. A class of optimization methods which has proved successful for finding the Bouc-Wen parameters are evolutionary algorithms. For example, Kyprianou et al. [15] used a differential evolution algorithm, Charalampakis et al. [16] used a hybrid evolutionary algorithm and Hornig [7] used a real coded genetic algorithm (RGA) to successfully identify the Bouc-Wen parameters using both simulated and experimental data. A benefit of these algorithms are their ability to avoid getting trapped in a local minima which increases the possibility of finding the best parameter set. The drawback of evolutionary methods are the number of iterations needed for the methods to converge. Since each iteration may consist of several function evaluations, these methods can be rather time consuming. However, the benefit of directly using measured forces as input to the simulation model and measured responses as reference signals makes the time domain approach and evolutionary algorithm attractive for parameter estimation based on experimental data.

The aim of the present paper is to develop a simulation and characterization

method for hysteretically-damped cutting tools, where the hysteresis function can be described by the Bouc-Wen model. This includes to find a fast time integration routine suitable for forced response simulation and nonlinear parameter identification in the time domain, to be used in a nonlinear optimization approach based on a real coded genetic algorithm [17].

2 Theoretical modeling

2.1 The Bouc-Wen hysteretic model

The Bouc-Wen hysteretic model is, for simplicity, here described by using a single-degree-of-freedom system with a mass m , a viscous damper c , a linear spring $k\alpha$, and a nonlinear hysteretic force $g(t)$. The system is excited by an external excitation force $f(t)$. The governing equation of the system is:

$$m\ddot{x}(t) + c\dot{x}(t) + k\alpha x(t) + g(t) = f(t) \quad (1)$$

where $g(t)$ is described by the Bouc-Wen differential equation [18] as:

$$\begin{aligned} g(t) &= (1 - \alpha)kz(t) \\ \dot{z}(t) &= \dot{x}(t)[\kappa - |z(t)|^n(\gamma + \beta \operatorname{sgn}(\dot{x}(t)) \operatorname{sgn}(z(t)))] \end{aligned} \quad (2)$$

The hysteretic variable, $z(t)$, is a "fictitious" displacement related to the time history displacement of $x(t)$ that accounts for the memory effect of the nonlinear restoring force. This means that the nonlinear restoring force is not only dependent on the current displacement but also on the past history displacements. The hysteretic feedback force is represented as the superposition of a linear elastic component, $\alpha kx(t)$, and a purely hysteretic part, $(1 - \alpha)kz(t)$. The parameter α ($0 < \alpha < 1$) is the post to pre-yielding stiffness ratio. Parameters κ, β (positive real numbers) and γ (real number) are nondimensional parameters which determine the amplitude and shape of the hysteresis loop. n is a scalar that governs the transition from elastic to plastic response. Figure 2 shows, for the purpose of illustrating the versatility of the Bouc-Wen model, hysteresis loops obtained by different combinations of the parameters β and γ ($\kappa = n = 1$), [19].

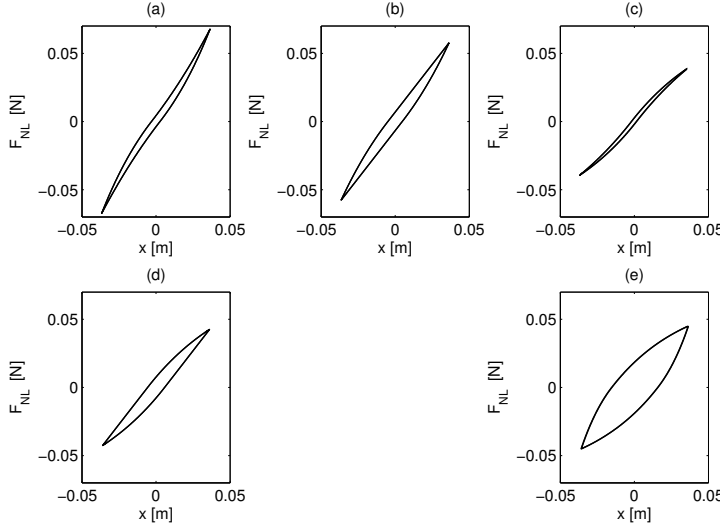


Figure 2: Hysteresis loops obtained by different combinations of γ and β . The system of equations. (1) and (2) was used with the following parameters, $m = 0.3$, $c = 0.01$, $k = 2$, $\alpha = 0.3$ and $\kappa = n = 1$. (a) $\gamma - \beta < \gamma + \beta$; (b) $\gamma + \beta = 0$, $\gamma - \beta < 0$; (c) $\gamma + \beta > \gamma - \beta > 0$; (d) $\gamma + \beta > 0$, $\gamma - \beta = 0$; (e) $\gamma + \beta > 0$, $\gamma - \beta < 0$.

2.2 Model of the studied system

Consider the system shown in Figure 3, a cantilever beam with a nonlinear damper consisting of a mass, m_b , coupled to the beam by a linear spring, $k_b\alpha$, a viscous damper, c_b , and a nonlinear element described by the Bouc-Wen Equation (2). This system can be represented in the frequency domain as:

$$\begin{bmatrix} H_{aa}(\omega) & H_{ab}(\omega) \\ H_{ba}(\omega) & H_{bb}(\omega) \end{bmatrix} \begin{bmatrix} F(\omega) - \mathcal{F}(g(x_a(t) - x_b(t))) \\ \mathcal{F}(g(x_a(t) - x_b(t))) \end{bmatrix} = \begin{bmatrix} X_a(\omega) \\ X_b(\omega) \end{bmatrix} \quad (3)$$

As seen in Equation (3), the system is modeled as a linear system excited with a force $F(\omega)$, and a “nonlinear” force $\mathcal{F}(g(x_a(t) - x_b(t)))$, where ω is the frequency variable and \mathcal{F} denote the Fourier transform. The nonlinear effect of the damper is modeled by artificial input forces acting on the underlying linear system. The underlying linear system is constituted by the aluminum

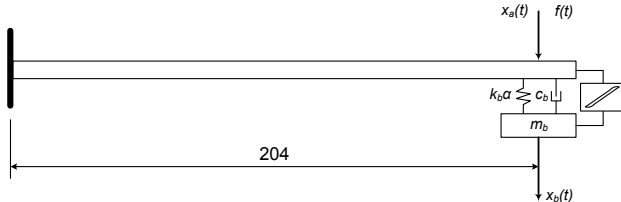


Figure 3: The studied system, a continuous system with a single-degree-of-freedom damper coupled together by linear and nonlinear elements. The beam is made of aluminum (cross section $30 \times 10 \text{ mm}^2$ and length 210 mm). This is a sketch of the rig used for experimental testing in section 5.

beam and mass of the damper (m_b) as well as the linear damping (c_b) and stiffness (k_b) between these two. A linear model of the beam (without the damper) can be obtained analytically, from a finite element model or from experimental measurements. A complete model of the underlying linear system can then be obtained by connecting the damper mass to the beam using the linear properties (stiffness, $k_b \alpha$, and damping c_b) of the damper by, for example receptance coupling, [20, 21]. Once the frequency response function matrix of the complete underlying linear system is known, the residues and poles are estimated. These are then used as the model of the underlying linear system in the forced response simulation routines presented in the next section.

3 Forced response simulation

There are several methods to calculate the time response of a mechanical system subjected to an arbitrary excitation. A few of these are: the convolution integral method, the state transition matrix method and the Runge-Kutta method with variations. A disadvantage with the traditional convolution integral method is the computational cost due to its non-recursive nature. However, the integral can be used to derive a recursive algorithm, a digital filter, which reduces the computational cost significantly compared with the traditional method, [22].

3.1 The filter coefficients

Working with discrete sampled data requires a transformation from the continuous time domain into the discrete time domain. The basis for a family of methods is the convolution integral:

$$x_p(t) = \int_0^t h_{pq}(t-\tau) f_q(\tau) d\tau \quad (4)$$

where p refers to the response node and q refers to the excitation node. The convolution integral can be used with any linear time invariant system. According to the modal superposition theorem a frequency response function can be expressed using partial fraction expansion of the residues R and poles λ as:

$$H_{pqr}(s) = \sum_{r=1}^M \frac{R_{pqr}}{s - \lambda_r} + \frac{R_{pqr}^*}{s - \lambda_r^*} \quad (5)$$

where r refers to the current mode and M denotes the total number of modes included and s is the Laplace variable. In the upcoming derivation of the digital filter, only one mode will be considered initially. The complex conjugate is also initially removed in order to illustrate the principle ideas as simple as possible. The function used in the derivation is thus:

$$H_{pq}^D(s) = \frac{R_{pq}}{s - \lambda} \quad (6)$$

The impulse response of $H_{pq}^D(s)$ is:

$$h_{pq}^d(t) = R_{pq} e^{\lambda t} \quad (7)$$

Changing to discrete time, the response $x_p(nT + T)$ can be calculated using the convolution integral from Equation (4) with x_p as output and f_q as input. T is the sampling interval. Thus:

$$\begin{aligned} x_p(nT + T) &= \int_0^{nT+T} R_{pq} e^{\lambda(nT+T-\tau)} f_q(\tau) d\tau \\ &= e^{\lambda T} x_p(nT) + R_{pq} e^{\lambda T} \int_0^T e^{-\lambda u} f_q(u + nT) du \end{aligned} \quad (8)$$

From this equation it is obvious that $x_p(nT+T)$ can be calculated with a recursion formula using only $x_p(nT)$ and the input signal in the interval $[nT, nT+T]$. The way the samples are treated in the evaluation of the last integral defines the method; for example, step invariant (zero-order hold) or ramp invariant (first-order hold). Step invariant treats the input sample as a constant, $f_q(nT)$, in the interval $[nT, nT+T]$ while ramp invariant makes a linear interpolation between the samples, $f_q(nT)$ and $f_q(nT + T)$. Applying step invariant interpolation, Equation (8) becomes:

$$\begin{aligned} x_p(nT + T) &= e^{\lambda T} x_p(nT) + R_{pq} e^{\lambda T} \int_0^T e^{-\lambda u} f_q(nT) du \\ &= e^{\lambda T} x_p(nT) + f_q(nT) \frac{R_{pq}}{\lambda} (e^{\lambda T} - 1) \end{aligned} \quad (9)$$

For ramp invariant, Equation (8) becomes:

$$\begin{aligned} x_p(nT + T) &= e^{\lambda T} x_p(nT) \\ &+ R_{pq} e^{\lambda T} \int_0^T e^{-\lambda u} \left(f_q(nT) + \frac{f_q(nT + T) - f_q(nT)}{T} u \right) du \\ &= e^{\lambda T} x_p(nT) \\ &+ \frac{R_{pq}}{\lambda^2 T} \left(f_q(nT) (1 - e^{\lambda T} (1 - \lambda T)) + f_q(nT + T) (e^{\lambda T} - \lambda T - 1) \right) \end{aligned} \quad (10)$$

Adding the complex conjugate and considering M modes, the Z-domain representation of Equation (9) becomes:

$$H_{pq}(Z) = \sum_{r=1}^M \left[\frac{Z^{-1} \frac{R_{pqr}}{\lambda_r} (e^{\lambda_r T} - 1)}{1 - Z^{-1} e^{\lambda_r T}} + \frac{Z^{-1} \frac{R_{pqr}^*}{\lambda_r^*} (e^{\lambda_r^* T} - 1)}{1 - Z^{-1} e^{\lambda_r^* T}} \right] \quad (11)$$

Equation (11) shows that one set of filter coefficients A_{pq} (denominator) and B_{pq} (numerator) is needed for each individual mode included in the simulation. By putting the numerator and denominator in vector form according to the specified time delays and then use convolution, the filter coefficients are obtained. In Equation (12), a formula for calculating the corresponding filter coefficients to Equation (11) is shown. N_{pqr} stands for numerator and D_{pqr} for denominator for mode r . Thus:

$$N_{pqr} = \left[0, \quad \frac{R_{pqr}}{\lambda_r} (\mathrm{e}^{\lambda_r T} - 1) \right] \quad (12\text{a})$$

$$D_{pqr} = [1, \quad -\mathrm{e}^{\lambda_r T}] \quad (12\text{b})$$

$$B_{pqr} = 2 \operatorname{Re}(N_{pqr}) * \operatorname{Re}(D_{pqr}) + 2 \operatorname{Im}(N_{pqr}) * \operatorname{Im}(D_{pqr}) \quad (12\text{c})$$

$$A_{pqr} = \operatorname{Re}(D_{pqr} * D_{pqr}^*) \quad (12\text{d})$$

These filter coefficients are valid for step invariant. However, based on Equation (10), filter coefficients for ramp invariant can be obtained in a straightforward manner following the same steps as shown for step invariant. When changing the interpolation method only the numerator in Equation (12) changes, the denominator stays the same regardless of which interpolation method that is used.

3.2 Setting up the digital filter

Once the filter coefficients for the frequency response functions in Equation (3) are obtained, a difference equation for the forced response of $x_a[n]$ and $x_b[n]$ can be setup as:

$$\begin{aligned} x_a[n] = & \sum_{r=1}^M \left[-g[n](B_{aar}^0 - B_{abr}^0) + \sum_{i=0}^{N_B} f[n-i]B_{aar}^i \right. \\ & \left. - \sum_{i=1}^{N_B} g[n-i](B_{aar}^i - B_{abr}^i) - \sum_{i=1}^{N_A} x_{ar}[n-i](A_{aar}^i + A_{abr}^i) \right] \end{aligned} \quad (13\text{a})$$

$$\begin{aligned} x_b[n] = & \sum_{r=1}^M \left[-g[n](B_{bar}^0 - B_{bbr}^0) + \sum_{i=0}^{N_B} f[n-i]B_{bar}^i \right. \\ & \left. - \sum_{i=1}^{N_B} g[n-i](B_{bar}^i - B_{bbr}^i) - \sum_{i=1}^{N_A} x_{br}[n-i](A_{bar}^i + A_{bbr}^i) \right] \end{aligned} \quad (13\text{b})$$

where N_B and N_A are the number of poles and zeros in the filter, respectively. Since the nonlinearity is dependent on the difference between $x_a[n]$ and $x_b[n]$, a new variable, $\Delta x[n]$, is introduced:

$$\Delta x[n] = x_a[n] - x_b[n] \quad (14)$$

Combining Equation (13) and (14), moving all unknown variables to the left side, putting the known values equal to a constant $C_x[n]$ and putting the sum of the known filter coefficients multiplied with $g[n]$ equal to a constant E_x yields:

$$\Delta x[n] + g[n]E_x = C_x[n] \quad (15)$$

An equation for $\Delta\dot{x}[n]$ can be obtained in the same manner. The difference is that the residues used when calculating the filter coefficients have to be in velocity format. The equation for $\Delta\dot{x}[n]$ becomes:

$$\Delta\dot{x}[n] + g[n]E_v = C_v[n] \quad (16)$$

The function in Equation (16) is still dependent on $\Delta x[n]$, since the nonlinearity is displacement dependent. However, the constants E_v and $C_v[n]$ are different from E_x and $C_x[n]$. Using this equation in the iteration process means that for any given guess of $\Delta x[n]$, the velocity in the same instance can be obtained. Replacing $g[n]$ in Equation (15) with the Bouc-Wen equation and solving for $z[n]$ gives:

$$z[n] = \frac{C_x[n] - \Delta x[n]}{(1 - \alpha)kE_x} \quad (17)$$

Since both $\Delta x[n]$ and $z[n]$ have to be treated as unknown variables, Equation (15) has to be solved iteratively. Equation (17) is used to get an estimate of $z[n]$ for a given estimate of $\Delta x[n]$. These estimates are then used to calculate $\dot{z}[n]$ according to Equation (2). $\dot{z}[n]$ is then numerically integrated, and the new estimate of $z[n]$ is put in Equation (18). The procedure is repeated from Equation (15) and the secant method is used to trap the solution.

$$z[n](1 - \alpha)kE_x + \Delta x[n] - C_x[n] = 0 \quad (18)$$

3.3 Error Analysis

Performing forced response simulations based on sampled data will lead to errors in the simulation results. A simplified error analysis where the system is assumed linear is presented in this section. Though simplified, the analysis

points out important error sources and is still useful when setting up a simulation.

The effect of different interpolation techniques, that is ramp invariant and step invariant, and their effects on the simulation results are discussed with respect to three error sources: aliasing, phase and bias errors. A schematic representation of the sampling and interpolation process for a linear system is shown in Figure 4.

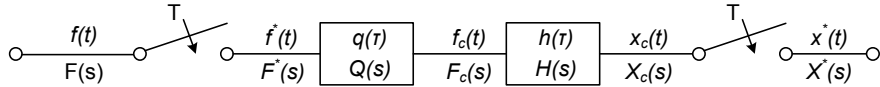


Figure 4: Schematic representation of the sampling and interpolation process.

A continuous input signal $f(t)$ is sampled into its discrete representation $f^*(t)$. When performing forced response simulations, the sampled signal, $f^*(t)$, is transformed into a continuous estimation, $f_c(t)$, of the original signal, $f(t)$. This is usually done by an interpolation filter, described by $q(\tau)$. The frequency response function of the interpolation filter is, in the frequency domain, multiplied with the system's frequency response function and thereby affects both the amplitude and phase response of the total system. Putting $s=j\omega$, the frequency responses for step, $Q_S(s)$, and ramp, $Q_R(s)$, invariant interpolation are given by Equations (19a) and (19b) [23] as:

$$Q_S(j\omega) = \frac{\sin\left(\frac{\omega T}{2}\right)}{\frac{\omega T}{2}} e^{-j\frac{\omega T}{2}} \quad (19a)$$

$$Q_R(j\omega) = \left(\frac{\sin\left(\frac{\omega T}{2}\right)}{\frac{\omega T}{2}} \right)^2 \quad (19b)$$

As seen in Equation (19a), the frequency response of the step invariant interpolation filter has a linear phase response corresponding to a constant delay, $T/2$, in the time domain. Thus, a phase error is introduced when using the step invariant interpolation. This phase error is important to consider when

performing simulations on nonlinear systems where the nonlinear forces are fed back into the system and may lead to instabilities. Also seen in Equation (19) is that the amplitude frequency response of the step and ramp invariant interpolation techniques are first and second order sinc-functions with zeros at multiples of the sampling frequency. This will reduce aliasing effects at the cost of a bias error. The bias error is system independent and only depends on the interpolation technique used, Equation (19). Thus, the bias error can be controlled by selecting a suitable sampling frequency with respect to the maximum frequency of interest. The effect of the different interpolation techniques on the amplitude response of a system's FRF is illustrated by comparing the analytical FRF of the system in Figure 5 with biased FRFs due to multiplication with step and ramp invariant interpolation filters in the frequency domain, Figure 6. The system in Figure 5 is a simplified model, describing the first bending mode and damper, of the beam structure in Figure 3. The modal mass (m_a), stiffness (k_a) and damping (c_a) of the first bending mode is coupled with the damper mass (m_b) using a linear spring ($k_b\alpha$) and a viscous damper (c_b).

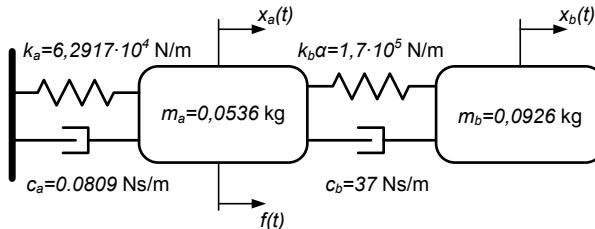


Figure 5: Simplified model of the beam and damper used in the simulations.

Another error source related to forced response simulations using sampled data is aliasing. Even if the input has aliasing protection, the system's response generally does not. Thus, the response spectrum will have contributions from the original spectrum, $H(\omega)Q(\omega)$, centered around multiples of the sampling frequency, ω_s . The aliased spectrum, $H_A(\omega)$, can be calculated as

$$H_A(\omega) = H(\omega)Q(\omega) + \sum_{l=1}^L H(\omega - l\omega_s)Q(\omega - l\omega_s) + H(\omega + l\omega_s)Q(\omega + l\omega_s) \quad (20)$$

where $Q(\omega)$ refers to the FRF of the interpolation method used, that is ramp or step invariant. As shown by Equation (20), the aliasing error is system

A Simulation and Characterization Method for Hysteretically-Damped Vibrations

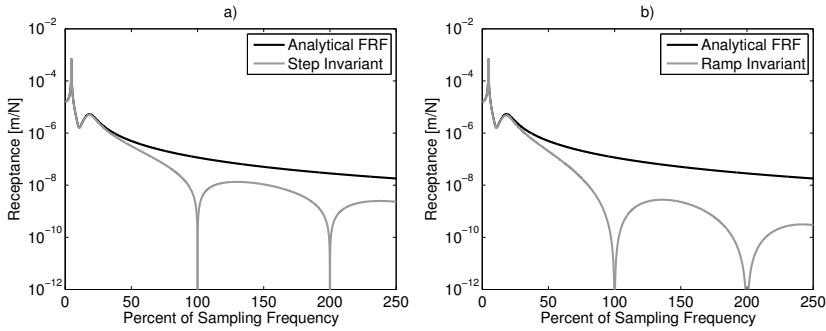


Figure 6: The systems theoretical FRF compared with the systems FRF multiplied with the FRFs of the interpolation filters: (a) Step invariant (b) Ramp invariant.

dependent and can therefore not be uniquely determined purely based on the interpolation technique used and sampling settings. However, as seen in Figure 6, the effect of aliasing can be substantially reduced by selecting a proper interpolation method.

To further illustrate the reasoning above, forced response simulations are carried out on the system in Figure 5. All the following comparisons are based on point flexibility in *a*. The excitation signal used is a unit impulse, low-pass filtered at $(f_s/2)$, where f_s is the sampling frequency. The sampling frequency used in the simulation is 2048 Hz, 90 seconds of data were collected in order to let the system decay to zero and the frequency response was calculated using a block size equal to the entire signal length and rectangular windowing was used. This provide a good estimation of the amplitude response of the system. The estimated error from the simulation is then compared to the theoretical error calculated using Equations (19) and (20). The results are shown in Figure 7. For comparison the same simulation was repeated using the fixed step solver Runge-Kutta 5, the amplitude errors from these simulations are shown in Figure 8.

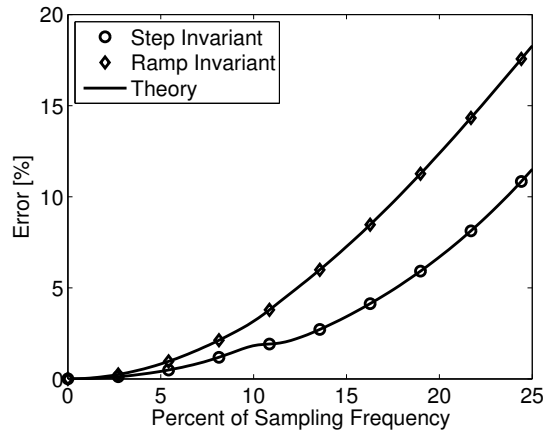


Figure 7: Comparison between simulated error using digital filters and theoretical error considering bias and aliasing effects using step and ramp invariant interpolation.

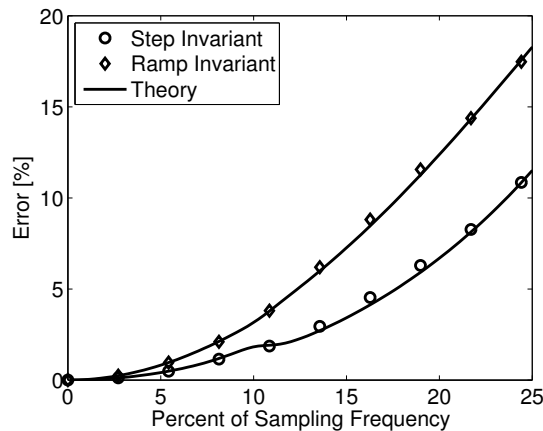


Figure 8: Comparison between simulated error using Runge-Kutta 5 and theoretical error considering bias and aliasing effects using step and ramp invariant interpolation.

Figures 7 and 8 shows that ramp invariant interpolation gives the largest error,

dominated by the bias error. Since the bias error is system independent, Equation (19), it can be controlled, without any prior knowledge about the system, by selecting a suitable sampling frequency. The advantages with ramp invariant compared to step invariant interpolation are that the system dependent aliasing errors are substantially reduced using ramp invariant interpolation and that step invariant interpolation introduces a phase error which might cause stability issues when performing simulations on nonlinear systems. Also seen in the simulations is that the amplitude errors using digital filters and Runge-Kutta 5 are comparable.

The error analysis presented in this section show that the dominant errors concerning forced response simulation using sampled data are bias and aliasing errors. These errors can be avoided by selecting an appropriate interpolation technique and sampling frequency. The simulations were performed on a linear system in order to be able to compute the exact amplitude response, the analytical FRF, in order to make relevant comparisons between simulated and theoretically predicted errors. The error analysis points out the importance of selecting an appropriate interpolation technique and sampling frequency when using discrete input data.

4 Parameter Estimation

The optimization approach adopted for the identification of the Bouc-Wen parameters in this paper is a real coded genetic algorithm [19, 24], this method is selected due to its robustness and ability to avoid getting trapped in local minima points, which increases the possibility of finding the best parameter set.

4.1 Parameter constraints

Ikhouane et al. [25] showed that the input-output behavior of the Bouc-Wen model is not described by a unique set of parameters, $[k, \alpha, \kappa, \beta, \gamma, n]$. Due to this, parameter identification methods relying on input-output data cannot uniquely determine the parameters of the Bouc-Wen model. To deal with this, some authors have compared the shape of the hysteresis loops instead of comparing the values of the identified parameters with their reference values, for example [7, 19]. Other authors usually fixes some of the parameters to arbi-

trary values, for example [5, 6, 15].

Ma et al. proved that the Bouc-Wen model can be reduced without affecting the system response by setting $\kappa = 1$. Furthermore, the constraint, $\kappa/(\gamma + \beta) = 1$, is used to further reduce the model [6, 16]. Also, as suggested in for example [15, 26] the parameter n is set to 2. Similarly constrained models have previously been used to successfully identify hysteresis behavior in for example a dry friction application (bolted-welded connection) [16], and to model the behavior of a rubber-bearing [6]. Applying these constraints, the unknown parameters related to the Bouc-Wen model are: k, α and β .

4.2 Identification procedure

It is assumed that there is both a linear and a nonlinear connection between the beam and damper mass, and that these linear parameters are unknown beforehand. Therefore, the total parameter vector to be estimated is, $\{P\} = \{c_b, k_b, \alpha, \beta\}$. As shown by for example Kyprianou et al. [15], the optimization result is improved by running several optimizations in series and successively reduce the search space. Here, a two stage parameter estimation procedure is proposed. To reduce the number of function calls needed, the parameter β is, in the first stage, estimated by a least square fit:

$$\{\dot{z} + \Delta\dot{x}(|z|^n - 1)\} = \{\Delta\dot{x}|z|^n - \Delta\dot{x}|z|^n \operatorname{sgn}(\Delta\dot{x}) \operatorname{sgn}(z)\} \beta \quad (21)$$

As seen in Equation (21), to identify β using least squares, estimates of $z, \dot{z}, \Delta\dot{x}$ and Δx are needed. Since z is an unmeasurable response it needs to be estimated based on Equation (18). Also, in an experimental case, the signals collected are usually velocity and/or acceleration. Thus, the measured signals need to be integrated in order to estimate z . This will introduce uncertainties into the parameter estimates and therefore it is not expected that the algorithm converges fully towards an optimal solution. However, the parameters obtained can be used to limit the search space in the second stage of the algorithm, where all unknown parameters are optimized by the genetic algorithm.

The reference signal used for comparison is the “nonlinear” feedback force from the damper, $\{m_b\ddot{x}_b\}$. The reason for using the force is that it can be estimated based on directly measurable quantities, and is therefore suitable to use with experimental data. Due to the fact that the viscous damping is one of the parameters to be estimated, reference signals from two or more force levels and/or

frequencies are needed in order to capture any velocity dependency present in the reference signal.

The problem is formulated as a minimization problem and the normalized mean square error (NMSE) between the reference, $\{m_b \ddot{x}_b\}$, and simulated, $\{m_b \hat{\ddot{x}}_b\}$, nonlinear feedback forces is calculated and used as the cost function, $C(\{P\})$ as:

$$C(\{P\}) = \frac{100}{M \sigma_{m_b \ddot{x}_b}^2} \sum_{l=1}^M (m_b \ddot{x}_b[l] - m_b \hat{\ddot{x}}_b[l])^2 \quad (22)$$

where $\sigma_{m_b \ddot{x}_b}^2$ is the variance of the measured “nonlinear” feedback force. When multiple reference signals are used, the NMSE is calculated for each signal and the average value, $\bar{C}(\{P\})$, used as error estimate. A schematic flow diagram of the optimization procedure is shown in Figure 9.

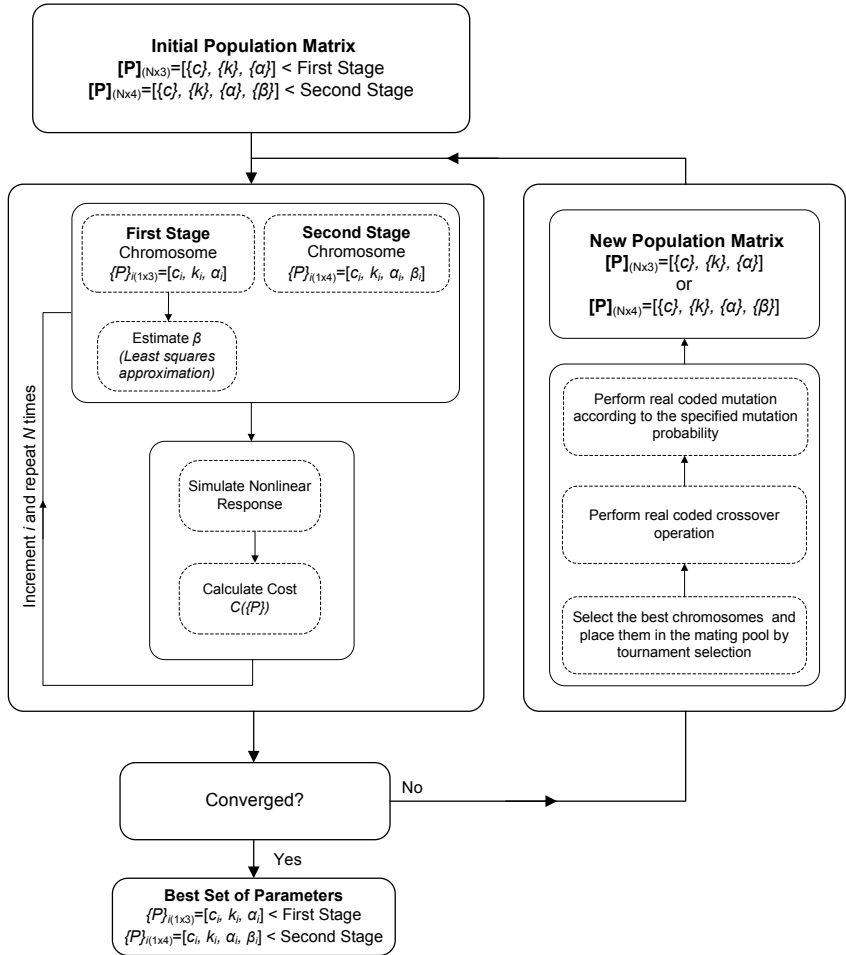


Figure 9: Schematic representation of the optimization procedure.

4.3 Simulation

To investigate the performance of the simulation and parameter estimation routine several optimization runs are completed using simulated data. The beam

structure in Figure 3 is used as basis in the simulations, and both the linear and nonlinear parameters connecting the beam and damper are estimated. The simplified model shown in Figure 10 is used in the simulations. This model describes the first bending mode of the beam and the damper mode.

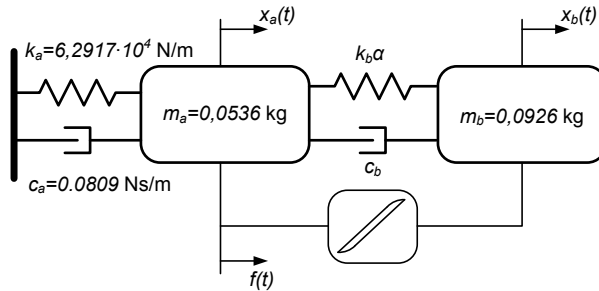


Figure 10: The nonlinear system used in the simulations.

Harmonic excitation is used and reference signals are simulated using three different forces:

- $f_1(t) = 26 \sin(2\pi 80t)$ N
- $f_2(t) = 8 \sin(2\pi 90t)$ N
- $f_3(t) = 3 \sin(2\pi 100t)$ N

The system is excited in point a , and the nonlinearity is connected between point a and b . The feedback force from the damper mass is extracted and used as reference signal, Equation (22).

The simulations are carried out in a noise free environment as well as with contaminating noise on the output channels (the feedback force of the damper mass). The noise added to the reference signals is scaled by the standard deviation of the output, for example a noise level of 0.1 means 10 percent of the standard deviation. Based on the error simulations presented in section 3.3, ramp invariant interpolation is used to avoid phase errors. The sampling frequency is set to 8192 Hz in order to capture the first orders of superharmonics present in the response. In each iteration, three forced responses of 0.8

seconds are simulated, the excitation signals are tapered to avoid as much transient effects as possible, allowing the system to reach its steady-state response quickly. For the system studied here, the computational savings using digital filters with respect to Runge-Kutta 4 and Runge-Kutta 5 are approximately 5 and 10 times, respectively.

The population, N , in the first stage is set to 10 and the algorithm is run for 100 generations. In the second stage, the population is set to 10 and the algorithm run for 200 generations. The mutation rate is set to 5 percent in both stages. The parameter search space used in the first stage is listed in Table 1. In the second stage the search space for β is set to $+/- 50$ percent of the result from the first stage estimation, the rest of the parameters are set to $+/- 5$ percent. Results from the simulations are shown in Table 2 and in Figure 11. To provide a measurement which only depends on the difference between the estimated and the true hysteretic feedback force and which is not affected by noise present in the reference signal, the function $\overline{C}_T(\{P\})$ is used. This function gives the average NMSE value between estimated and true hysteresis force.

Table 1: Reference parameters used in the simulations, upper and lower bounds are related to the first stage in the optimization process.

	c_b [Ns/m]	k_b [N/m]	α	β	γ	κ	n
True Value	37	$1.7 \cdot 10^5$	0.2	$2 \cdot 10^8$	$-2 \cdot 10^8$	1	2
Lower Bound	1	$5 \cdot 10^4$	0	—	—	—	—
Upper Bound	50	$5 \cdot 10^5$	1	—	—	—	—

As seen in Table 2, the optimization procedure is able to find the reference parameters within reasonable error margin. The estimation of the linear parameters are within 0.5 percent of the true values for all noise levels. At higher noise levels, the estimates of β and α has a higher deviation than the rest of the parameters. However, the difference between the reference and predicted hysteresis loops are still small as seen from the cost function, $\overline{C}_T(\{P\})$ in Table 2. The results also show that the population size and number of generations used are enough for the algorithm to converge towards an acceptable error.

Table 2: Results from the parameter estimation.

Parameter	Noise level			True Value
	0	0.05	0.10	
c_b	37.1977	37.2019	37.2095	37
$k_b \cdot 10^{-5}$	1.6919	1.6951	1.6942	1.7
α	0.2043	0.2056	0.2505	0.2
$\beta \cdot 10^{-8}$	2.0379	2.1055	2.2211	2
$\gamma \cdot 10^{-8}$	-2.0379	-2.1055	-2.2211	-2
κ	-	-	-	1
n	-	-	-	2
$\overline{C}_T(\{P\})[\%]$	0.0018	0.0025	0.0238	

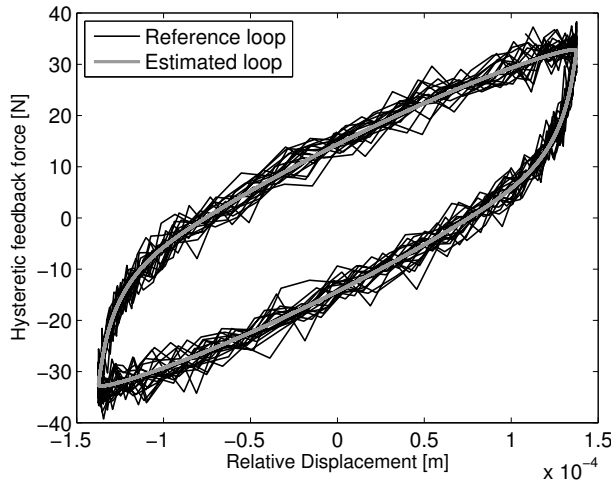


Figure 11: Example of estimated hysteresis loop and reference hysteresis loop with 10 percent noise. Excitation force, $f_3(t) = 3 \sin(2\pi 100t)$ N.

5 Experimental validation

The test rig used in the experimental tests consists of a cantilever beam with a mass suspended between two sets of plate springs, see Figures 3 and 12.

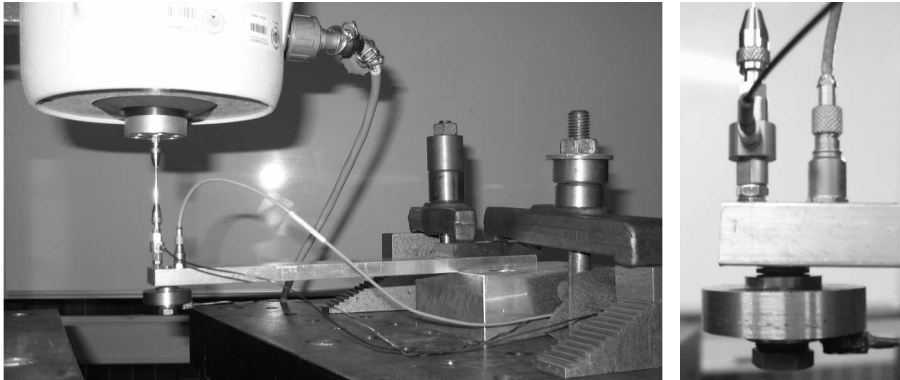


Figure 12: Pictures of the test rig

The hysteretic effect is caused by dry-friction between the plate springs when the system is vibrating, this system displays clear nonlinear effects when excited around its first resonance frequency (the first bending mode) which changes between approximately 90 and 100 Hz depending on the amplitude of the excitation force. The simulation model shown in Figure 10, is also used for the experimental tests. The reference signals are obtained from displacement controlled measurements using a harmonic excitation at different frequencies, $f = [80, 90, 100]$ Hz. Each measurement was taken when the relative displacement between the beam and damper mass was 0.14 mm.

The hysteresis force from all three measurements are used as reference functions in the optimization. The parameter constraints imposed on the model in section 4.1 is also applied in the experimental tests, that is $\kappa = 1$, $n = 2$ and $\kappa/(\beta + \gamma) = 1$. The measured excitation forces are used as input to the simulation. The search boundaries used in the first stage are shown in Table 3. In the second stage the search space for β is set to $+/- 50$ percent of the result from the first stage estimation, the rest of the parameters are set to $+/- 10$ percent. Mutation rate is set to 5 percent. Results from the parameter estimation are displayed in Figures 13-14 and in Table 3.

A Simulation and Characterization Method for Hysteretically-Damped Vibrations

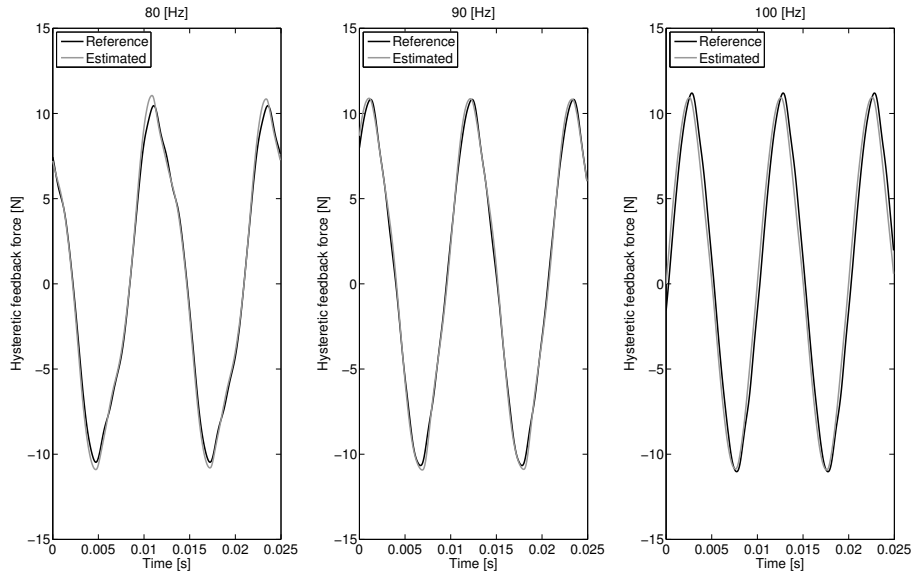


Figure 13: Comparison between measured and estimated nonlinear feedback forces.

Table 3: Results from the parameter estimation using experimental data, LB and UB refers to “lower bound” and “upper bound” limiting the search space used in the first stage of the optimization.

Parameter	Identified values	LB	UB
c_b	6.8825	1	10
k_b	$1.3289 \cdot 10^5$	$5 \cdot 10^4$	$9 \cdot 10^5$
α	0.6901	0	1
β	$3.0324 \cdot 10^8$	-	-
γ	$-3.0324 \cdot 10^8$	-	-
$\overline{C}(\{P\})[\%]$	1.0976		

The results in Figure 13 show a good correlation between estimated and measured nonlinear feedback forces. This is also confirmed by the average NMSE

in Table 3. As seen in Figure 14, the measured and simulated hysteresis loops also matches well, indicating that the relative displacement between the beam and damper is also captured in the simulation model. In summary, these result show that the Bouc-Wen model is capable of describing the nonlinear effects observed in the dry friction damper with the parameter constraints imposed on the model. Several optimization runs has been made and the algorithm has always converged towards a satisfactory solution.

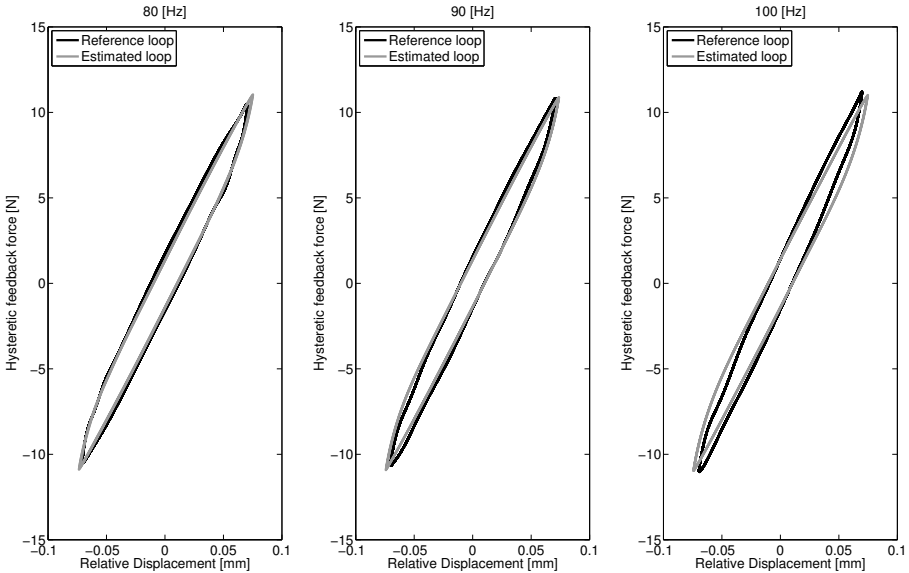


Figure 14: Comparison between measured and estimated hysteresis loops.

6 Discussion and Future Work

An analysis method for use with hysteretically-damped cutting-tools has been presented. The method builds on the Bouc-Wen model and utilizes digital filters for efficient forced response simulations in combination with a real coded genetic algorithm for parameter estimation. The filter based time integration routine is approximately one order of magnitude faster than typical Runge-

Kutta routines for the applications studied in this paper.

A two stage parameter estimation approach, combining least squares estimates with nonlinear optimization using a real coded genetic algorithm, is suggested to obtain both the linear and nonlinear parameters connecting the studied structure and damper. This approach reduces the number of function calls needed, and allows the search space for all parameters to be narrowed down before the second stage estimation. The methods was applied on both simulated and experimental data and the results show that the suggested parameter estimation routine is robust even with reference data contaminated by noise. The algorithm also found accurate estimates of the linear parameters, which is especially important for the model to be valid over a wide range of excitation frequencies and amplitudes. The experimental results confirms the possibility to use the Bouc-Wen model to describe the dry-friction hysteresis present in the test-rig.

Future investigations include experimental testing and parameter identification on rubber and silicone type materials. The presented method will be modified to handle nonlinear systems with a ground-hook nonlinearity to facilitate the study of alternative hysteresis effects, for example tool clamping effects. Also, a way to estimate the simulation errors for forced response simulation on nonlinear systems using sampled input data is of interest in future research.

References

- [1] Yusuf Altintas. *Manufacturing Automation - Metal Cutting Mechanics, Machine Tool Vibrations, and CNC Design*. Cambridge university press, 2000.
- [2] Kai Cheng. *Machining dynamics : fundamentals, applications and practices*. Springer, London, 2009.
- [3] Tony L. Schmitz and Kevin S. Smith. *Machining dynamics : Frequency Response to Improved Productivity*. Springer, New York, 2009.
- [4] Yi-Kwei Wen. Method for random vibration of hysteretic systems. *Journal of the Engineering Mechanics Division*, 102(2):249 – 263, 1976.

- [5] Y.Q. Ni, J.M. Ko, and C.W. Wong. Identification of non-linear hysteretic isolators from periodic vibration tests. *Journal of Sound and Vibration*, 217(4):737 – 756, 1998.
- [6] Yin Qiang, Zhou Li, and Wang Ximeng. Parameter identification of hysteretic model of rubber-bearing based on sequential nonlinear least-square estimation. *Earthquake Engineering and Engineering Vibration*, 9(3):375 – 83, Sept. 2010.
- [7] K. H. Hornig. Parameters characterization of the bouc/wen mechanical hysteresis model for sandwich composite materials by using real coded genetic algorithms. Technical report, Mechanical Engineering Department, Ross Hall, Auburn, Alabama, 2000.
- [8] Mohammed Ismail, Faycal Ikhouane, and Jose Rodellar. The hysteresis bouc-wen model, a survey. *Archives of Computational Methods in Engineering*, 16(2):161 – 188, 2009.
- [9] S. L. Lau, Y. K. Cheung, and S. Y. Wu. Incremental harmonic balance method with multiple time scales for aperiodic vibration of nonlinear systems. *Journal of Applied Mechanics, Transactions ASME*, 50(4a):871 – 876, 1983.
- [10] Hideyuki Tamura, Yoshihiro Tsuda, and Atsuo Sueoka. Higher approximation of steady oscillations in nonlinear systems with single degree of freedom - suggested multi-harmonic balance method. *Bulletin of the JSME*, 24(195):1616 – 1625, 1981.
- [11] C.W. Wong, Y.Q. Ni, and J.M. Ko. Steady-state oscillation of hysteretic differential model. ii: Performance analysis. *Journal of Engineering Mechanics*, 120(11):2299 – 2324, 1994.
- [12] A. Josefsson, M. Magnevall, and K. Ahlin. Control algorithm for sine excitation on nonlinear systems. *Proceedings of the IMAC-XXIV*, 2006.
- [13] M. Magnevall, A. Josefsson, and K. Ahlin. Experimental verification of a control algorithm for nonlinear systems. *Proceedings of the IMAC-XXIV*, 2006.
- [14] Satish Nagarajaiah, Andrei M. Reinhorn, and Michalakis C. Constantinou. Nonlinear dynamic analysis of 3-d-base-isolated structures. *Journal of Structural Engineering*, 117(7):2035 – 2054, 1991.

A Simulation and Characterization Method for Hysteretically-Damped Vibrations

- [15] A. Kyprianou, K. Worden, and M. Panet. Identification of hysteretic systems using the differential evolution algorithm. *Journal of Sound and Vibration*, 248(2):289 – 314, 2001.
- [16] A.E. Charalampakis and V.K. Koumousis. Identification of bouc-wen hysteretic systems by a hybrid evolutionary algorithm. *Journal of Sound and Vibration*, 314(3-5):571 – 585, 2008.
- [17] Randy L. Haupt and Sue Ellen Haupt. *Practical Genetic Algorithms*. John Wiley & Sons, second edition, 2004.
- [18] C.W. Wong, Y.Q. Ni, and S.L. Lau. Steady-state oscillation of hysteretic differential model. i: Response analysis. *Journal of Engineering Mechanics*, 120(11):2271 – 2298, 1994.
- [19] R. H. Sues, S. T. Mau, and Y. K. Wen. Systems identification of degrading hysteretic restoring forces. *Journal of Engineering Mechanics*, 114(5):833 – 846, 1988.
- [20] Bjorn Jetmundsen, Richard L. Bielawa, and William G. Flannelly. Generalized frequency domain substructure synthesis. *Journal of the American Helicopter Society*, 33(1):55 – 64, 1988.
- [21] W. Liu and D.J. Ewins. Substructure synthesis via elastic media. part ii: Coupling analysis. In *Proceedings of SPIE - The International Society for Optical Engineering*, volume 4062 (I, pages 1160 – 1166, San Antonio, TX, USA, 2000).
- [22] K. Ahlin, M. Magnevall, and A. Josefsson. Simulation of forced response in linear and nonlinear mechanical systems using digital filters. ISMA, 2006.
- [23] Z. Kowalcuk. Discrete approximation of continuous-time systems: a survey. *IEE Proceedings, Part G: Circuits, Devices and Systems*, 140(4):264 – 278, 1993.
- [24] George Lindfield and John Penny. *Numerical Methods Using MATLAB*. Prentice-Hall, Inc., second edition, 2004.
- [25] P. Ikhouane and J. Rodellar. On the hysteretic bouc-wen model. part i. forced limit cycle characterization. *Nonlinear Dynamics*, 42(1):63 – 78, 2005/10/.

- [26] Bo-Jen Chen, C.S. Tsai, L.L. Chung, and Tsu-Cheng Chiang. Seismic behavior of structures isolated with a hybrid system of rubber bearings. *Structural Engineering and Mechanics*, 22(6):761 – 783, 2006.

Paper F

**High Frequency Measurements of
Cutting Forces in Milling by
Inverse Filtering**

Paper F is published as:

Magnevall, M., Lundblad, M., Ahlin, K., Broman, G. High Frequency Measurements of Cutting Forces in Milling by Inverse Filtering, *Accepted for publication in Machining Science and Technology*, November, 2011.

High Frequency Measurements of Cutting Forces in Milling by Inverse Filtering

Martin Magnevall^{1,2}

Mikael Lundblad¹

Kjell Ahlin²

Göran Broman^{2,3}

¹ AB Sandvik Coromant, SE-811 81 Sandviken, Sweden

² Blekinge Institute of Technology, SE-371 79 Karlskrona, Sweden

³ Luleå University of Technology, SE-971 87 Luleå, Sweden

Abstract

Accurate estimates of cutting forces are important in the evaluation of different cutting tool geometries and concepts. However, dynamic influences from the measurement system affect the result, which can make the obtained cutting force data erroneous and misleading. This paper presents a method to obtain an inverse filter which compensates for the dynamic influences of the measurement system. Using this approach, unwanted dynamic effects of the measurement system can be counteracted, making it possible to retain information related to the cutting forces contained in the high frequency region. The advantage of the proposed method is illustrated by comparing simulated, inverse- and low-pass filtered forces to unfiltered forces under different cutting conditions. The results show that inverse filtering increases the usable frequency range of the force dynamometer and thereby provide more reliable results compared to both low-pass and unfiltered forces.

Keywords: cutting force, dynamometer, inverse filter, deconvolution

1 Introduction

Cutting forces are one of the most important quantities in the metal machining process. The cutting forces govern power and torque requirements in the machine tool and drive heat generation which catalyzes tool wear and determines the magnitude and direction of residual stresses in the machined component. Cutting forces also cause deflection of the cutting tool, machine tool and work piece and may have a negative influence on the machined components quality. The cutting forces are therefore important parameters in evaluation of different cutting tool geometries and concepts. However, dynamic influences from the measurement system affect the result and make it difficult to obtain accurate cutting force data. A commonly used method to remove unwanted dynamic effects from the measured cutting forces is low-pass filtering. Low-pass filtering removes all information above a specified cut-off frequency and may therefore also remove important information related to the true cutting forces contained in frequencies above the cut-off frequency. This is especially evident in milling with transient cutting conditions when the rise times are short and the cutting forces thereby have high frequency content. Therefore, it is difficult to get reliable estimates of the amplitudes and rise times by low-pass filtering transient cutting forces, especially at high cutting speeds.

Accurate estimates of both rise times and force amplitudes are important, e.g., when evaluating and comparing different tools and insert geometries. An alternative approach, to low-pass filtering, that improves the cutting force estimates, i.e. increases the effective frequency range of the force dynamometer, is therefore of great interest.

For example, Tlusty et al. [1] used accelerometers to compensate for the inertia and structural damping of the dynamometer, thereby increasing the effective frequency range. This method has been proven to work under certain conditions, but encounters difficulties around resonance frequencies when the system inertia or damping is large. The method also has problems handling systems with more than one dominating mode, [2]. Park and Altintas [3] and Altintas and Park [4] used a Kalman filtering technique to compensate for unwanted dynamics, process and measurement noise of a spindle integrated force sensor. The same method has also been applied to cutting force measurements in micro end milling, [5]. The Kalman filtering technique has been proven to work in experimental tests and is well suited when problems with measurement or

process noise is expected. Jensen et al. [2] developed a method to obtain an invertible filter of a non-minimum phase frequency response function (FRF) of a force dynamometer. The method was tested on experimental data with promising results. The basic principle of the method is to divide the system's transfer function into one stable and one unstable causal IIR-filter. The unstable causal IIR-filter is transformed into a non-causal stable FIR-filter. Then, by using these two filters in series a stable inverse filter is obtained. Depending on the location of the non-minimum phase zeros of the system's transfer function, the length of the non-causal FIR-filter can become large, introducing long time delays. However if the method is applied on large data sequences, this will not cause a problem. Castro et al. [6] and Girardin [7] used an approach where the dynamic effects from the force dynamometer are removed in the frequency domain by multiplying with the inverse of the system's FRF matrix. Since the measured cutting forces need to be transformed into the frequency domain, average amplitudes of the frequency components are obtained, which requires the studied signals to be stationary.

In the case when the force dynamometer can be considered linear and the cross-frequency responses between the directions x , y and z are negligible, a minimum-phase inverse filter can be constructed and used to counteract the dynamometer dynamics and thereby increase the usable bandwidth of the dynamometer. A procedure for creating a minimum-phase inverse filter is described in this paper and applied in both simulations and on experimental data from milling under various cutting conditions.

2 Inverse Filtering

Consider the FRF $H(\omega)$ between the applied force $F_R(\omega)$ and the force output from the dynamometer $F_D(\omega)$, Equation (1).

$$H(\omega) = \frac{F_D(\omega)}{F_R(\omega)} \quad (1)$$

In an ideal case, i.e. when there are no dynamic influences from the dynamometer, the magnitude of $H(\omega)$ is equal to unity and the phase equal to zero for all frequencies. However, due to e.g., the mass and shape of the work piece, the stiffness and damping of the force dynamometer and the distance between the actual cutting position and the positions of the force transducers in the

dynamometer, the magnitude and phase of the frequency response between applied force and force output will deviate from the ideal values and thus the measured force will differ from the applied force. By applying an inverse filter, describing $H^{-1}(\omega)$, on the recorded force signal these unwanted dynamic effects can be counteracted. If $H(\omega)$ is stable and minimum-phase (all zeros of the system lies within the unit circle in the z -domain) then the system is directly invertible. Usually, mechanical systems are stable and mixed-phase (zeros both inside and outside the unit circle). If the system has zeros outside the unit circle it cannot be directly inverted, since the result will then have unstable poles and the filter output exponentially tends toward infinity. However, a mixed or maximum-phase FRF can be transformed into a minimum-phase FRF while still keeping the amplitude characteristics but changing the phase. An invertible filter describing the characteristics of the minimum-phase FRF can then be estimated as described in this section.

2.1 Transformation into minimum-phase

A mixed- or maximum-phase transfer function can be transformed into a minimum phase transfer function by, e.g., using the Hilbert transform [8] or cepstrum [9, 10]. In this paper real cepstrum is used to transform the FRF of the force dynamometer into minimum-phase.

Let $h(n)$ be a real sequence with $H(\omega)$ as its Fourier transform. Its real and complex cepstrum $\hat{c}(n)$ and $\hat{h}(n)$ are defined as:

$$\hat{C}(\omega) = \Re(\hat{H}(\omega)) = \log|H(\omega)| \quad (2a)$$

$$\hat{c}(n) = \mathcal{F}^{-1}(\hat{C}(\omega)) \quad (2b)$$

$$\hat{H}(\omega) = \log(H(\omega)) \quad (2c)$$

$$\hat{h}(n) = \mathcal{F}^{-1}(\hat{H}(\omega)) \quad (2d)$$

where $\log|H(\omega)|$ refers to the natural logarithm of $|H(\omega)|$ and \mathcal{F}^{-1} denotes the inverse Fourier transform. Some useful relations between minimum-phase and maximum-phase sequences and their complex cepstrums are, [10]:

- If $h(n)$ is a minimum-phase sequence, $\hat{h}(n)$ will be a causal sequence.

- If $h(n)$ is a maximum-phase sequence, $\hat{h}(n)$ will be an anti-causal sequence.

Let the minimum-phase counterpart to $h(n)$ be denoted by $h_{min}(n)$ and its complex cepstrum denoted by $\hat{h}_{min}(n)$. The Kramers-Kronig relations for a causal sequence states that the entire sequence can be described by its even part. The relationship between the even part of $\hat{h}(n)$ and its Fourier transform is given by [11]:

$$\hat{h}_e(n) = \mathcal{F}^{-1}(\Re(\hat{H}(\omega))) = \hat{c}(n) \quad (3)$$

Since $\hat{h}(n)$ is a causal sequence when $h(n)$ is minimum-phase, $\hat{h}_{min}(n)$ can be estimated as:

$$\hat{h}_{min}(n) = \begin{cases} 2\hat{c}(n) & n > 0 \\ \hat{c}(n) & n = 0 \\ 0 & n < 0 \end{cases} \quad (4)$$

According to Equation (2) the minimum-phase transfer function $H_{min}(\omega)$ is obtained by:

$$H_{min}(\omega) = e^{\mathcal{F}(\hat{h}_{min}(n))} \quad (5)$$

2.2 Obtaining an invertible digital filter

Empirical Transfer Function Estimate (ETFE) is used for model identification of the estimated minimum-phase FRF, $H_{min}(\omega)$ [12]. This method is based on non-parametric frequency response characteristics and describes the identified FRF using a polynomial model. The identification is performed in MATLAB® using the function `invfreqz` from the Signal Processing Toolbox. The identified model is a discrete representation of the minimum-phase transfer function of the force dynamometer, $h_{min}(n)$, and can be represented as:

$$H_{min}(z) = \frac{B(z)}{A(z)} = \frac{b(1) + b(2)z^{-1} + \dots + b(nb+1)z^{-nb}}{a(1) + a(2)z^{-1} + \dots + a(na+1)z^{-na}} \quad (6)$$

The result is an invertible IIR-filter described by the coefficients b and a , where nb and na are the total number of coefficients in the numerator and denominator, respectively. nb and na are selected by visual inspection ensuring a satisfactory fit between the measured and estimated FRFs.

3 Simulations

To verify the proposed method and identify usable frequency ranges for the inverse filters, simulations using a model of the force dynamometer obtained from experimental data are performed. The model is based on the FRF matrix of the force dynamometer, with the work piece, mounted in the machine tool. The FRF matrix was estimated using impulse excitation in x - and y -directions, results are shown in Figures 1 and 2.

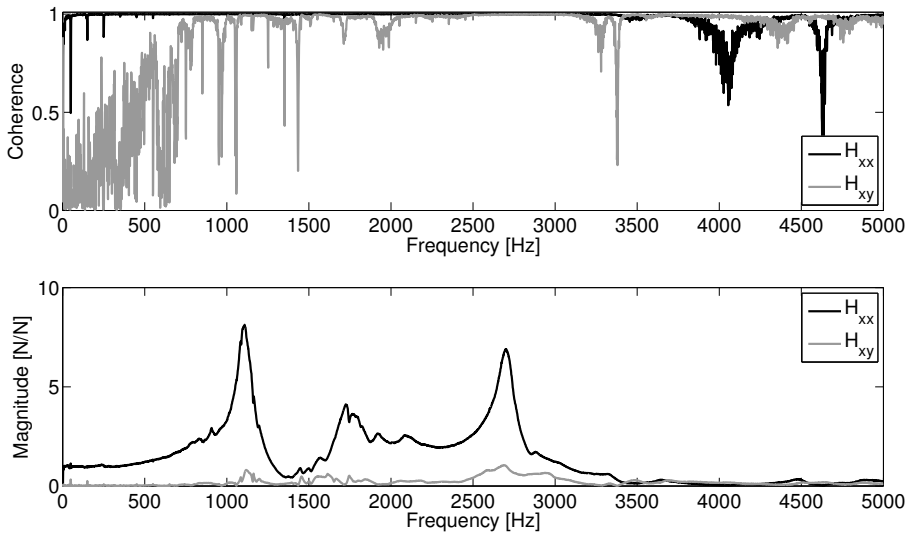


Figure 1: Measured FRFs of the force dynamometer from impulse excitation. The dynamometer is excited in the x -direction and responses collected in x - and y -directions.

High Frequency Measurements of Cutting Forces in Milling by Inverse Filtering

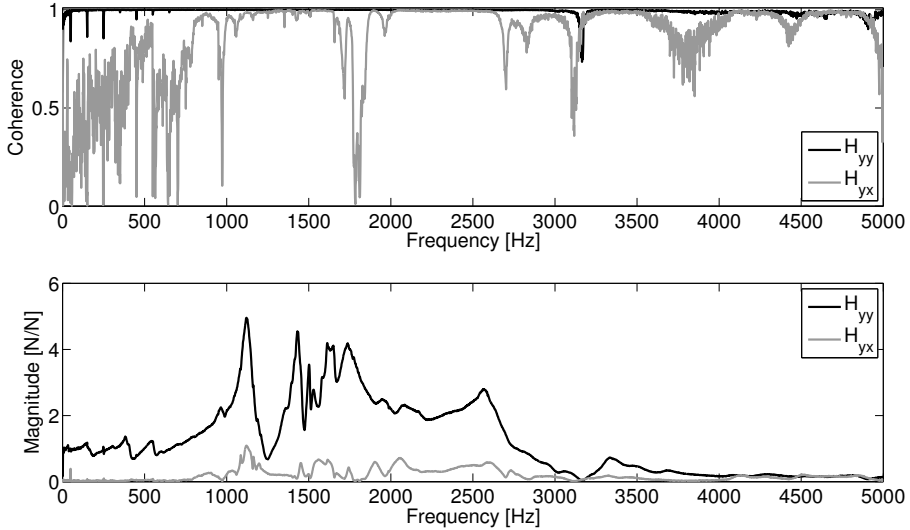


Figure 2: Measured FRFs of the force dynamometer from impulse excitation. The dynamometer is excited in the y -direction and responses collected in y - and x -directions.

The cross-frequency response in the region 0 to 3000 Hz is small in both directions. Also, the coherence functions are close to unity up to approximately 3000 Hz, implying linear relationships between inputs and outputs. These results indicate that a linear model, with negligible cross frequency response, of the force dynamometer is valid for frequencies up to 3000 Hz.

Based on the FRF measurements of the dynamometer, inverse filters in both x and y - directions are constructed and evaluated with respect to both amplitude and phase correction. Comparisons between the measured FRFs and the minimum-phase FRFs are shown in Figures 3 and 4. To clearly show the amplitude and phase characteristics of the inverse filters, the combined FRFs are also displayed; these are calculated as:

1. Inverse Fourier transform the measured mixed-phase FRF, $H(\omega)$, the result is the impulse response.
2. Apply the inverse filter to the obtained impulse response, the result is a

unit impulse.

3. The combined FRF is the Fourier transform of the signal obtained from the inverse filter.

If the inverse filter behaves perfectly, the magnitude of the combined FRF should be unity and the phase zero for all frequencies.

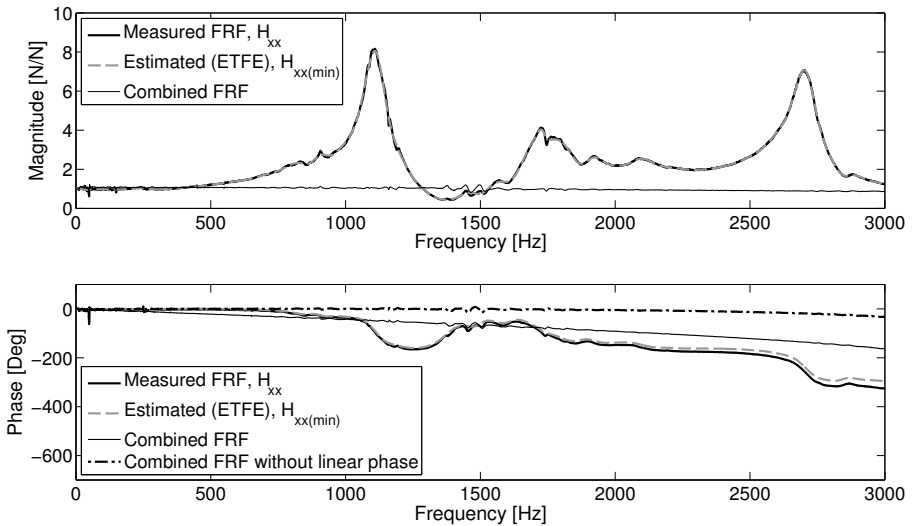


Figure 3: Magnitude and phase responses of $H_{xx}(\omega)$, $H_{xx(min)}(\omega)$ and the combined FRF, $nb = 200$ and $na = 55$. The dynamometer's dominant modes are: 1110 Hz, 1725 Hz, 2700 Hz.

The magnitudes of $H_{xx}(\omega)$ and $H_{yy}(\omega)$ matches well with their respective minimum-phase FRFs $H_{xx(min)}(\omega)$ and $H_{yy(min)}(\omega)$. The combined FRFs indicate a good amplitude correction over the entire frequency range, even at dominant modes. Due to the minimum-phase transformation, the phase responses of measured and minimum-phase FRFs differ, which is clearly visible in the phase responses of the combined FRFs. However, the phase responses of the combined FRFs are dominated by linear trends which can be related to constant delays in the time domain and will not affect the amplitude responses of the inverse filtered signals. Thus, the phase responses affecting the

High Frequency Measurements of Cutting Forces in Milling by Inverse Filtering

inverse filtered signals are obtained by removing the linear phase trends from the combined FRFs.

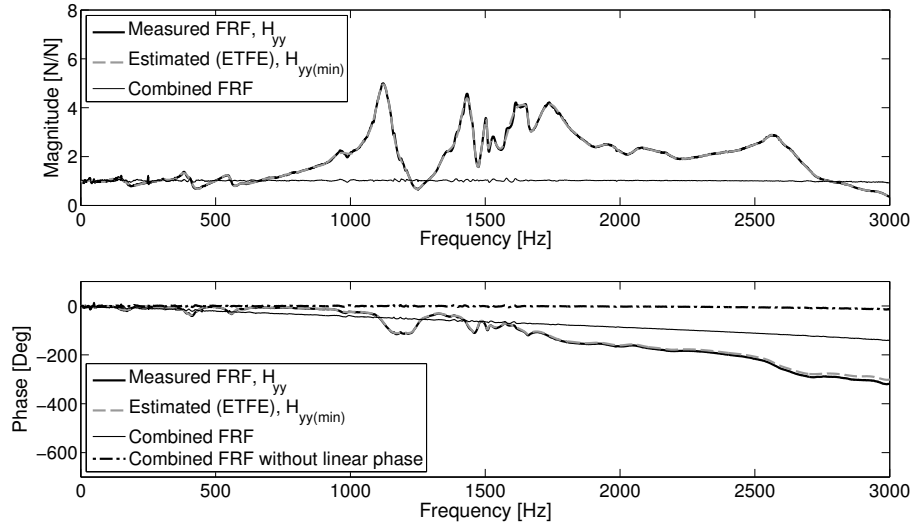


Figure 4: Magnitude and phase responses of $H_{yy}(\omega)$, $H_{yy(\min)}(\omega)$ and the combined FRF, $nb = 200$ and $na = 55$. The dynamometer's dominant modes are: 1120 Hz, 1430 Hz, 1630 Hz, 1750 Hz and 2550 Hz.

As seen in Figures 3 and 4, the phases of the combined FRFs have deviated approximately 7 degrees from zero at 2500 Hz. Therefore, it is expected that frequencies above 2500 Hz will be out of range for the inverse filter. To avoid influences from the resonances at 2550 Hz in the x -direction and 2700 Hz in the y -direction, the frequency limit of the inverse filters was set to 2400 Hz in both directions, higher frequencies are removed by low-pass filtering. Low-pass filtering also removes any high-frequency noise present in the inverse filtered signal. High frequency noise is common when performing inverse filtering due to the nature of the filter. The reason being that mechanical systems normally acts as low-pass filters, attenuating high frequencies. When these systems are inverted they will instead act as high-pass filters and therefore respond badly to high frequency noise. The low-pass filter design used in the simulations is a Butterworth filter of order 3. To remove any phase distortion caused by the low-pass filter, zero-phase filtering is performed by filtering the data in both

forward and reverse directions using the MATLAB[®] function `filtfilt`.

To test the behavior of the inverse filters, simulations are carried out for the cutting speeds and feed rates listed in Table 1. Down milling and 50 percent radial immersion is used to excite the dynamometer with a high frequency transient signal and thereby clear effects from the dynamometer dynamics appear. The simulations are carried out using both x and y as feed directions. Mechanistic modeled cutting forces are used as input (see Table 2), these are filtered through ETFEs of the measured mixed-phase transfer functions, $h_{xx}(n)$, $h_{xy}(n)$ and $h_{yy}(n)$, $h_{yx}(n)$. Each output is then inverse filtered and compared to the reference cutting force (simulated input force), Figures 5 and 6. The simulated output forces have contributions both from the point FRFs and the cross FRFs. Due to the phase distortion caused by the minimum-phase transformation, superposition of e.g. $h_{xx(min)}(n)$ and $h_{xy(min)}(n)$ does not apply. Therefore only $h_{xx(min)}(n)$ or $h_{yy(min)}(n)$ are used in the inverse filters. Thus, for the results to be accurate, the effect of the cross FRFs have to be negligible.

The similarity between the signals is estimated by calculating the ratio of the energy in the difference between reference and inverse filtered force, $E(f_R(t) - f_I(t))$, and the energy in the reference signal, $E(f_R(t))$, according to:

$$\eta = \min \left[\left(1 + \frac{R_{f_I f_I}(0) - \bar{f}_I^2 - 2(R_{f_R f_I}(\tau) - \bar{f}_R \bar{f}_I)}{R_{f_R f_R}(0) - \bar{f}_R^2} \right) \cdot 100 \right] \quad (7)$$

where $R_{f_R f_R}(0)$ and $R_{f_I f_I}(0)$ are the autocorrelations at zero time delay between reference and inverse filtered forces, respectively. $R_{f_R f_I}(\tau)$ refers to the cross correlation between reference and inverse filtered forces, where τ is the time delay between the two signals, [13]. \bar{f}_R and \bar{f}_I are the average values of the reference and inverse filtered forces, respectively. The best fit between the signals is found at the time delay, τ , where the energy in the difference between the two signals has a minimum. If $\eta = 0$ the two signals are identical.

The simulation results show that the inverse filters are able to counteract the dynamic influences and reconstruct the reference cutting forces within a small error margin for all cutting speeds and feed rates listed in Table 1. As seen in Figures 5a) and 6a) the difference between reference and inverse filtered forces increases as the cutting speed increases. This is expected since the cutting speed affect ramp up times and thereby the frequency content in the reference

High Frequency Measurements of Cutting Forces in Milling by Inverse Filtering

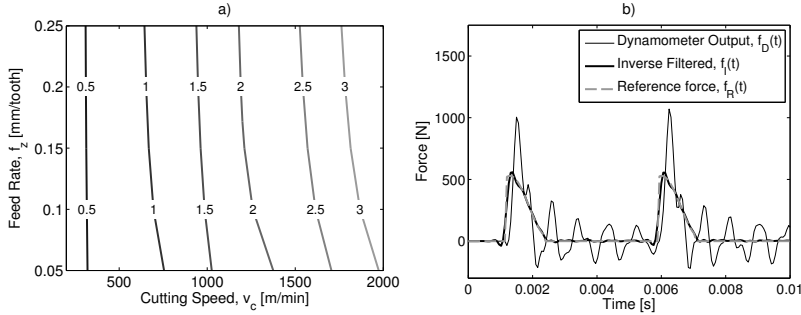


Figure 5: Simulation results with feed in x -direction; a) The isolines of η [%], Equation (7). b) Comparison between dynamometer output, inverse filtered and reference input forces (Cutting speed, $v_c = 2000$ [m/min]; Feed rate, $f_z = 0.25$ [mm/tooth]).

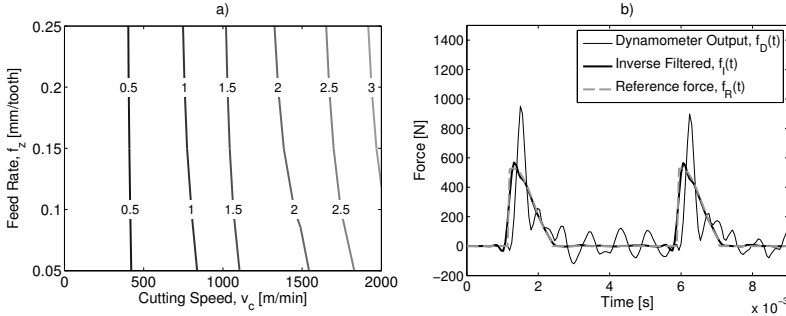


Figure 6: Simulation results with feed in y -direction; a) The isolines of η [%], Equation (7). b) Comparison between dynamometer output, inverse filtered and reference input forces (Cutting speed, $v_c = 2000$ [m/min]; Feed rate, $f_z = 0.25$ [mm/tooth]).

force signal. Higher cutting speed leads to higher frequencies in the reference force. Thus, the frequency range of the inverse filter may not be enough to fully describe the transient behavior in the force signal at high cutting speeds. Comparisons between reference and inverse filtered forces using maximum feed rate and cutting speed are shown in Figures 5b) and 6b). Additionally, simulations were performed without considering the effect of the cross FRFs on the

dynamometer outputs. Neglecting the cross FRFs did not show any significant changes in the results confirming that the cross FRFs are negligible.

4 Experimental tests

The proposed method was evaluated in experimental cutting tests using different cutting speeds, feed rates and radial immersion. To be able to test the method over a large span of cutting speeds, the tests were performed in aluminum. Forces in both x - and y -directions were recorded and inverse filtered. The results are compared with unfiltered, low-pass filtered and simulated cutting forces. The simulated cutting forces are mechanistic modeled and the cutting coefficients are estimated from milling tests in the work piece used in the experimental tests, see Table 2, [14]. The test setup is illustrated in Figure 7. Equipment and cutting data used are listed in Table 1.

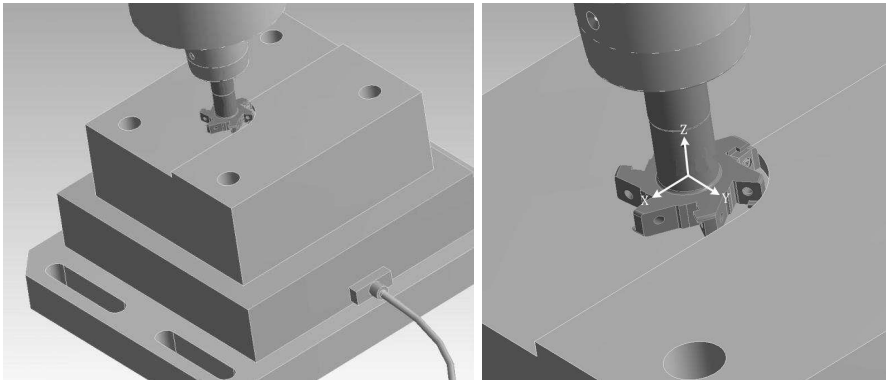


Figure 7: The test setup showing force dynamometer, workpiece and cutter used in the measurements.

The cut-off frequency used for direct low-pass filtering of the cutting forces was set by visually inspecting the FRFs in Figures 1 and 2. As seen, the frequency response of the force dynamometer is relatively flat up to 600 Hz. Information contained in the region above 600 Hz is expected to be effected by the force dynamometer dynamics and generate an erroneous output. Thus, the cut-off frequency used for direct low-pass filtering was set to 600 Hz. The cut-off frequency used for low-pass filtering the inverse filtered signals is the same as

High Frequency Measurements of Cutting Forces in Milling by Inverse Filtering

used in the simulations, 2400 Hz. The filter design and filtering techniques used in the simulations are also used in the experimental tests. Figures 8-10 show results from tests with different radial immersion and cutting speeds.

Table 1: Equipment and cutting data used in the cutting force measurements.

Machine Tool	MORI SEIKI NV5000
Cutting Tool	Sandvik R331.35-050A20EM100
Insert	Sandvik N331.1A-08 45 08H-NL H10
Work Piece Material	AISI 7075
Force Dynamometer	Kistler 9255B
Charge Amplifier	Kistler 5011
Cutter diameter, D_{cap}	50 [mm]
Radial cutting depth, a_e	10; 25; 40 [mm]
Axial cutting depth, a_p	3 [mm]
Number of teeth, z_c	1
Cutting speeds, v_c	200; 400; 800; 1200; 1490; 2000 [m/min]
Tooth passing frequencies, f_t	21.2; 42.4; 84.8; 127.3; 158.1; 212.2 [Hz]
Feed rates, f_z	0.05; 0.1; 0.15; 0.2; 0.25 [mm/tooth]

Table 2: Estimated cutting force coefficients from milling tests.

v_c	K_{tc}	K_{te}	K_{rc}	K_{re}	K_{ac}	K_{ae}
200	732.26	26.38	163.71	15.65	-52.07	18.90
400	693.05	18.37	128.67	9.66	-36.80	14.771
800	638.00	17.92	99.43	11.33	-5.47	12.69
1200	649.03	21.78	42.14	14.67	-23.76	4.61
1490	617.35	19.71	24.12	12.77	-87.01	16.72
2000	597.66	17.40	24.44	11.61	-105.45	15.61
m/min	N/mm ²					

The results show that inverse filtered cutting forces are able to predict both amplitude and ramp-up in a reliable manner. Compared with simulated forces the difference in amplitude is small for all cutting conditions tested. Both amplitude and ramp-up prediction is better for inverse filtered compared to

low-pass filtered forces. The difference is especially clear for transient cutting conditions and high cutting speeds. Another issue using low-pass filtering is that changes in the estimated cutting forces with respect to cut-off frequency makes it difficult to tell if and when the obtained results are accurate. Also, using low-pass filtering the cut-off frequency should be set to the highest possible value in order to preserve as much information as possible. This requires measurements of the dynamometers frequency response for each specific set-up. Thus, to properly select a cut-off frequency for low-pass filtering, the same number of frequency response measurements are needed as are needed to construct an inverse filter. Since the frequency range, in this case, was extended by 400 percent using inverse filtering compared to low-pass filtering, the results become more reliable and less sensitive to changes in cutting conditions.

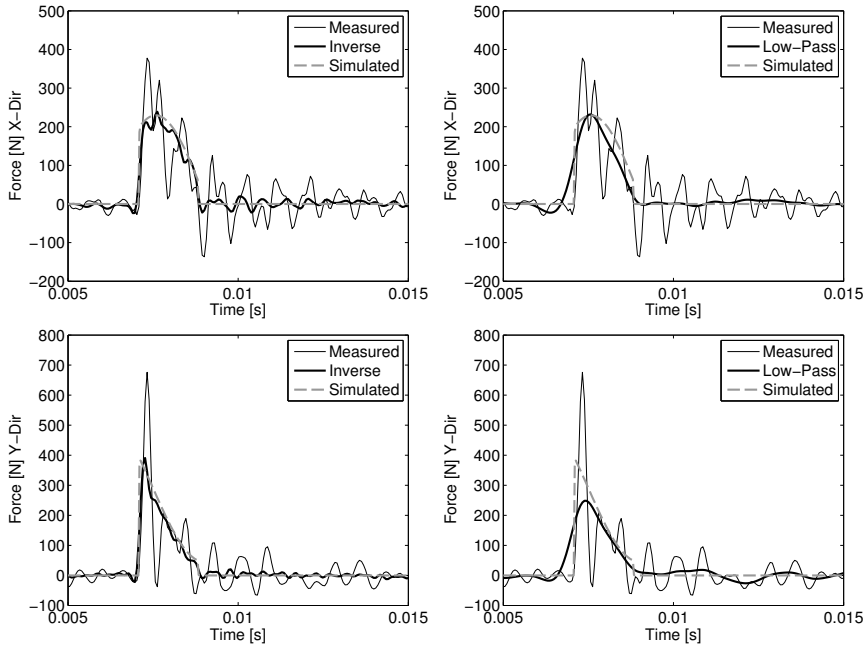


Figure 8: Comparison of unfiltered, simulated, inverse filtered and low-pass filtered cutting forces. Down milling; Cutting speed, $v_c = 800$ m/min; Tooth passing frequency, $f_t = 84.8$ Hz; Feed rate, $f_z = 0.2$ mm/tooth; Radial immersion $a_e = 10$ mm.

High Frequency Measurements of Cutting Forces in Milling by Inverse Filtering

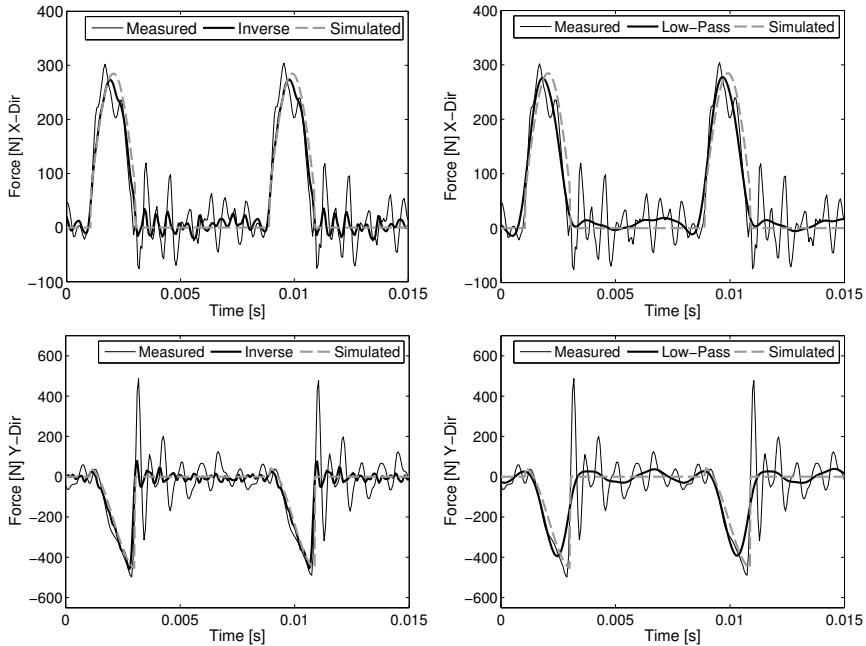


Figure 9: Comparison of unfiltered, simulated, inverse filtered and low-pass filtered cutting forces. Up milling; Cutting speed, $v_c = 1200$ m/min; Tooth passing frequency, $f_t = 127.3$ Hz; Feed rate, $f_z = 0.2$ mm/tooth; Radial immersion $a_e = 25$ mm.

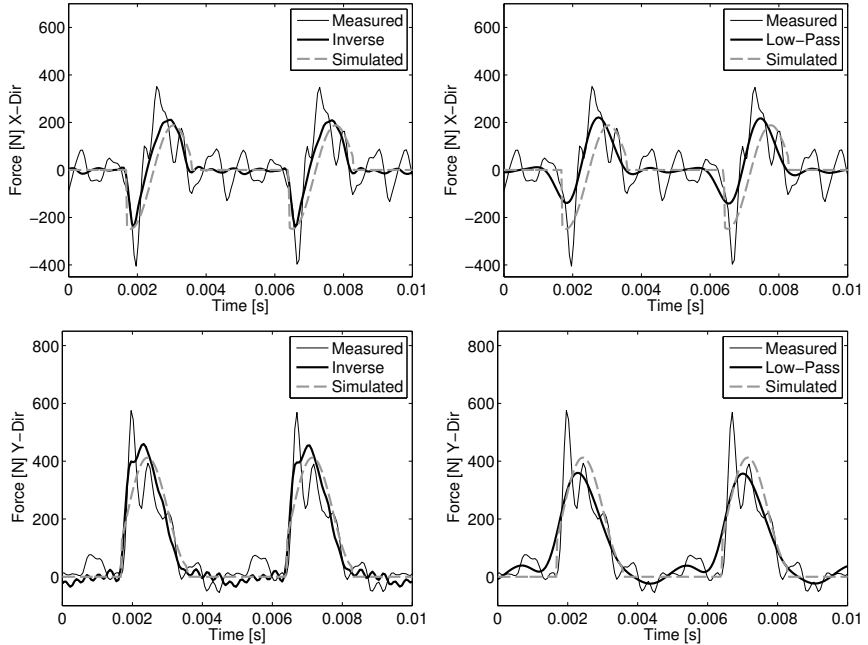


Figure 10: Comparison of unfiltered, simulated, inverse filtered and low-pass filtered cutting forces. Down milling; Cutting speed, $v_c = 2000$ m/min; Tooth passing frequency, $f_t = 212.2$ Hz; Feed rate, $f_z = 0.2$ mm/tooth; Radial immersion $a_e = 40$ mm.

5 Conclusions

A method to create an inverse filter for improved cutting force measurements based on minimum-phase FRFs has been presented. The method is based on the assumptions that the force dynamometer can be described by a linear model and that the cross FRFs of the system are negligible. These assumptions were verified by simulations, combining both measured mixed-phase and minimum-phase FRFs of the force dynamometer, confirming the inverse filters validity within the boundaries of the cutting conditions used in the measurements. The method successfully counteracted the dynamometer dynamics in experimental

tests with different feed rates, cutting directions and cutting speeds. The results show that a more reliable estimation of the cutting forces can be obtained using the proposed method compared to traditional low-pass filtering, especially under transient cutting conditions and high cutting speeds. Since the dynamic corrections are performed in the time domain, compensation can be performed on both stationary and non-stationary signals, which allows the method to be used under both constant and varying cutting conditions. The method can be used to study detailed force responses such as transient entering and/or exiting forces, which is important, e.g., for cutting tool design.

References

- [1] J. Tlusty, D.Y. Jang, and Y.S. Tarn. Measurements of milling force over a wide frequency range. In *Proceedings of the 15th NAMRC*, pages 273–280, 1987.
- [2] Steven A. Jensen, Yung C. Shin, and Patricia Davies. Inverse filtering of unwanted system dynamics in cutting force measurement. *American Society of Mechanical Engineers, Dynamic Systems and Control Division (Publication) DSC*, 58:167–174, 1996.
- [3] Simon S. Park and Yusuf Altintas. Dynamic compensation of spindle integrated force sensors with kalman filter. *Journal of Dynamic Systems, Measurement, and Control*, 126(3):443–452, 2004.
- [4] Y. Altintas and S.S. Park. Dynamic compensation of spindle-integrated force sensors. *CIRP Annals - Manufacturing Technology*, 53(1):305 – 308, 2004.
- [5] S.S. Park and M. Malekian. Mechanistic modeling and accurate measurement of micro end milling forces. *CIRP Annals - Manufacturing Technology*, 58(1):49 – 52, 2009.
- [6] Luis Ricardo Castro, Pascal Viéville, and Paul Lipinski. Correction of dynamic effects on force measurements made with piezoelectric dynamometers. *International Journal of Machine Tools and Manufacture*, 46(14):1707 – 1715, 2006.

- [7] Remond D. Rigal J.-F. Girardin, F. High frequency correction of dynamometer for cutting force observation in milling. *Journal of Manufacturing Science and Engineering, Transactions of the ASME*, 132(3):0310021–0310028, 2010.
- [8] Malcolm J. Hawksford. Minimum-phase signal processing for loudspeaker systems. In *Audio Engineering Society Convention 100*, 5 1996.
- [9] Soo-Chang Pei and Huei-Shan Lin. Minimum-phase FIR filter design using real cepstrum. *IEEE Transactions on Circuits and Systems II-Express Briefs*, 53(10):1113–1117, 2006.
- [10] Alan V. Oppenheim and Ronald W. Schafer. *Discrete-time signal processing*. Pearson Education, Upper Saddle River, N.J., 3. ed., international ed. edition, 2010.
- [11] John G. Proakis and Dimitris G. Manolakis. *Digital signal processing : principles, algorithms and applications*. Prentice-Hall, Upper Saddle River, N.J., 3. ed. edition, 1996.
- [12] Lennart Ljung. *System identification : theory for the user*. Prentice Hall, Upper Saddle River, N.J., 2. ed. edition, 1999.
- [13] Julius S. Bendat and Allan G. Piersol. *Engineering applications of correlation and spectral analysis*. Wiley, New York, 2. ed. edition, 1993.
- [14] Yusuf Altintas. *Manufacturing automation : metal cutting mechanics, machine tool vibrations, and CNC design*. Cambridge University Press, Cambridge, 2000.

ABSTRACT

Trial and error and the use of highly time-consuming methods are often necessary for investigation and characterization of nonlinear systems. However, for the rather common case where a nonlinear system has linear relations between many of its degrees of freedom there are opportunities for more efficient approaches. The aim of this thesis is to develop and validate new efficient simulation and experimental methods for characterization of mechanical systems with localized nonlinearities. The purpose is to contribute to the development of analysis tools for such systems that are useful in early phases of the product innovation process for predicting product properties and functionality. Fundamental research is combined with industrial case studies related to metal cutting. Theoretical modeling, computer simulations and experimental testing are utilized in a coordinated approach to iteratively evaluate and improve the methods. The nonlinearities are modeled as external forces acting on the underlying linear system. In this way, much of the linear theories behind forced response simulations can be utilized. The linear parts of the system are described using digital filters and modal superposition, and the response of the system is recursively solved for together with the artificial external forces. The result is an efficient simulation method, which in conjunction with experimental tests, is used to validate the proposed characterization methods.

A major part of the thesis addresses a frequency domain characterization method based on broadband excitation. This method uses the measured responses to create artificial nonlinear inputs to the parameter estimation model. Conventional multiple-input/multiple-output techniques are then used to separate the linear system from the nonlinear parameters. A specific result is a generalization of this frequency domain method, which allows for characterization of continuous systems with an arbitrary number of localized zero-memory nonlinearities in a structured way. The efficiency and robustness of this method is demonstrated by both simulations and experimental tests. A time domain simulation and characterization method intended for use on systems with hysteresis damping is also developed and its efficiency is demonstrated by the case of a dry-friction damper. Furthermore, a method for improved harmonic excitation of nonlinear systems using numerically optimized input signals is developed. Inverse filtering is utilized to remove unwanted dynamic effects in cutting force measurements, which increases the frequency range of the force dynamometer and significantly improves the experimental results compared to traditional methods. The new methods form a basis for efficient analysis and increased understanding of mechanical systems with localized nonlinearities, which in turn provides possibilities for more efficient product development as well as for continued research on analysis methods for nonlinear mechanical structures.

